W&M ScholarWorks

Dissertations, Theses, and Masters Projects   Theses, Dissertations, & Master Projects

2015

The Influence of Short-Term Events on the Hydrographic and Biological Structure of the Southwestern Ross Sea

Randolph M. Jones
College of William and Mary - Virginia Institute of Marine Science

Follow this and additional works at: https://scholarworks.wm.edu/etd

Part of the Marine Biology Commons, and the Oceanography Commons

This Thesis is brought to you for free and open access by the Theses, Dissertations, & Master Projects at W&M ScholarWorks. It has been accepted for inclusion in Dissertations, Theses, and Masters Projects by an authorized administrator of W&M ScholarWorks. For more information, please contact scholarworks@wm.edu.

THE INFLUENCE OF SHORT-TERM EVENTS ON THE HYDROGRAPHIC AND

BIOLOGICAL STRUCTURE OF THE SOUTHWESTERN ROSS SEA

_____

A Thesis

Presented to

The Faculty of the School of Marine Science

The College of William and Mary in Virginia

In Partial Fulfillment

of the Requirements for the Degree of

Master of Science
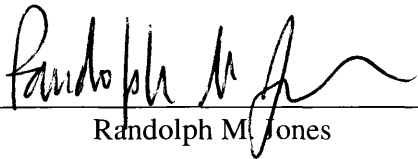
_____

by

Randolph M. Jones
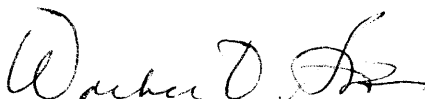
2015

APPROVAL SHEET

This thesis is submitted in partial fulfillment of

the requirements for the degree of

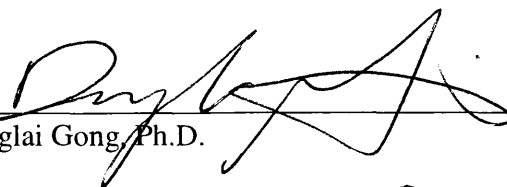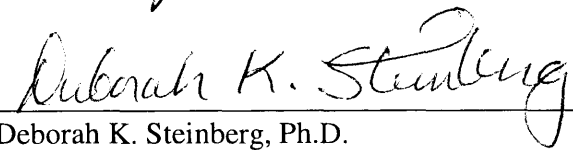Master of Science

Randolph M. Jones

Approved, by the Committee, November 2015

Walker O. Smith, Jr., Ph.D.
Committee Chairman/Advisor

Marjorie A.M. Friedrichs, Ph.D.

Donglai Gong, Ph.D.

Deborah K. Steinberg, Ph.D.

TABLE OF CONTENTS

ACKNOWLEDGEMENTS

LIST OF TABLES

LIST OF FIGURES

vii

LIST OF APPENDICES

ABSTRACT

Relative to the rest of the Southern Ocean, the Ross Sea continental shelf experiences very high productivity and phytoplankton biomass, which supports an extensive food web including high concentrations of upper trophic level biomass. Conventional observational methods, including ship-based sampling, instrumented moorings, satellite imagery, and computer-based modelling, have illustrated the seasonal progression of the phytoplankton bloom over the past four decades. While we have been sampling phytoplankton variability in the Ross Sea on a variety of relatively large scales, with observations at specific locations or times, over spans of time, or at specific depths, our understanding of smaller scales of variability (on the order of a few hours or several kilometers) is still poor. Utilizing two seasons (2010-2011 and 2012-2013) of high-resolution autonomous glider deployments in the southwestern Ross Sea, I examined the mechanisms driving both the transitions between stages of the phytoplankton bloom and the short-term perturbations in average 0-50 m chlorophyll. By including the available raw fluorescence data from both glider seasons and three mooring seasons, I determined that the 2012-2013 season had greater than average variability, with greater levels of variability observed in only two other seasons. Differences in the timing of bloom transitions were relatively constrained; the transition from bloom to post-bloom levels occurred within a temporal span of 6 d. These findings were likely the result of the location of the 2012-2013 glider adjacent to Ross Island and the Ross Ice Shelf, where complex bathymetry, turbulent flows, and the presence of an ice field contributed to the greater observed variability. To investigate the mechanisms driving the short-term perturbations in chlorophyll, I examined the relationships between average chlorophyll, average temperature, and mixed layer depth measured by the gliders and wind speed measured by two automatic weather stations atop the Ross Ice Shelf. Over the course of the 2012-2013 season, perturbations or responses in chlorophyll were heavily influenced by the degree of temporal coupling between wind events and the depth of mixing. Longer delays of 12-24 h observed prior to the biomass maximum shortened following the transition to biomass dissipation to 2-12 h. Furthermore, by causing aggregate formation and rapid vertical flux, physical forcing factors contributed to the observed short-term perturbations through reductions in biomass in surface layers and the appearance of chlorophyll in deeper layers. These results suggest that the small-scale observing capabilities of autonomous gliders allow for an improved understanding of the mechanisms that drive variability and short-term perturbations in shallow chlorophyll in the southwestern Ross Sea.

THE INFLUENCE OF SHORT-TERM EVENTS ON THE HYDROGRAPHIC

AND BIOLOGICAL STRUCTURE OF THE SOUTHWESTERN ROSS SEA

CHAPTER 1

'Project Introduction and Background'

Research Background and Motivation

Investigations over the past four decades into the phytoplankton of the Ross Sea have generated an extensive data set on the physiological ecology, growth, and distribution of the two main phytoplankton groups, haptophytes and diatoms (El-Sayed et al., 1983; Smith and Nelson, 1985; Arrigo et al., 1999, 2000, 2010; Smith et al., 2000, 2011a, 2013). Together, they contribute the vast majority of primary production observed over the Ross Sea continental shelf (Arrigo et al., 1999), which supports an extensive food web with substantial upper trophic level biomass (Ballard et al., 2012). While the region is known to be one of the least impacted by direct human activities (Halpern et al., 2008), the building momentum of climate change will lead to rapid ecosystem shifts in the near future with consequences for phytoplankton dynamics (Orr et al., 2005; Constable et al., 2014; Smith et al., 2014b).

Conventional survey methods combined with a multi-generational series of ocean color satellite data (e.g., Coastal Zone Color Scanner or CZCS, Sea-Viewing Wide Field-of-View Sensor or SeaWiFS, and Moderate Resolution Imaging Spectroradiometer or MODIS) have increased our understanding of phytoplankton dynamics and of the seasonal climatology at broad spatial and temporal scales (Arrigo et al., 1998a; Smith et al., 2000, 2011a), but these observational methods can be greatly limited by atmospheric and ocean conditions, cost, and resolution of important mesoscale or sub-mesoscale features, which are important to biological processes (e.g., McGillicuddy et al., 2007). As a recent addition to ocean observing capabilities, buoyancy-propelled autonomous underwater vehicles, known as gliders, have the ability to counter some of these limitations and produce high-resolution, long-duration data for study areas from 10's to

1000's of kilometers in size (Eriksen et al., 2001). There are two main limitations of glider technology: slower speed and, in high-latitudes, the requirement of sea-ice free surface conditions for GPS and data connectivity (Rudnick and Cole, 2011; Smith et al., 2014c). Their use, as demonstrated by Kaufman et al. (2014), has permitted the examination of finer scales of spatial and temporal variability than are not available through ship-based survey methods or satellite analyses.

The principal objective of this research is *to better elucidate mechanisms driving key events within the seasonal progression of phytoplankton (e.g., delineating stages of biomass accumulation, bloom maximal concentrations, biomass dissipation, and post-bloom) and the mechanisms behind observed event-scale perturbations in the seasonal phytoplankton climatology of the southwestern Ross Sea* by utilizing the sampling capabilities of gliders. The material in the following section describes the Southern Ocean and the Ross Sea in detail, as a background for the entire thesis.

The Southern Ocean

The Southern Ocean, here defined as waters south of 50°S, comprises 12.6% (45.5 million km^2) of the surface area of the world's oceans (Amante and Eakins, 2009), and plays a critical role in the global climate system (Gille, 2002) and marine biogeochemical cycles (Le Quéré et al., 2007; Arrigo et al., 2008b), as well as hosting a diverse array of marine ecosystems (Smetacek and Nicol, 2005). A major driver of these influences on both global and regional scales (e.g., impacting the Ross Sea) is the circulation pattern of the Southern Ocean, which is dominated by the largest volume transport on Earth, the Antarctic Circumpolar Current (ACC) encircling the globe near

4

60°S. Between 50°S and the Antarctic land mass, a set of latitudinal frontal systems creates rapid changes in surface properties over relatively small spatial scales (e.g., km) and delineates different water masses (Figure 1). One of the most predominant water masses in the Southern Ocean is Circumpolar Deep Water (CDW), a relatively warm (> 2°C), salty, low-oxygen, and nutrient-replete layer which is carried eastward at mid-depths (~2,500 m) by the ACC (Orsi and Wiederwohl, 2009; Smith et al., 2012a). The eastward circulation of the ACC and latitudinal frontal systems support sloped density surfaces that rise to the south, which provide a route for CDW to shoal adiabatically as it moves southward across the ACC towards the continental shelf break. This process adds variability to the temperature and salinity properties of CDW (Orsi et al., 1995a). Above the voluminous CDW lies colder Antarctic Surface Water (AASW), which in contrast to CDW exhibits relatively uniform properties from the Polar Front to the Antarctic continent.

Induced by wind and buoyancy forcing and constrained by topography, two large clockwise gyres occur south of the ACC – the Weddell and the Ross Gyres (Wang and Meredith, 2008). The eastern limb of the latter entrains waters of the CDW, which is cooled as it circulates around the Gyre and undergoes diapycnal mixing with colder (−1.5 °C), low-salinity (~34.0) AASW. These interactions attenuate the warm and salty properties of CDW (hereafter referred to modified CDW or MCDW), and bring it to shallower depths (~700-800 m; Orsi and Wiederwohl, 2009). The westward-flowing southern limb of the Ross Gyre creates a coastal jet that follows the bathymetry of the continental shelf break. On- and off-shelf transport processes are largely the result of this coastal jet interacting with a series of troughs and banks oriented roughly north-south on

5

the Ross Sea continental shelf, leading to intrusions of MCDW into the troughs. Additional processes that transport water onto the continental shelf include deep, southward Ekman flow diverging from the shallower eastward ACC current, flow inertia interacting with bathymetric features, atmospherically forced exchanges of water, and on-shelf advection due to ice shelf circulation (Dinniman et al., 2003; Klinck and Dinniman, 2010).

The Ross Sea

With connectivity to Southern Ocean global circulation and a highly productive water column, the Ross Sea is important both regionally and globally. Being the site of High Salinity Shelf Water (HSSW) production, generated by the winter formation of sea ice and simultaneous brine rejection, it is a physically critical region as HSSW production drives deep vertical mixing, after which HSSW is then advected off the shelf to form Antarctic Bottom Water (AABW), a major component of the global thermohaline circulation (Orsi and Wiederwohl, 2009). Substantial deposits of biogenic silica occur in the Ross Sea, which are major components of the biogeochemical cycle of silica for the entire ocean (Mincks et al., 2005). It is highly productive, supporting large concentrations of phytoplankton biomass as well as some of the largest standing stocks of higher trophic levels in the ocean (Smith et al., 2014c). It has been estimated that the Ross Sea is responsible for 28% of the annual carbon fixation in the entire Southern Ocean (Arrigo et al., 1998b), and its biomass and annual productivity are greater than observed elsewhere in Antarctica (Arrigo et al., 2008b; Smith and Comiso, 2008). It supports the largest standing stocks of penguins, seals, and killer whales in the Southern Ocean, as well as

high densities (albeit poorly quantified) of Antarctic toothfish and baleen whales (Ballard et al., 2012). Due to its relative inaccessibility, it has been called the least anthropogenically modified continental shelf system in the world (Halpern et al., 2008). The Ross Sea is, however, being impacted by atmospheric input of CO_2 (Orr et al., 2005), and its salinity is decreasing at a substantial rate (Jacobs and Giulivi, 2010), likely due to advection of low salinity water from the Amundsen-Bellingshausen sector.

The Ross Sea continental shelf, which is 986,000 km^2 in area (average depth of ~530 m with the shelf break at ~700 m; Smith et al., 2012b), is bounded by the Transantarctic Mountains and Victoria Land to the west, the Antarctic continent to the south, Cape Colbeck to the east, and by the shelf break to the north (Figure 2). The Ross Ice Shelf, which covers the southern extent of the Ross Sea, is the largest in the world (530,000 km^2), with a mean thickness of ~370 m (Smith et al., 2012b). It covers a significant portion of the entire continental shelf, and is a site of active seawater exchanges with the rest of the shelf region.

Circulation of the Ross Sea

Water masses over the Ross Sea continental shelf play a critical role in determining conditions that influence the seasonal phytoplankton bloom (Smith et al., 2007). The overall circulation pattern on the Ross Sea continental shelf is complex (Figure 3), with the trough and bank bathymetry, the westward Antarctic Slope Current, the action of atmospheric forcing, and the dynamics of sea ice formation influencing circulation patterns (Dinniman et al., 2003, 2007). AASW, which is relatively less saline and cold, flows onto the continental shelf near Cape Colbeck and dominates the surface

flows of the southern Ross Sea (Whitworth et al., 1998). Sea ice dynamics and summer

solar heat inputs create substantial short- and long-term spatial and temporal variability in

the properties of AASW (Whitworth et al., 1998; Orsi and Wiederwohl, 2009; Smith et

al., 2011a). Cooling of AASW or shoaled MCDW by katabatic winds, sea ice formation,

and brine rejection drives the formation of salty and dense Shelf Water, which mixes

completely to depth and fills the troughs. An east-west salinity gradient results from

differences in winter sea ice production rates and further categorizes Shelf Water as

either Low Salinity Shelf Water (<34.62, LSSW) produced in the eastern Ross Sea, or

HSSW (>34.62) produced in the west (Jacobs and Giulivi, 1998; Orsi and Wiederwohl,

2009; Smith et al., 2012a). Shelf waters mix further with MCDW to form AABW, which

is supplied to the global deep ocean, making the Ross Sea an important source of deep

AABW to the world's oceans (Jacobs et al., 1985; Whitworth et al., 1998; Gordon et al.,

2009; Muench et al., 2009). Warm (albeit modified from its source off the continental

shelf) MCDW flows at mid-depths (~300 m) under the Ross Ice Shelf in a few locations,

where it melts the base of the ice shelf to form cold (−2.0°C at depth), relatively fresh

melt-water (Ice Shelf Water or ICW; Smith et al., 2012a).

Sea Ice

The presence of ice plays a large role in the regulation of productivity and is

temporally variable across the region. Sea ice covers the majority (~98%) of the Ross Sea

during austral winter, with katabatic winds driving the formation of a small polynya (an

area of reduced ice cover surrounded by dense concentrations of ice) near the Ross Ice

Shelf and in other coastal locations (Bromwich et al., 1998). By late spring, increasing

8

solar radiation adds heat to surface waters, which accelerates ice melt and polynya

expansion (Arrigo et al., 2000), and also enhances biological processes (Arrigo and

McClain, 1994). The onset of austral spring (late October) leads to phytoplankton blooms

in the open water regions of the expanding polynya (Smith and Comiso, 2008). During

austral summer (January-February), sea ice coverage is reduced and thus plays a lesser

role in determining phytoplankton bloom dynamics; however, ice melt-induced

stratification can persist throughout summer, thereby influencing productivity (Figure 4).

Ice concentrations typically increase rapidly during March and rapidly cover the entire

continental shelf.

Ross Sea Phytoplankton

The Ross Sea continental shelf is a comparatively small area (4-5% of the surface

area of the Southern Ocean), but accounts for 28% of the annual production of carbon

(Arrigo et al., 1998a; Smith and Comiso, 2008). In turn, this substantial phytoplankton

stock supports a vibrant food web, and thus plays a pivotal role in driving the biological

dynamics of the ecosystem (Smith et al., 2007, 2012b, 2014a). Ross Sea phytoplankton

are typically dominated by two groups, haptophytes and diatoms. *In situ* distributions and

climatologies (Smith et al., 2000, 2010, 2011a, 2013) suggest a typical seasonal bloom

progression in which haptophytes bloom in spring and are followed by diatoms. In winter

and early spring nutrients are elevated (nitrate is ca. 30 μM and iron is ca. 1.0 nM; Smith

et al., 2003b; Sedwick et al., 2011). Phytoplankton growth begins in late October or early

November, upon reduction in sea ice, shoaling of mixed layer depths, increased

irradiance in surface waters, and lengthening photoperiod (24-h photoperiod by late

October). Maximal growth rates and relatively low grazing and sinking losses typically

lead to a biomass maximum in mid- to late December, followed by reduced levels in

January, which normally persist until sea ice covers the region in February-March (Smith

et al., 2014a). Growth during this final period is generally low and considered to be

limited by iron bioavailability (Smith et al., 2012b).

The haptophyte *Phaeocystis antarctica* tends to dominate the initial accumulation

of biomass due to its ability to photosynthesize at low irradiances characteristic of early

spring (Moisan and Mitchell, 1999; Kropuenske et al., 2009). Following a biomass

maximum in December, its growth may be limited by micronutrient (iron) availability

(Sedwick et al., 2000), and biomass rapidly disappears from the euphotic zone by

processes of aggregation, horizontal or vertical transport, and/or grazing (Smith et al.,

2000, 2011b). Diatoms tend to form blooms after the seasonal decline of *P. antarctica*

when summer mixed layer depths are shallower and irradiance in surface waters greater

(Leventer and Dunbar, 1996; Kropuenske et al., 2009), although the magnitude of

summer diatom blooms is extremely variable (Peloquin and Smith, 2007). Diatom

blooms are ubiquitous over the continental shelf, with higher abundances associated with

the marginal ice zones and the western ice edge of the Ross Sea polynya (Arrigo et al.,

1999). There the *in situ* ice melt results in highly stratified water columns, shallow mixed

layers (approx. 20 m or less), and high irradiance conditions (Arrigo et al., 1999, 2000;

Smith et al., 2012b). The two groups have markedly different elemental ratios

(haptophytes, specifically *P. antarctica*: 139C:19N:1P; diatoms: 76C:12N:1P), and

distinct particulate organic carbon (POC) to chlorophyll *a* (Chl) ratios (low POC:Chl

ratios for haptophytes and high POC:Chl ratios for diatoms; DiTullio and Smith, 1996;

Arrigo et al., 2000; Kaufman et al., 2014), which in turn may affect biogeochemical cycling through production and export processes.

Biogeochemical cycling

Given the productivity of surface waters, the subsequent biomass accumulation, and the high export efficiencies of detritus and aggregates to the benthos (Smith et al., 2011b), there is potential for export to the deep ocean if benthic organic matter is resuspended during winter deep-water formation and transported off the shelf. However, these processes are temporally offset and complex, and export is typically spatially removed from deep water formation sites (Peloquin and Smith, 2007; Arrigo et al., 2008b). Export efficiencies are highly dependent upon the phytoplankton composition, sinking rates of particles, mesozooplankton abundance and activity, fecal pellet/aggregation production, and disaggregation processes (Asper and Smith, 1999, 2003).

Despite the high levels of productivity, macronutrients (e.g., nitrate, phosphate, and silicate) are rarely depleted, likely due to lowered growth rates over a short and cold growing season and a limiting supply of the micronutrient iron (Sedwick et al., 2000, 2011; Smith et al., 2014a). Sources of iron in the Ross Sea include seafloor sediments, sea and glacial ice, intrusions onto the shelf of MCDW, and mineral aerosols (Sedwick and DiTullio, 1997; Winton et al., 2014; McGillicuddy et al., 2015). The availability of iron in high nutrient, low chlorophyll (HNLC) waters limits phytoplankton accumulation and resultant export to depth (Martin et al., 1990; Boyd, 2002).

Large-scale climactic variability may also lead to changes in the productivity of phytoplankton and result in shifts in the biogeochemical cycling of nutrients. One measure of this variability, the Southern Annular Mode or SAM, measures the north-south pressure differential across the region, and drives the westerly winds inducing the flow of the ACC (Lovenduski and Gruber, 2005; Böning et al., 2008). A positive SAM index leads to increased winds, strengthening the Antarctic Divergence, an Ekman-induced upwelling that parallels the Ross Sea continental shelf break, and is associated with increased phytoplankton biomass (Arrigo et al., 2008a). Greater than 64% of the interannual variance in chlorophyll *a* concentrations on the Ross Sea continental shelf can be attributed to SAM, thus underscoring the importance of these large-scale atmospheric-ocean interconnections to shifts or changes in biogeochemical cycling under future climate scenarios (Arrigo et al., 2008b; Smith et al., 2014a).

Ross Sea Higher Trophic Levels

The food web of the Ross Sea is generally well characterized (Pinkerton and Bradford-Grieve, 2010, 2014), although some components are far more quantified than others. Surprisingly little is known about the abundance and activity of the middle trophic levels, specifically copepods, krill, pteropods, and silverfish. Krill, often thought to be the most important grazer of phytoplankton in coastal Antarctic waters, is comprised primarily of crystal krill (*Euphausia crystallorophius*) in the Ross Sea (Azzali et al., 2006), as Antarctic krill (*E. superba*) are found only near the shelf-break and in the deeper waters of the northern Ross Sea continental shelf (Ainley and Jacobs, 1981). Crystal krill are omnivorous and opportunistic in their diet (Deibel and Daly, 2007), and

their distribution, abundance, and variability in the Ross Sea is largely unknown.
Copepods are poorly studied in the Ross Sea, and in general their abundance is thought to
be low. Indeed, Deibel and Daly (2007) suggested that copepod biomass was only 15% of
that in the Antarctic Peninsula region. Pteropods also occur, but exhibit extreme
variability in their biomass (Hunt et al., 2008). Antarctic silverfish (*Pleuragramma
antarcticum*) feed on copepods and larval krill, and have a spatially variable distribution
in the region (La Mesa et al., 2010; O'Driscoll et al., 2011; La Mesa and Eastman, 2012).
The trophic relationships amongst these groups is also poorly known, and their impact on
phytoplankton is generally thought to be small (Tagliabue and Arrigo, 2003).

Higher trophic levels are much better known from long-term studies of behavior,
reproduction, and activity. Adélie penguins (*Pygoscelis adeliae*) have large rookeries in
various locations along the Ross Sea coast (Smith et al., 2014a), and the colony at Cape
Crozier (Ross Island) has 120,000 breeding pairs – the largest colony known in the
Antarctic. Similarly, Emperor penguins (*Aptenodytes forsteri*) have numerous colonies,
and represent 25% of the total numbers of this species for the entire continent. Crabeater
seals (*Lobodon carcinophagus*) are also very abundant (Burns et al., 2004), as are leopard
seals (*Hydrurga leptonyx*), predators of penguins and crabeater seals. Baleen whales are
also common in the Ross Sea, although the numbers and activities are poorly constrained.
Finally, killer whales (*Orca orcinus*) are conspicuous upper trophic predators. Three
ecotypes occur – one which feeds mainly upon Antarctic minke whales (*Balaenoptera
bonaerensis*), another that feeds primarily on seals, and another that has only been
observed to feed upon Antarctic toothfish (*Dissostichus mawsoni*; Pitman and Ensor,
2003). Of the large fish species present in the Ross Sea, one of the most important is the

Antarctic toothfish (*Dissostichus mawsoni*). Toothfish are now being commercially harvested, but their role in the food web cannot be assessed, as data for much of its life history, its abundance and distribution, and even its feeding behavior are conspicuously absent. Thus, concerns about the harvest of such large fish have been voiced (Abrams, 2014; Hanchet et al., 2015).

Potential Future Changes in the Ross Sea

The Ross Sea continental shelf is presently experiencing increasing ice concentrations, decreased open ice duration, and decreased salinities (Stammerjohn et al., 2008, 2012; Jacobs and Giulivi, 2010), but projections indicate that the region will likely experience atmospheric warming over 2°C in the next 50 years (Bracegirdle and Kolstad, 2010). Along with altered winds and transfer of atmospheric heat into the ocean, these future atmospheric changes will drive a reduction in ice concentrations in summer (56% reduction in 50 years, 78% in 100 years from present) and an increase in the ice-free duration (5 and 28 days longer in 50 and 100 years, respectively; Smith et al., 2014b). These changes in oceanographic properties (Table 1) may in turn cause changes in the timing, productivity, intensity, and composition of phytoplankton blooms, and will likely lead to marked changes to the food web. Specifically, these changes will likely induce marked modifications in the food web through reductions in the growth and biomass of crystal krill and silverfish; these reductions will likely in turn impact the growth, survival and reproduction of higher trophic levels dependent on them (e.g., Emperor penguins, Adélie penguins, crabeater seals, baleen whales). Therefore, a major re-organization of

the Ross Sea food web is to be expected in the coming decades (Pinkerton and Bradford-Grieve, 2010; Constable et al., 2014).

REFERENCES

Abrams, P.A., 2014. How precautionary is the policy governing the Ross Sea Antarctic toothfish (*Dissostichus mawsoni*) fishery? Antarctic Science 26, 3–14.

Ainley, D.G., Jacobs, S.S., 1981. Sea-bird affinities for ocean and ice boundaries in the Antarctic. Deep Sea Research Part A 28, 1173–1185. doi:10.1016/0198-0149(81)90054-6

Amante, C., Eakins, B.W., 2009. ETOPO1 1 arc-minute global relief model: procedures, data sources and analysis. US Department of Commerce, National Oceanic and Atmospheric Administration, National Environmental Satellite, Data, and Information Service, National Geophysical Data Center, Marine Geology and Geophysics Division.

Arrigo, K.R., DiTullio, G.R., Dunbar, R.B., Robinson, D.H., Van Woert, M.L., Worthen, D.L., Lizotte, M.P., 2000. Phytoplankton taxonomic variability in nutrient utilization and primary production in the Ross Sea. Journal of Geophysical Research 105, 8827–8846.

Arrigo, K.R., McClain, C.R., 1994. Spring Phytoplankton Production in the Western Ross Sea. Science 266, 261–263. doi:10.1126/science.266.5183.261

Arrigo, K.R., Mills, M.M., Kropuenske, L.R., Van Dijken, G.L., Alderkamp, A.C., Robinson, D.H., 2010. Photophysiology in two major southern ocean phytoplankton taxa: Photosynthesis and growth of *Phaeocystis antarctica* and *Fragilariopsis cylindrus* under different irradiance levels. Integrative and Comparative Biology 50, 950–966. doi:10.1093/icb/icq021

Arrigo, K.R., Robinson, D.H., Worthen, D.L., Dunbar, R.B., DiTullio, G.R., Van Woert, M.L., Lizotte, M.P., 1999. Phytoplankton Community Structure and the Drawdown of Nutrients and CO_2 in the Southern Ocean. Science 283, 365–367. doi:10.1126/science.283.5400.365

Arrigo, K.R., Robinson, D.H., Worthen, D.L., Schieber, B., Lizotte, M.P., 1998a. Bio-optical properties of the southwestern Ross Sea. Journal of Geophysical Research 103, 21683–21695.

Arrigo, K.R., van Dijken, G.L., Bushinsky, S., 2008a. Primary production in the Southern Ocean, 1997–2006. Journal of Geophysical Research 113, 1–27. doi:10.1029/2007JC004551

Arrigo, K.R., van Dijken, G.L., Long, M.C., 2008b. Coastal Southern Ocean: A strong anthropogenic CO_2 sink. Geophysical Research Letters 35, 1–6.

16

doi:10.1029/2008GL035624

Arrigo, K.R., Worthen, D.L., Schnell, A., Lizotte, M.P., 1998b. Primary production in Southern Ocean waters. Journal of Geophysical Research 103, 15587–15600.

Asper, V.L., Smith, W.O., 1999. Particle fluxes during austral spring and summer in the southern Ross Sea, Antarctica. Journal of Geophysical Research 104, 5345–5359.

Asper, V.L., Smith, W.O., 2003. Abundance, distribution and sinking rates of aggregates in the Ross Sea, Antarctica. Deep Sea Research Part I 50, 131–150. doi:10.1016/S0967-0637(02)00146-2

Azzali, M., Leonori, I., De Felice, A., Russo, A., 2006. Spatial–temporal relationships between two euphausiid species in the Ross Sea. Chemistry and Ecology 22, S219–S233. doi:10.1080/02757540600670836

Ballard, G., Jongsomjit, D., Veloz, S.D., Ainley, D.G., 2012. Coexistence of mesopredators in an intact polar ocean ecosystem: The basis for defining a Ross Sea marine protected area. Biological Conservation 156, 72–82. doi:10.1016/j.biocon.2011.11.017

Böning, C.W., Dispert, A., Visbeck, M., Rintoul, S.R., Schwarzkopf, F.U., 2008. The response of the Antarctic Circumpolar Current to recent climate change. Nature Geoscience 1, 864–869. doi:10.1038/ngeo362

Boyd, P.W., 2002. Environmental Factors Controlling Phytoplankton Processes in the Southern Ocean. Journal of Phycology 38, 844–861.

Bracegirdle, T.J., Kolstad, E.W., 2010. Climatology and variability of Southern Hemisphere marine cold-air outbreaks. Tellus A 62, 202–208. doi:10.1111/j.1600-0870.2009.00431.x

Bromwich, D.H., Liu, Z., Rodgers, A.N., Van Woert, M.L., 1998. Winter atmospheric forcing of the Ross Sea polynya. Ocean, Ice, and Atmosphere: Interactions at the Antarctic Continental Margin 75, 101–133.

Burns, J.M., Costa, D.P., Fedak, M.A., Hindell, M.A., Bradshaw, C.J.A., Gales, N.J., McDonald, B., Trumble, S.J., Crocker, D.E., 2004. Winter habitat use and foraging behavior of crabeater seals along the Western Antarctic Peninsula. Deep Sea Research Part II 51, 2279–2303. doi:10.1016/j.dsr2.2004.07.021

Constable, A.J., Melbourne-Thomas, J., Corney, S.P., Arrigo, K.R., Barbraud, C., Barnes, D.K.A., Bindoff, N.L., Boyd, P.W., Brandt, A., Costa, D.P., Davidson, A.T., Ducklow, H.W., Emmerson, L., Fukuchi, M., Gutt, J., Hindell, M.A., Hofmann, E.E., Hosie, G.W., Iida, T., Jacob, S., Johnston, N.M., Kawaguchi, S., Kokubun, N., Koubbi, P., Lea, M.A., Makhado, A., Massom, R.A., Meiners, K., Meredith, M.P., Murphy, E.J., Nicol, S., Reid, K., Richerson, K., Riddle, M.J., Rintoul, S.R., Smith, W.O., Southwell, C., Stark, J.S., Sumner, M., Swadling, K.M., Takahashi, K.T.,

Trathan, P.N., Welsford, D.C., Weimerskirch, H., Westwood, K.J., Wienecke, B.C., Wolf-Gladrow, D.A., Wright, S.W., Xavier, J.C., Ziegler, P., 2014. Climate change and Southern Ocean ecosystems I: How changes in physical habitats directly affect marine biota. Global Change Biology 20, 3004–3025. doi:10.1111/gcb.12623

Deibel, D., Daly, K.L., 2007. Zooplankton Processes in Arctic and Antarctic Polynyas, in: Elsevier Oceanography Series. Elsevier, pp. 271–322. doi:10.1016/S0422-9894(06)74009-0

Dinniman, M.S., Klinck, J.M., Smith, W.O., 2003. Cross-shelf exchange in a model of the Ross Sea circulation and biogeochemistry. Deep Sea Research Part II 50, 3103–3120. doi:10.1016/j.dsr2.2003.07.011

Dinniman, M.S., Klinck, J.M., Smith, W.O., 2007. Influence of sea ice cover and icebergs on circulation and water mass formation in a numerical circulation model of the Ross Sea, Antarctica. Journal of Geophysical Research 112, 1–13. doi:10.1029/2006JC004036

DiTullio, G.R., Smith, W.O., 1996. Spatial patterns in phytoplankton biomass and pigment distributions in the Ross Sea. Journal of Geophysical Research 101, 18467–18477. doi:10.1029/96JC00034

El-Sayed, S.Z., Biggs, D.C., Holm-Hansen, O., 1983. Phytoplankton standing crop, primary productivity, and near-surface nitrogenous nutrient fields in the Ross Sea, Antarctica. Deep Sea Research Part A 30, 871–886.

Eriksen, C.C., Osse, T.J., Light, R.D., Wen, T., Lehman, T.W., Sabin, P.L., Ballard, J.W., Chiodi, A.M., 2001. Seaglider: a long-range autonomous underwater vehicle for oceanographic research. IEEE Journal of Oceanic Engineering 26, 424–436. doi:10.1109/48.972073

Gille, S.T., 2002. Warming of the Southern Ocean since the 1950s. Science 295, 1275–1277. doi:10.1126/science.1065863

Gordon, A.L., Orsi, A.H., Muench, R., Huber, B.A., Zambianchi, E., Visbeck, M., 2009. Western Ross Sea continental slope gravity currents. Deep Sea Research Part II 56, 796–817. doi:10.1016/j.dsr2.2008.10.037

Halpern, B.S., Walbridge, S., Selkoe, K.A., Kappel, C. V., Micheli, F., D'Agrosa, C., Bruno, J.F., Casey, K.S., Ebert, C., Fox, H.E., Fujita, R., Heinemann, D., Lenihan, H.S., Madin, E.M.P., Perry, M.T., Selig, E.R., Spalding, M., Steneck, R.S., Watson, R., 2008. A global map of human impact on marine ecosystems. Science 319, 948–952. doi:10.1126/science.1149345

Hanchet, S.M., Dunn, A., Parker, S., Horn, P., Stevens, D., Mormede, S., 2015. The Antarctic toothfish (*Dissostichus mawsoni*): biology, ecology, and life history in the Ross Sea region. Hydrobiologia 761, 397–414. doi:10.1007/s10750-015-2435-6

18

Hunt, B.P.V., Pakhomov, E.A., Hosie, G.W., Siegel, V., Ward, P., Bernard, K.S., 2008. Pteropods in Southern Ocean ecosystems. Progress in Oceanography 78, 193–221. doi:10.1016/j.poecan.2008.06.001

Jacobs, S.S., Fairbanks, R.G., Horibe, Y., 1985. Origin and evolution of water masses near the Antarctic continental margin: evidence from $H_2{}^{18}O/H_2{}^{16}O$ ratios in seawater. Oceanography of the Antarctic Continental Shelf 43, 59–85.

Jacobs, S.S., Giulivi, C.F., 1998. Interannual ocean and sea ice variability in the Ross Sea. Ocean, Ice, and Atmosphere: Interactions at the Antarctic Continental Margin 75, 135–150.

Jacobs, S.S., Giulivi, C.F., 2010. Large Multidecadal Salinity Trends near the Pacific–Antarctic Continental Margin. Journal of Climate 23, 4508–4524. doi:10.1175/2010JCLI3284.1

Kaufman, D.E., Friedrichs, M.A.M., Smith, W.O., Queste, B.Y., Heywood, K.J., 2014. Biogeochemical Variability in the Southern Ross Sea as Observed by a Glider Deployment. Deep Sea Research Part I 92, 93–106.

Klinck, J.M., Dinniman, M.S., 2010. Exchange across the shelf break at high southern latitudes. Ocean Science 6, 513–524. doi:10.5194/os-6-513-2010

Kropuenske, L.R., Mills, M.M., van Dijken, G.L., Bailey, S., Robinson, D.H., Welschmeyer, N.A., Arrigo, K.R., 2009. Photophysiology in two major Southern Ocean phytoplankton taxa: Photoprotection in *Phaeocystis antarctica* and *Fragilariopsis cylindrus*. Limnology and Oceanography 54, 1176–1196. doi:10.4319/lo.2009.54.4.1176

La Mesa, M., Catalano, B., Russo, A., Greco, S., Vacchi, M., Azzali, M., 2010. Influence of environmental conditions on spatial distribution and abundance of early life stages of Antarctic silverfish, *Pleuragramma antarcticum* (Nototheniidae), in the Ross Sea. Antarctic Science 22, 243–254. doi:10.1017/S0954102009990721

La Mesa, M., Eastman, J.T., 2012. Antarctic silverfish: Life strategies of a key species in the high-Antarctic ecosystem. Fish and Fisheries 13, 241–266. doi:10.1111/j.1467-2979.2011.00427.x

Le Quéré, C., Rödenbeck, C., Buitenhuis, E.T., Conway, T.J., Langenfelds, R., Gomez, A., Labuschagne, C., Ramonet, M., Nakazawa, T., Metzl, N., Gillett, N., Heimann, M., 2007. Saturation of the southern ocean CO_2 sink due to recent climate change. Science 316, 1735–1738. doi:10.1126/science.1136188

Leventer, A.R., Dunbar, R.B., 1996. Factors influencing the distribution of diatoms and other algae in the Ross Sea. Journal of Geophysical Research 101, 489–500.

Lovenduski, N.S., Gruber, N., 2005. Impact of the Southern Annular Mode on Southern Ocean circulation and biology. Geophysical Research Letters 32, 1–4.

doi:10.1029/2005GL022727

Martin, J.H., Fitzwater, S.E., Gordon, R.M., 1990. Iron deficiency limits phytoplankton growth in Antarctic waters. Global Biogeochemical Cycles 4, 5–12.

McGillicuddy, D.J., Anderson, L.A., Bates, N.R., Bibby, T.S., Buesseler, K.O., Carlson, C.A., Davis, C.S., Ewart, C., Falkowski, P.G., Goldthwait, S.A., Hansell, D.A., Jenkins, W.J., Johnson, R., Kosnyrev, V.K., Ledwell, J.R., Li, Q.P., Siegel, D.A., Steinberg, D.K., 2007. Eddy/Wind Interactions Stimulate Extraordinary Mid-Ocean Plankton Blooms. Science 316, 1021–1026. doi:10.1126/science.1136256

McGillicuddy, D.J., Sedwick, P.N., Dinniman, M.S., Arrigo, K.R., Bibby, T.S., Greenan, B.J.W., Hofmann, E.E., Klinck, J.M., Smith, W.O., Mack, S.L., Marsay, C.M., Sohst, B.M., van Dijken, G.L., 2015. Iron supply and demand in an Antarctic shelf ecosystem. Geophysical Research Letters 42, 8088–8097. doi:10.1002/2015GL065727

Mincks, S.L., Smith, C.R., DeMaster, D.J., 2005. Persistence of labile organic matter and microbial biomass in Antarctic shelf sediments: evidence of a sediment "food bank." Marine Ecology Progress Series 300, 3–19. doi:10.3354/meps300003

Moisan, T., Mitchell, B.G., 1999. Photophysiological acclimation of *Phaeocystis antarctica* Karsten under light limitation. Limnology and Oceanography 44, 247–258.

Muench, R., Padman, L., Gordon, A.L., Orsi, A.H., 2009. A dense water outflow from the Ross Sea, Antarctica: Mixing and the contribution of tides. Journal of Marine Systems 77, 369–387. doi:10.1016/j.jmarsys.2008.11.003

O'Driscoll, R.L., Macaulay, G.J., Gauthier, S., Pinkerton, M.H., Hanchet, S.M., 2011. Distribution, abundance and acoustic properties of Antarctic silverfish (*Pleuragramma antarcticum*) in the Ross Sea. Deep Sea Research Part II 58, 181–195. doi:10.1016/j.dsr2.2010.05.018

Orr, J.C., Fabry, V.J., Aumont, O., Bopp, L., Doney, S.C., Feely, R.A., Gnanadesikan, A., Gruber, N., Ishida, A., Joos, F., Key, R.M., Lindsay, K., Maier-Reimer, E., Matear, R., Monfray, P., Mouchet, A., Najjar, R.G., Plattner, G.-K., Rodgers, K.B., Sabine, C.L., Sarmiento, J.L., Schlitzer, R., Slater, R.D., Totterdell, I.J., Weirig, M.-F., Yamanaka, Y., Yool, A., 2005. Anthropogenic ocean acidification over the twenty-first century and its impact on calcifying organisms. Nature 437, 681–686. doi:10.1038/nature04095

Orsi, A.H., Whitworth, T., Nowlin, W.D., 1995a. On the meridional extent and fronts of the Antarctic Circumpolar Current. Deep Sea Research Part I 42, 641–673. doi:10.1016/0967-0637(95)00021-W

Orsi, A.H., Whitworth, T., Nowlin, W.D., 1995b. On the meridional extent and fronts of the Antarctic Circumpolar Current. Deep Sea Research Part I 42, 641–673.

Orsi, A.H., Wiederwohl, C.L., 2009. A recount of Ross Sea waters. Deep Sea Research Part II 56, 778–795. doi:10.1016/j.dsr2.2008.10.033

Peloquin, J.A., Smith, W.O., 2007. Phytoplankton blooms in the Ross Sea, Antarctica: Interannual variability in magnitude, temporal patterns, and composition. Journal of Geophysical Research 112, 1–12. doi:10.1029/2006JC003816

Pinkerton, M.H., Bradford-Grieve, J.M., 2010. A balanced model of the food web of the Ross Sea, Antarctica. CCAMLR Science 17, 1–31.

Pinkerton, M.H., Bradford-Grieve, J.M., 2014. Characterizing foodweb structure to identify potential ecosystem effects of fishing in the Ross Sea, Antarctica. ICES Journal of Marine Science 71, 1542–1553.

Pitman, R.L., Ensor, P., 2003. Three forms of killer whales (*Orcinus orca*) in Antarctic waters. Journal of Cetacean Research and Management 5, 131–139.

Rudnick, D.L., Cole, S.T., 2011. On sampling the ocean using underwater gliders. Journal of Geophysical Research 116, 1–12. doi:10.1029/2010JC006849

Sedwick, P.N., DiTullio, G.R., 1997. Regulation of algal blooms in Antarctic shelf waters by the release of iron from melting sea ice. Geophysical Research Letters 24, 2515–2518.

Sedwick, P.N., DiTullio, G.R., Mackey, D.J., 2000. Iron and manganese in the Ross Sea, Antarctica: Seasonal iron limitation in Antarctic shelf waters. Journal of Geophysical Research 105, 11321–11336. doi:10.1029/2000JC000256

Sedwick, P.N., Marsay, C.M., Sohst, B.M., Aguilar-Islas, A.M., Lohan, M.C., Long, M.C., Arrigo, K.R., Dunbar, R.B., Saito, M.A., Smith, W.O., DiTullio, G.R., 2011. Early season depletion of dissolved iron in the Ross Sea polynya: Implications for iron dynamics on the Antarctic continental shelf. Journal of Geophysical Research 116, 1–19. doi:10.1029/2010JC006553

Smetacek, V., Nicol, S., 2005. Polar ocean ecosystems in a changing world. Nature 437, 362–368. doi:10.1038/nature04161

Smith, W.O., Ainley, D.G., Arrigo, K.R., Dinniman, M.S., 2014a. The Oceanography and Ecology of the Ross Sea. Annual Review of Marine Science 6, 469–487. doi:10.1146/annurev-marine-010213-135114

Smith, W.O., Ainley, D.G., Cattaneo-Vietti, R., 2007. Trophic interactions within the Ross Sea continental shelf ecosystem. Philosophical Transactions of the Royal Society Series B 362, 95–111. doi:10.1098/rstb.2006.1956

Smith, W.O., Ainley, D.G., Cattaneo-Vietti, R., Hofmann, E.E., 2012a. The Ross Sea continental shelf: regional biogeochemical cycles, trophic interactions, and potential future changes, in: Rodgers, A., Johnston, N., Murphy, E., Clarke, A. (Eds.),

Antarctic Ecosystems: An Extreme Environment in a Changing World. Blackwell Publishing Ltd., pp. 213–242.

Smith, W.O., Asper, V.L., Tozzi, S., Liu, X., Stammerjohn, S.E., 2011a. Surface layer variability in the Ross Sea, Antarctica as assessed by in situ fluorescence measurements. Progress in Oceanography 88, 28–45. doi:10.1016/j.pocean.2010.08.002

Smith, W.O., Comiso, J.C., 2008. Influence of sea ice on primary production in the Southern Ocean: A satellite perspective. Journal of Geophysical Research 113, 1–19. doi:10.1029/2007JC004251

Smith, W.O., Dinniman, M.S., Hofmann, E.E., Klinck, J.M., 2014b. The effects of changing winds and temperatures on the oceanography of the Ross Sea in the 21st century. Geophysical Research Letters 41, 1624–1631.

Smith, W.O., Dinniman, M.S., Klinck, J.M., Hofmann, E.E., 2003. Biogeochemical climatologies in the Ross Sea, Antarctica: Seasonal patterns of nutrients and biomass. Deep Sea Research Part II 50, 3083–3101. doi:10.1016/j.dsr2.2003.07.010

Smith, W.O., Dinniman, M.S., Tozzi, S., DiTullio, G.R., Mangoni, O., Modigh, M., Saggiomo, V., 2010. Phytoplankton photosynthetic pigments in the Ross Sea: Patterns and relationships among functional groups. Journal of Marine Systems 82, 177–185. doi:10.1016/j.jmarsys.2010.04.014

Smith, W.O., Goetz, K.T., Kaufman, D.E., Queste, B.Y., Asper, V.L., Costa, D.P., Dinniman, M.S., Friedrichs, M.A.M., Hofmann, E.E., Heywood, K.J., Klinck, J.M., Kohut, J.T., Lee, C.M., 2014c. Multiplatform, Multidisciplinary Investigations of the Impacts of Modified Circumpolar Deep Water in the Ross Sea, Antarctica. Oceanography 27, 180–185.

Smith, W.O., Marra, J., Hiscock, M.R., Barber, R.T., 2000. The seasonal cycle of phytoplankton biomass and primary productivity in the Ross Sea, Antarctica. Deep Sea Research Part II 47, 3119–3140.

Smith, W.O., Nelson, D.M., 1985. Phytoplankton Bloom Produced by a Receding Ice Edge in the Ross Sea: Spatial Coherence with the Density Field. Science 227, 163–166.

Smith, W.O., Sedwick, P.N., Arrigo, K.R., Ainley, D.G., Orsi, A.H., 2012b. The Ross Sea in a Sea of Change. Oceanography 25, 90–103.

Smith, W.O., Shields, A.R., Dreyer, J.C., Peloquin, J.A., Asper, V.L., 2011b. Interannual variability in vertical export in the Ross Sea: Magnitude, composition, and environmental correlates. Deep Sea Research Part I 58, 147–159. doi:10.1016/j.dsr.2010.11.007

Smith, W.O., Tozzi, S., Long, M.C., Sedwick, P.N., Peloquin, J.A., Dunbar, R.B.,

Hutchins, D.A., Kolber, Z., DiTullio, G.R., 2013. Spatial and temporal variations in variable fluoresence in the Ross Sea (Antarctica): Oceanographic correlates and bloom dynamics. Deep Sea Research Part I 79, 141–155. doi:10.1016/j.dsr.2013.05.002

Spreen, G., Kaleschke, L., Heygster, G., 2008. Sea ice remote sensing using AMSR-E 89-GHz channels. Journal of Geophysical Research: Oceans 113, 1–14. doi:10.1029/2005JC003384

Stammerjohn, S.E., Martinson, D.G., Smith, R.C., Yuan, X., Rind, D., 2008. Trends in Antarctic annual sea ice retreat and advance and their relation to El Niño–Southern Oscillation and Southern Annular Mode variability. Journal of Geophysical Research 113, 1–20. doi:10.1029/2007JC004269

Stammerjohn, S.E., Massom, R.A., Rind, D., Martinson, D.G., 2012. Regions of rapid sea ice change: An inter-hemispheric seasonal comparison. Geophysical Research Letters 39, 1–8. doi:10.1029/2012GL050874

Tagliabue, A., Arrigo, K.R., 2003. Anomalously low zooplankton abundance in the Ross Sea: An alternative explanation. Limnology and Oceanography 48, 686–699. doi:10.4319/lo.2003.48.2.0686

Talley, L.D., Pickard, G.L., Emery, W.J., Swift, J.H., 2011. Descriptive Physical Oceanography: An Introduction, 6th ed. ed. Academic Press.

Wang, Z., Meredith, M.P., 2008. Density-driven Southern Hemisphere subpolar gyres in coupled climate models. Geophysical Research Letters 35. doi:10.1029/2008GL034344

Whitworth, T., Orsi, A.H., Kim, S.-J., Nowlin, W.D., Locarnini, R.A., 1998. Water masses and mixing near the Antarctic Slope Front. Ocean, Ice, and Atmosphere: Interactions at the Antarctic Continental Margin 75, 1–27. doi:10.1029/AR075p0001

Winton, V.H.L., Dunbar, G.B., Bertler, N.A.N., Millet, M.-A., Delmonte, B., Atkins, C.B., Chewings, J.M., Andersson, P., 2014. The contribution of aeolian sand and dust to iron fertilization of phytoplankton blooms in southwestern Ross Sea, Antarctica. Global Biogeochemical Cycles 28, 423–436. doi:10.1002/2013GB004574

Table 1: A summary of potential responses of biota to changes in environmental variables in the Ross Sea. PAR = photosynthetically active radiation, UV = ultraviolet radiation, T = temperature, Z_{mix} = depth of mixed layer. Acidification (OA) includes altered carbonate chemistry and decreased pH. Sea ice includes consideration of thickness, concentration, and extent without differentiating the factor/s causing change in each group of organisms. The symbols used in the table denote a positive (+) or negative (−) direct effect of an increase in the variable on particular taxa. '?' indicates where there is likely to be a response but the direction is uncertain (i.e., the result may be variable in space, time or for specific taxa or the evidence is equivocal). Modified from Constable et al. (2014).

Taxon	PAR	UV	T	OA	Z_{mix}	Sea Ice
Diatoms	+ (< 3°C) − (> 3°C)	−	+	+	+	−
Flagellates, haptophytes	−	−	−	+	+	+
Microzooplankton			+	?	−	−
Bacteria & viruses		−	+		−	−
Zooplankton			+			
Salps			+			−
Antarctic krill		−		−		−
Crystal krill		−		−		+
Nototheniid fish			−			
Myctophid fish			+			
Crabeater/Weddell seals						+
Emperor penguins						−
Adélie penguins						−
Baleen whales						−
Pelagic birds			−			−
Benthos						−
Calcifying benthos				−		−

24
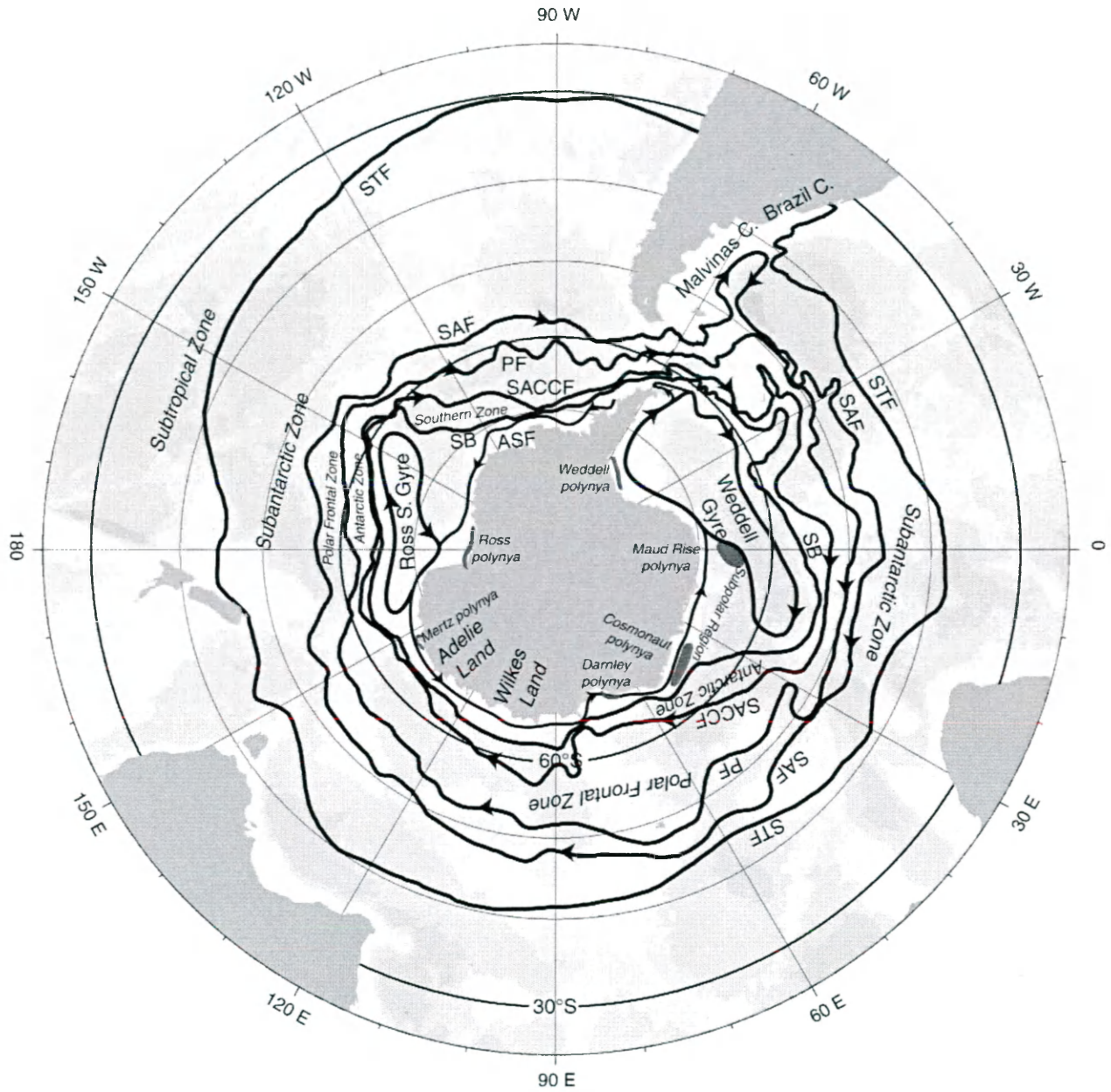
Figure 1: A map of the geography, principal fronts, and oceanographic zones of the Southern Ocean (Talley et al., 2011). The Southern Ocean is bounded to the north by the Subtropical Front (STF) and to the south by the Antarctic land mass. Contained within the eastward Antarctic Circumpolar Current (ACC) are four fronts: the Sub-Antarctic Front (SAF), the Polar Front (PF), the Southern ACC Front (SACCF), and the Southern Boundary (SB). Adjacent to the Antarctic landmass flows the westward Antarctic Slope Front (ASF), which follows the continental slope. Frontal locations from Orsi et al. (1995b). Major polynyas are shown as dark gray patches.
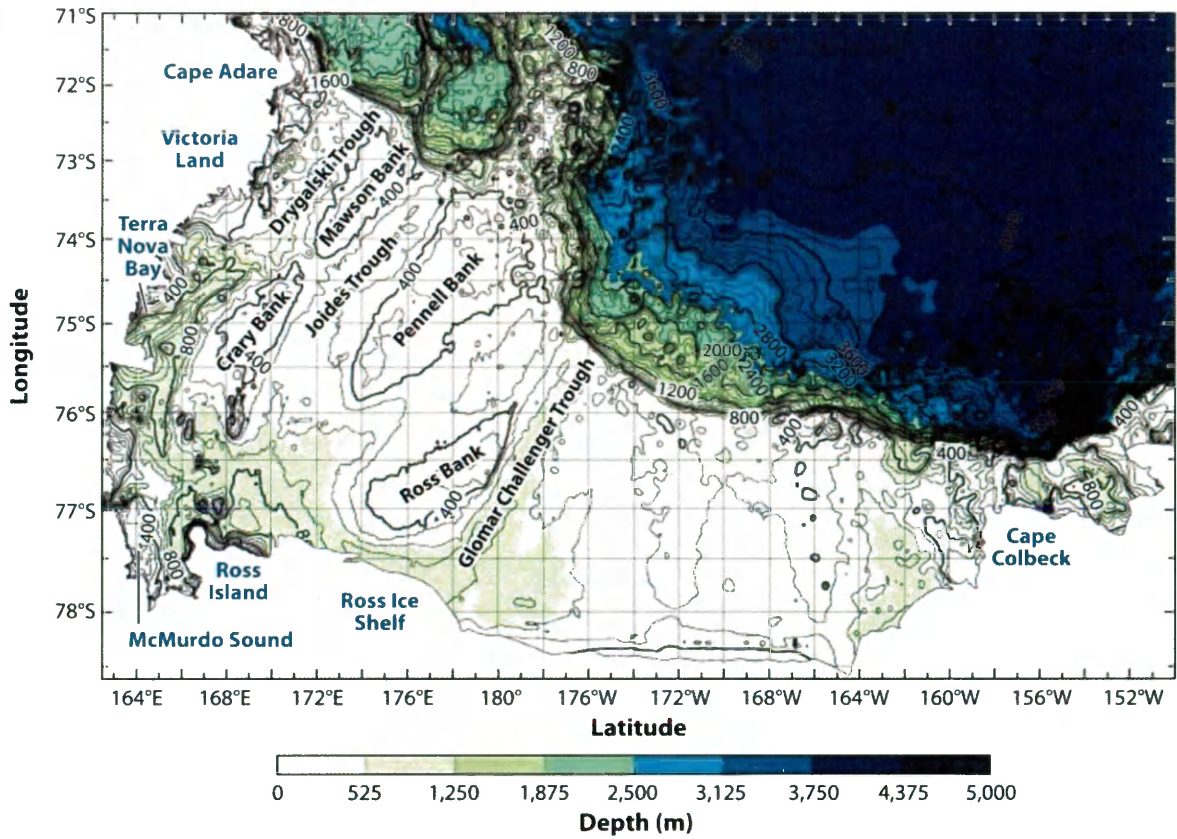
Figure 2: Bathymetric map of the Ross Sea. Bathymetry and contours (100 m interval) based on the ETOPO1 global relief model (Smith et al., 2014a).
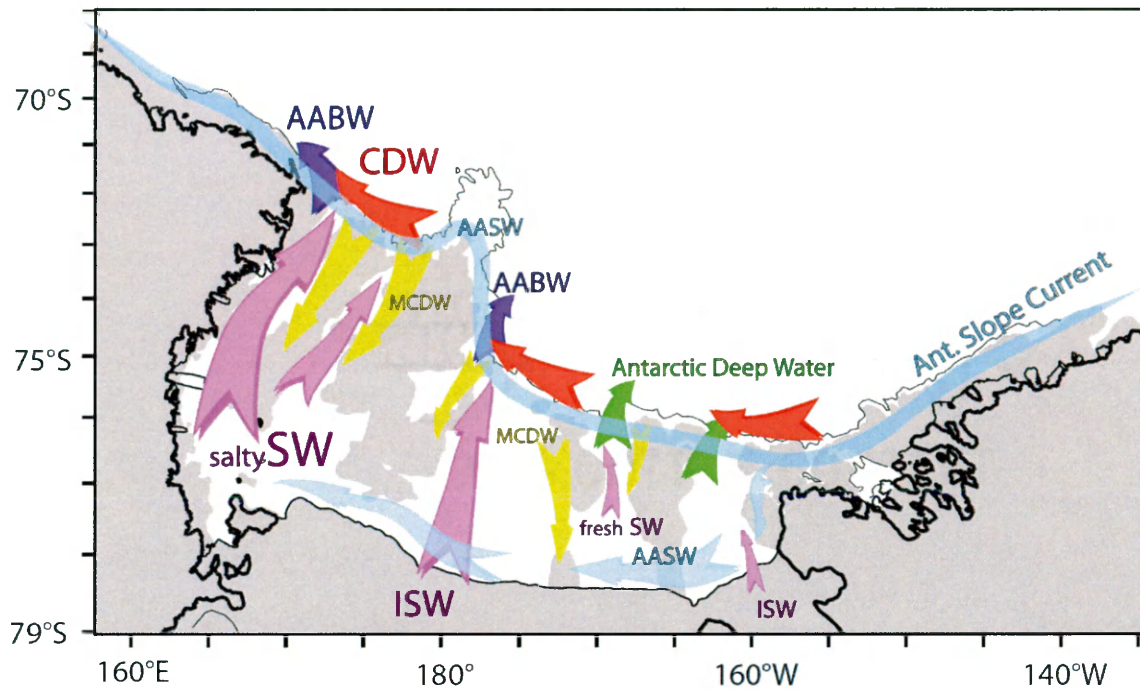
Figure 3: Schematic of the circulation patterns of the Ross Sea continental shelf, south of the eastward Antarctic Circumpolar Current (ACC; not shown). The width of the arrow indicates the relative strength of each water mass, and arrow color indicates individual water masses. Water masses include the Antarctic Surface Water (AASW; light blue), Circumpolar Deep Water (CDW; orange), Modified Circumpolar Deep Water (MCDW; yellow), Shelf Water and Ice Shelf Water (SW and ISW; purple), and Antarctic Bottom Water (AABW; dark blue). Modified from Smith et al. (2012a).
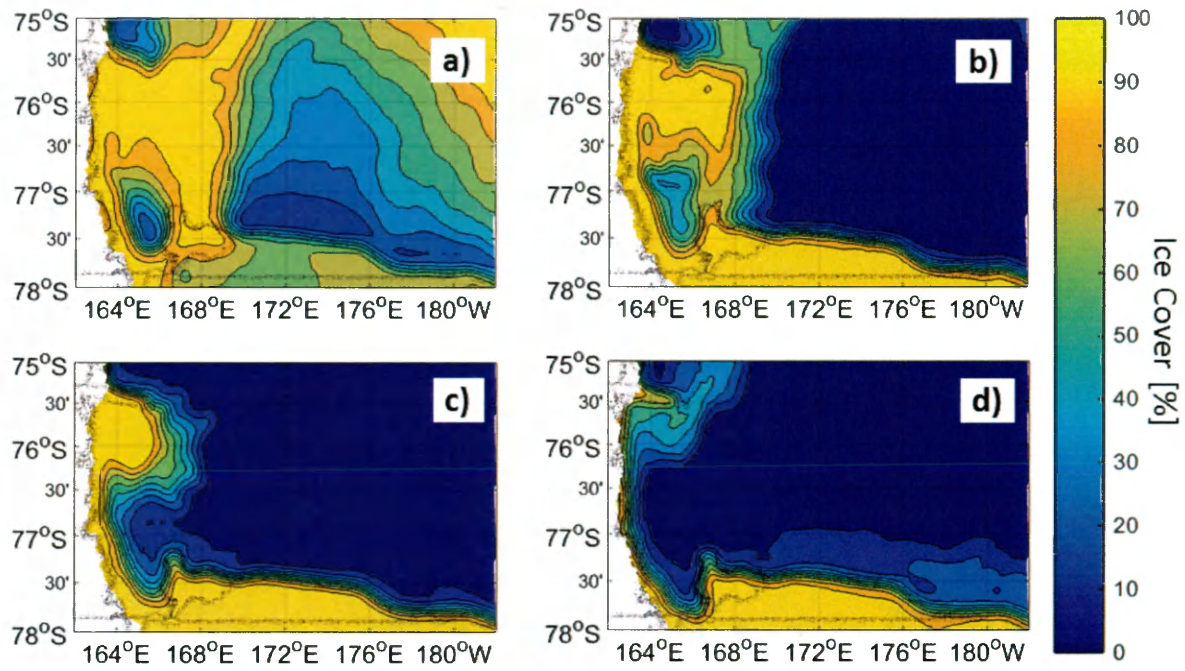
Figure 4: Monthly mean sea ice for the period of glider deployment: (**a**) November 2012, (**b**) December 2012, (**c**) January 2013, and (**d**) February 2013. Data from the microwave radiometer Special Sensor Microwave Imager Sounder (SSMIS/F18; Spreen et al., 2008). Open water (0% sea ice cover) is dark blue; full 100% sea ice cover is yellow. Contours are intervals of 10% sea ice cover.

CHAPTER 2

'Autonomous Glider Observations of Perturbations in the Seasonal Phytoplankton

Bloom Progression in the Southern Ross Sea, Antarctica'

ABSTRACT

Relative to the rest of the Southern Ocean, the Ross Sea continental shelf experiences very high productivity and phytoplankton biomass, which supports an extensive food web including high concentrations of upper trophic level biomass. Conventional observational methods, including ship-based sampling, instrumented moorings, satellite imagery, and computer-based modelling, have illustrated the seasonal progression of the phytoplankton bloom over the past four decades. While we have been sampling phytoplankton variability in the Ross Sea on a variety of relatively large scales, with observations at specific locations or times, over spans of time, or at specific depths, our understanding of smaller scales of variability (on the order of a few hours or several kilometers) is still poor. Utilizing two seasons (2010-2011 and 2012-2013) of high-resolution autonomous glider deployments in the southwestern Ross Sea, I examined the mechanisms driving both the transitions between stages of the phytoplankton bloom and the short-term perturbations in average 0-50 m chlorophyll. By including the available raw fluorescence data from both glider seasons and three mooring seasons, I determined that the 2012-2013 season had greater than average variability, with greater levels of variability observed in only two other seasons. Differences in the timing of bloom transitions were relatively constrained; the transition from bloom to post-bloom levels occurred within a temporal span of 6 d. These findings were likely the result of the location of the 2012-2013 glider adjacent to Ross Island and the Ross Ice Shelf, where complex bathymetry, turbulent flows, and the presence of an ice field contributed to the greater observed variability. To investigate the mechanisms driving the short-term perturbations in chlorophyll, I examined the relationships between average chlorophyll, average temperature, and mixed layer depth measured by the gliders and wind speed measured by two automatic weather stations atop the Ross Ice Shelf. Over the course of the 2012-2013 season, perturbations or responses in chlorophyll were heavily influenced by the degree of temporal coupling between wind events and the depth of mixing. Longer delays of 12-24 h observed prior to the biomass maximum shortened following the transition to biomass dissipation to 2-12 h. Furthermore, by causing aggregate formation and rapid vertical flux, physical forcing factors contributed to the observed short-term perturbations through reductions in biomass in surface layers and the appearance of chlorophyll in deeper layers. These results suggest that the small-scale observing capabilities of autonomous gliders allow for an improved understanding of the mechanisms that drive variability and short-term perturbations in shallow chlorophyll in the southwestern Ross Sea.

30

INTRODUCTION

The Ross Sea and Use of Gliders to Measure Event-Scale Perturbations

The Ross Sea is one of the most studied regions in the Southern Ocean, in large part due to being the site of the continent's major logistics center (McMurdo Station) as well as historical investigations by numerous Antarctic explorers (e.g., Ross, Shackleton). Specifically, extensive research in the Ross Sea has examined the complexities of phytoplankton dynamics and their inter- and intra-annual variability in space and time (El-Sayed et al., 1983; Smith and Nelson, 1985; Arrigo et al., 1999; Smith et al., 2000, 2011a, 2013; Peloquin and Smith, 2007; Long et al., 2011). Much of this work has been completed utilizing conventional observational platforms: research vessels, moored arrays, and a multi-generational series of remote sensing satellites. Recently, an increased utilization of autonomous underwater vehicles, specifically underwater gliders, have added complementary observing capabilities to the Ross Sea region (Kaufman et al., 2014; Smith et al., 2014c; Queste et al., 2015b). Gliders provide observations of the small spatial scale variability (over days and less than 10 km) within phytoplankton blooms. They also provide insight into the mechanisms that drive variations or deviations in the seasonal bloom dynamics in the southwestern Ross Sea due to their ability to acquire high-resolution and sustained (even in sub-optimal conditions) observations. This research utilizes underwater gliders to investigate the causes of short-term (several hours to days) deviations from the seasonal climatology of the upper water column chlorophyll

31

a concentrations (hereafter called event-scale perturbations), which have been difficult to study by conventional observational means.

Seasonal Phytoplankton Climatology and Environmental Factors Regulating Phytoplankton

The Ross Sea continental shelf has been characterized as being the most productive region in the Southern Ocean, contributing 28% of the productivity of the Southern Ocean (Arrigo et al., 1998c). Studies of the region have indicated the importance of this intense productivity and the substantial phytoplankton standing stocks in sustaining the food web (Smith et al., 2014a). These food web linkages are critically important and support large populations of middle and upper trophic level species. However, the processes regulating the food web are poorly understood, as the substantial standing stocks of phytoplankton appear to be relatively spatially or temporally uncoupled from the distributions of middle and upper trophic level species (Arrigo et al., 2000; Pinkerton and Bradford-Grieve, 2014; Ainley et al., 2015). Therefore, a greater understanding of the seasonal climatology of chlorophyll *a* and the complex set of physical and biological environmental factors that regulate phytoplankton stocks is needed to more fully assess the energetics of the food web.

Two phytoplankton functional groups, haptophytes and diatoms, are responsible for the majority of production in the Ross Sea (Smith et al., 2014a). The southern Ross Sea is the site of a large spring phytoplankton bloom that is dominated by the haptophyte, *Phaeocystis antarctica* (Smith and Gordon, 1997; Arrigo et al., 1999). This species reaches very high biomass levels (up to 25 mg chlorophyll m^{-3}; Smith et al., 2003), but

32

its biomass rapidly declines in late December and early January (Smith et al., 2000, 2011b, 2014a), after which biomass of all phytoplankton groups generally remains low (Peloquin and Smith, 2007). Despite this high spring productivity, concentrations of macronutrients (nitrate, phosphate, silicate) are rarely depleted, as the system is largely limited by irradiance via attenuation by ice cover or by deep vertical mixing during this period (Smith et al., 2000). Concentrations of the micronutrient iron are low in spring and summer ($\leq$0.1 nM; Sedwick et al., 2000, 2011), and are considered limiting following the rapid biomass decline, and in fact may initiate the reduction (Smith et al., 2003a). In some years, however, a diverse assemblage of diatoms forms extensive secondary blooms in late summer (Peloquin and Smith, 2007), the magnitude of which can be equal to those found in spring (Smith et al., 2011a). These temporal patterns of phytoplankton biomass have been confirmed by satellite observations (Arrigo and McClain, 1994; Arrigo and van Dijken, 2003, 2004; Arrigo et al., 2008; Smith and Comiso, 2008). These studies have also demonstrated marked spatial variability, but combined satellite-observational investigations have not adequately explained the causes of such variations.

The major reasons for this observed temporal (seasonal bloom progression) and spatial variability (mesoscale dynamics) are believed to be both physical and biological. Beginning with bloom initiation in late October, the dominant controlling mechanisms are related to light availability: decreasing ice coverage, seasonally increasing irradiance, lengthening photoperiods, and shoaling mixed layer depths (Smith and Gordon, 1997; Smith et al., 2000). Irradiance during winter (prior to bloom initiation) is zero, as the sun remains below the horizon for the entire 24-h photoperiod from late April until mid-August (Figure 5). Irradiance penetration through sea ice and snow cover (on average

0.67-0.82 m and 0.13-0.18 m thickness, respectively; Worby et al., 2008) is very low

during spring and fall, with an attenuation of ~97% (Arrigo, 2014). Following the period

of rapid sea-ice retreat (from late October to late December; Smith and Gordon, 1997;

Parkinson and Cavalieri, 2012), cloud cover can attenuate incident irradiance by ~50%

(Arrigo and van Dijken, 2004), but with sea ice retreat, increased solar angle, and

moderate water column stabilization, phytoplankton productivity and biomass quickly

increases, leading to large accumulations of particulate organic matter in the surface layer

(Smith and Sakshaug, 1990; Smith and Gordon, 1997; Arrigo et al., 1998b; Smith et al.,

2000).

Water column stratification also dictates the conditions that are amenable to

bloom initiation and accumulation (Smith et al., 2000; Smith and Jones, 2015). Deep

winter mixing, which sometimes occurs throughout the entire water column, gives way to

shoaling mixed layers under increasing heat inputs, input of sea-ice melt, and reduced

frequencies of storm and mixing events (Figure 5). The relatively stable, shallow mixed

layer along with increasing irradiances encourages high, yet light-limited, growth rates,

with an accumulation of biomass occurring from late October to the bloom maximum in

mid-December. To achieve high biomass conditions typical of mid-December,

production values must be high during November-December, attaining ~3-4 g C m^{-2} d^{-1}

(Nelson et al., 1996; Smith et al., 1996; Arrigo et al., 1998c).

A biomass maximum typically occurs in mid- to late December, and further

growth is apparently limited by availability of the micronutrient iron (Figure 5; Smith et

al., 2000; Sedwick et al., 2011). Observations of secondary phytoplankton blooms

(typically comprised of diatoms) have been made (Peloquin and Smith, 2007), yet it

34

remains difficult to explain how substantial productivity is supported during the presumed summer micronutrient limitation. The relief of iron limitation through the delivery of iron to surface waters by deep mixing, melting sea or glacial ice, land-derived inputs, physiological acclimation to a low iron environment, rapid recycling of iron from earlier blooms, and/or atmospheric mineral aerosols may explain this phenomenon (Sedwick et al., 2011; McGillicuddy et al., 2015). However, most of these iron input processes are spatially restricted, whereas secondary blooms are not. Overall, while the pattern of a primary followed by a secondary bloom may occur in most years, temporal and spatial variability in this pattern appears largely due to changes in environmental conditions dictated by irradiance, vertical water column structure, and the degree of iron limitation, as well as the ensuing species response to these conditions (DiTullio and Smith, 1996; Arrigo et al., 1999; Peloquin and Smith, 2007; Sedwick et al., 2011).

The termination of the biomass maxima is largely thought to be the result of grazing losses and vertical flux of aggregated phytoplankton material (Dunbar et al., 1998; Smith et al., 2000, 2011b; Arrigo and van Dijken, 2003). Smith et al. (2000, 2011b) demonstrated that two independent environmental factors created a temporal disconnect of ~30 days between the maxima of productivity and biomass. Initially, limited iron availability leads to a reduction in production, with grazing and particle aggregation/sinking losses experiencing a lag before becoming significant, thus leading to a reduction of biomass. Although the bloom rapidly dissipates, upper water column irradiance remains optimal for phytoplankton growth.

Event-Scale Perturbations in Seasonal Phytoplankton Climatology

Over the course of a growing season, the processes that cause phytoplankton biomass to accumulate and/or dissipate can be illustrated through the generation of a climatology, which depicts the overall mean trends and the general level of variability (Figure 6). Net growth rates over time – that is, the change in phytoplankton biomass through time (or other statistical treatments of trends) – can be calculated from climatologies of chlorophyll, providing a convenient means for comparisons across geographic regions or temporal periods. Previous climatologies for phytoplankton in the Ross Sea determined from remotely sensed or *in situ* shipboard observations exist (Arrigo et al., 1998c; Smith et al., 2003b, 2006, 2010), and have typically been calculated over time steps from days to years. While this relatively coarse time step may be appropriate for observational studies, it falls short of the temporal resolution required to appropriately observe event-scale perturbations.

Event-scale perturbations in upper water column chlorophyll a are defined as excursions of one standard deviation above or below the overall mean of the linearly de-trended data. They typically persist over short periods (on the order of several hours to several days) and are driven by physical and biological processes, each potentially with even shorter time scales. These processes include wind mixing or storm events, water mass circulation, and vertical fluxes and grazing. Thus, to appropriately explore the linkages between processes and the resulting perturbations, an observational method is needed with small-scale resolution. An underwater autonomous vehicle equipped with hydrographic, bio-optical, and oxygen sensors, such as a glider, is capable of providing the necessary observations; L'Hévéder et al. (2013) and Kaufman et al. (2014) demonstrated that with careful study design (e.g., considering the spatial extent of the

36

study area, placement of glider cruise tracks, reoccupation of glider points or transects, potential for multiple gliders, and consideration of study objectives), gliders provide a necessary level of finer-scale observation required to discern mesoscale phytoplankton dynamics.

Previous studies have observed event-scale perturbations and have broadly attributed these features to a combination of physical or biological processes, or have simply attributed them to noise (Banse, 1996; DiTullio and Smith, 1996; Asper and Smith, 1999; Peloquin and Smith, 2007; Smith et al., 2011a; Kaufman et al., 2014). Event-scale perturbations are included in the larger set of mesoscale and submesoscale features, such as eddies, fronts, internal waves, and vertical mixing, which are ubiquitous in the ocean, with high levels of observed variability on various spatial and temporal scales (Garçon et al., 2001; Boyd, 2002). Using shipboard observations and remote sensing imagery, more recent studies, such as Arrigo et al. (1998a) and Peloquin and Smith (2007), noted events that would be defined by this study as perturbations and variability among successive years of phytoplankton bloom composition, timing, and magnitude, positing that the influences of an interplay of factors were causal. In a biologically complex system like the Ross Sea, it is critical to be able to identify the causal factors of these perturbations and differentiate them from the noise inherent in the overall spatio-temporal variability. On one hand, adding capacity for the observation (e.g., gliders) to resolve features and the underlying processes that force them should lead to increased understanding of the system. However, limitations in sampling designs (i.e., the inability to determine synoptic three-dimensional observations of physical and biogeochemical measurements) leave researchers unable to derive a full understanding of

the system. It thus appears that one course would be to quantify and differentiate variability in the system of interest, while utilizing new technologies to examine perturbations on small-scales.

Introduction to Autonomous Platforms

The use of autonomous platforms to observe the physical and biological processes in the ocean has become an important means by which measurements of oceanic properties are collected. Moorings have long been used to collect current directions and speeds, as well as continuous records of temperature and salinity at one depth. More recently, profiling floats have been deployed throughout the ocean (Riser and Johnson, 2008); these floats collect information on the hydrographic properties in the water column, as well as dissolved oxygen concentrations. Newer versions collect estimates of phytoplankton biomass, nutrient concentrations (e.g., nitrate; http://www.mbari.org/chemsensor/APEXISUS.htm; Johnson and Coletti, 2002), and downwelling irradiance/PAR (Mignot et al., 2015). A more recent technological advance has been the development of gliders, autonomous underwater vehicles (AUVs) that navigate by buoyancy and undulate from the surface to depth and relay the data collected to a remote base station via satellite link (Eriksen et al., 2001). Such gliders can remain at sea for up to 9 months, depending on the types of dives, the sensors on each platform, and the installed battery capacity. A major advantage of these sampling technologies is that they are uninfluenced by storm events (unlike ships), and often are able to collect data in extremely difficult environments. For example, gliders have sampled 100's of km along transects across ocean basins (Glenn et al., 2011), been utilized in high latitude, ice-

38

covered regions such as the Southern Ocean (Thompson et al., 2014), sampled typhoons, hurricanes, and storm conditions (Glenn et al., 2008; Mrvaljevic et al., 2013; Miles et al., 2015), worked during the North Atlantic spring (Mahadevan et al., 2012), and have recently been deployed in the Ross Sea, a region that has heavy ice cover and frequent storms, both of which restrict oceanographic sampling (Kaufman et al., 2014; Queste et al., 2015b).

While the engineering, design, and capacities of underwater gliders may provide advantages over traditional observational platforms, they also lead to some disadvantages. The majority of their past operations have been in regions of open water free from ice cover, although operation in the vicinity of ice is possible with the addition of obstacle- or ice-avoidance systems (Abrahamsen, 2014), and under-ice operation has been achieved (Curry et al., 2014). Underwater buoyancy-driven gliders, in the absence of blade-propelled design, are limited to slow speeds of < 0.25 m s^{-1} and typically cover horizontal distances of ~0.5-5 km dive^{-1} or ~15-30 km d^{-1} (Rudnick et al., 2004). Depending on depth and other parameters, spatial coverage is limited to distinct transects, referred to as sections. Thus, when considering study design that requires increased coverage, one glider may be insufficient to cover more than a relatively small (e.g., 10's of km) survey region; the addition of multiple gliders provides the increased coverage needed over a larger region (L'Hévéder et al., 2013).

There is also a need to address the potential for a mismatch between the spatial and temporal scales of underwater glider observations and the temporal and spatial scales of the features of interest. Currently, glider observations cannot provide a synoptic, three-dimensional view of physical or biogeochemical measurements, as measurements are

39

influenced by both temporal and spatial variability (Piterbarg et al., 2014). Depending on the temporal and spatial scales of a physical or biogeochemical feature of interest, gliders are typically limited to resolving features with scales of a few days in time and a few km in space. Conscientious sampling design and execution may minimize some of these complications.

Phytoplankton dynamics, on spatial and temporal scales that match well with glider design, appear to be good candidates for exploration using gliders. Previous research efforts have provided an understanding of the oceanographic processes in the region using ship-based sampling, although the data are limited by the temporal and spatial restrictions of ship operations. To demonstrate this, Kaufman et al. (2014) down-sampled glider-based observations of physical and biological variables in the Ross Sea for comparison with ship-board observations. They found that large scale (~30 km) sampling (such as ships provide) were unable to detect correlations between physical and biological data that were resolved in the full glider data set. Hence, data collected on high spatial and temporal scales can provide an alternate view of the processes occurring within the water column.

This study sampled the southern Ross Sea using gliders during two field efforts, one conducted in 2010-2011 and one in 2012-2013, and utilizes an instrumented mooring from a third field effort in 2003-2006. The spatial extent of sampling in both of the gliders was restricted to small regions (~80-100 km^2), allowing the temporal resolution of the areas to be quantified; the mooring corroborated the temporal resolution of variability. These data were then used to investigate the impact of event-scale

perturbations on the temporal patterns of phytoplankton, as well as the potential changes

within the seasonal progression.

STUDY HYPOTHESES

I wanted to test the following hypotheses:

- Short-term events (such as storms and high energy surface-atmospheric motions) introduce significant variability to the temporal sequence of phytoplankton biomass;

- These perturbations in chlorophyll are associated with enhanced fluxes of particulate matter to depth that are not correlated with enhanced mixed layer depths; and

- These events alter the rates of accumulation and dissipation of chlorophyll biomass observed immediately after the event.

METHODS AND DATA ANALYSIS

Overview of Glider Observations

Three iRobot Seaglider™ (Model: 1KA) autonomous underwater vehicles were deployed into the Ross Sea polynya over the course of two seasons. All three gliders were instrumented with a suite of sensors, which included a Seabird CT Sail (conductivity and temperature), an Aanderaa 4330F Oxygen Optode (dissolved oxygen), and a Wet Labs ECO Triplet Puck (chlorophyll *a* fluorescence and optical backscatter at two different wavelengths, 470 and 700 nm). These data are available from the Biological and Chemical Oceanography Data Management Office website at http://www.bco-dmo.org/.

Glider Study Areas and Instrumentation

During the 2010-2011 GOVARS (Glider Observations of Variability in the Ross Sea) project, two Seagliders (Serial Numbers: SG502 and SG503), capable of diving to approximately 600 m or shallower when limited by bathymetry, were deployed in the vicinity of Ross Island and retrieved by the *RVIB Nathaniel B. Palmer* (cruise NBP11-01). Seaglider SG502 was deployed from the sea ice edge into McMurdo polynya (77.534°S, 165.075°E) on November 22, 2010 at 09:50 UTC (22:50 local time), spending the first ~150 dives in McMurdo Sound before heading north to ~76.7°S. It then turned to the east, transiting along 76.7°S beneath an ice bridge north of Ross Island, and crossed into the Ross Sea polynya (76.693°S, 169.310°E) on December 14, 2010. For the remainder of the deployment, it sampled a latitudinal transect between 172°E and 180°E

43

at 76.5°S, crossing the Central Basin and Ross Bank, reversing course at the eastern end of Ross Bank, and returning to the Central Basin (Figure 7a). It completed a total of 702 dives over 60 d and was retrieved by the *RVIB Palmer* (76.446°S, 173.349°E) on January 20, 2011 at 12:41 UTC (01:41 local time, January 21, 2011).

Seaglider SG503 was deployed into the Ross Sea polynya from the fast ice edge near Cape Crozier (77.435°S, 169.499°E) on November 29, 2010 at 08:56 UTC (21:56 local time). Initially, it headed northeast from Cape Crozier before turning to the east along 76.6°S across the Central Basin to the eastern end of Ross Bank (~179.7°E) before turning and returning to ~176.2°E. There it commenced a meridional 'bow-tie' track between 76 and 77°S, with the northern limb of the bow-tie over the trough between Pennell and Ross Banks, and the southern limb over the 400 m isobath of the western end of Ross Bank, which it repeated twice (Figure 7a). Prior to being retrieved by the *RVIB Palmer* (73.101°S, 175.101°E) on January 30, 2011 at 15:21 UTC (04:21 local time, January 31, 2011), it completed a total of 923 dives over 63 d. Flight patterns for the GOVARS gliders were designed to sample spatial variability (across a long latitudinal transect; SG502) and temporal variability (by repeating the meridional bow-tie pattern; SG503). The SG503 Wet Labs ECO Triplet Puck failed on the third day of deployment (during dive 55), which limited the collection of chlorophyll *a* fluorescence and optical backscattering data, but did not affect collection of temperature, conductivity, or dissolved oxygen data.

The second season (2012-2013) utilized a single Seaglider (SG503), modified with greater length overall and increased payload capacity. It was deployed from the fast ice near Ross Island (77.438°S, 169.746°E) on November 22, 2012 at 09:25 UTC (22:25

44

local time). It initially headed to the northeast for the first 50 dives before returning to near the point of deployment. For the remainder of the study (dives 81-571), the glider followed a 'radiator' pattern (with three main latitudinal transects and several perpendicular, longitudinal transects; 25 km E/W x 50 km N/S), sampling multiple times along certain transects (Figure 7b) and diving to up to approximately 800 m. The glider completed 571 dives over 78 d and was retrieved (76.771°S, 167.729°E) by the *RVIB Palmer* (cruise NBP12-10) on February 8, 2013 at 00:44 UTC (13:44 local time). In addition to instrumentation onboard the GOVARS gliders (SeaBird CT Sail, Aanderaa Oxygen Optode 4330F, and Wet Labs ECO Triplet Puck), this glider was outfitted with a downward-looking Imagenex 853 Echo Sounder Module for quantifying middle trophic level abundance. Data were collected approximately every 5 seconds; the Wet Labs ECO Puck and Imagenex 853 Echo Sounder were disabled below 250 m (200 m for the echo sounder after glider dive 53) to conserve battery power. The radiator flight pattern for the 2012-2013 glider was implemented to provide repeated coverage of the penguin foraging region in the vicinity of the Cape Crozier colony (Ainley et al., 2015).

Calibration and Correction of Glider Data

With the absence of early season, ship-based support and small boat capabilities, glider calibration was limited to one CTD cast performed by *RVIB Palmer* during recovery of each glider; additionally, water samples were collected at the ice edge during the second season deployment of SG503. The RVIB *Palmer* CTD profiles and associated *in situ* water samples were used to calibrate glider temperature, salinity, dissolved oxygen, and chlorophyll fluorescence data. Hysteresis, defined as the delay between

measured and actual values at one depth (i.e., instrument lag), which in the thermal and

conductivity probe records data from a different depth due to the time required for the

instrument mass to equilibrate thermally with the surrounding seawater, occurred through

strong gradients in the temperature, conductivity, and dissolved oxygen data on

successive glider casts. Temperature and conductivity hysteresis were corrected by cross-

calibration with the CTD profiles and application of a temporal offset. In the oxygen

optode, there is an instrument lag of approximately 8 seconds, as the dissolved oxygen in

the surrounding water requires time to diffuse across the optode sensing foil (Queste,

2013; Queste et al., 2015a). These corrections and other pre-analysis calculations were

performed on the glider data sets using the 'uea-seaglider-toolbox', developed by Bastien

Y. Queste and available at https://bitbucket.org/bastienqueste/uea-seaglider-toolbox/

(accessed August 8, 2014).

Glider fluorescence counts and particulate backscattering coefficients ($b_{bp}(\lambda)$,

calculated from the glider optical backscattering counts; Stramski et al., 1998, 1999),

were processed by regressing data from the final glider dive against *in situ* data (n=12).

Samples for chlorophyll *a* were analyzed by fluorometry using the acid-addition method

on a Turner 10-AU fluorometer (JGOFS, 1996), and particulate matter concentrations

were determined by filtering known volumes of seawater through combusted GFF filters,

drying at 60°C, and conducting pyrolysis on an elemental analyzer to obtain particulate

organic carbon (POC) concentrations (Gardner et al., 2000). Glider fluorescence counts

(FL) for 2010-2011 and 2012-2013 were converted into chlorophyll *a* concentrations

(Chl) using the regression:

$$\text{Chl} = (\text{FL} - 141) * 0.00225; \text{n} = 12; R^2 = 0.94; p < 0.01$$

derived from the calibration cast for 2010-2011 (due to issues with the 2012-2013 calibration data set; Kaufman et al., 2014). To calculate b_{bp} (λ), glider optical backscattering counts were: 1) converted to total volume scattering, β (117°, 470 nm), by subtracting dark counts and multiplying by a factory-calibrated scale factor, 2) subtracting the volume scattering of seawater, β_w (Morel, 1974), from the total volume scattering to obtain volume scattering of particulates, β_p, and 3) multiplying by a factor of $2\pi\chi$, where χ is 1.1 (Boss and Pegau, 2001). A regression based on the calibration cast:

$$\text{POC} = (42{,}850 * b_{bp}(470 \text{ nm})) + 57.47; \text{n} = 11; R^2 = 0.55; p < 0.01$$

was used to convert 2012-2013 b_{bp} (λ) into POC concentrations. Regression relationships for the 2010-2011 SG502 glider, which are available in Kaufman et al. (2014) were used to convert 2010-2011 b_{bp} (λ) into POC concentrations.

Derived or Calculated Glider Variables

To prepare the calibrated, core data sets for analyses, individual glider dives were separated into their descending and ascending legs (hereafter referred to as 'downcasts' and 'upcasts'), with the deepest point in the dive marking the delineation between the downcast and upcast. With GPS positioning data only available when the glider was oriented tail-up at the ocean surface, the GPS position obtained just prior to and just following a dive were interpolated to estimate GPS position data for that dive.

From the resulting core data sets for the three Seagliders, a number of physical

and biological parameters were calculated or derived to summarize each cast. Values for

sea surface temperature, salinity, and density were calculated by averaging observations

from the top 5 m of the water column. Mixed layer depth (MLD) was computed using a

potential density threshold method (Thomson and Fine, 2003), which defines the MLD as

the minimum depth at which a 0.01 kg m^{-3} increase is observed over the density (σ_θ) at 3

m. Average integrated temperatures, densities, and chlorophyll concentrations were

calculated using trapezoidal integration.

Glider Temporal Period Definitions

To investigate changes in the effects of physical and biological variables across

the seasonal progression of the phytoplankton bloom, temporal periods were identified

using average 0-50 m chlorophyll glider data. Three periods, "accumulation",

"dissipation", and "post-dissipation", were defined and corresponded with biomass

accumulation, biomass maintenance/decrease, and post-decrease, respectively.

Temporal period delineation was primarily driven by the longer record of

observations available from the 2012-2013 SG503 Seaglider deployment (Figure 8). The

SG503 accumulation period began when the glider entered into the radiator pattern on

December 1, 2012 at 00:00 UTC and ended on December 14, 2012 at 00:00 UTC

approximately 12 h prior of the maximum average 0-50 m chlorophyll. The accumulation

period spanned 13 d, and comprised 184 casts with average cast duration of

approximately 1.5 h (glider casts 152-335). The dissipation period began December 14,

2012 at 00:00 UTC (approximately 12 h following the maximum average 0-50 m

chlorophyll) and ended on January 7, 2013 at 00:00 UTC, 24 d later. The duration of this period is approximately 2x longer than the accumulation period, as the bloom dissipates over a longer time. Yet, the definition of the period ending avoids extending into the period when biomass is no longer markedly decreasing (characteristic of the post-dissipation period). The dissipation period was comprised 366 casts with average cast duration of approximately 1.4 h (glider casts 336-701). The post-dissipation period began January 7, 2013 at 00:00 UTC and ended 12 d later on January 19, 2013 at 00:00 UTC (average cast duration of approximately 1.6 h; casts 702-868; Figure 8).

Temporal periods for the 2010-2011 SG502 Seaglider were based on those chosen for the 2012-2013 SG503 Seaglider, but were shifted forward in time by 24 h – a limit imposed by the emergence of the glider from beneath the ice into the Ross Sea Polynya on December 15, 2010. An accumulation period was not observed by SG502. Therefore, the SG502 dissipation period began December 15, 2010 at 00:00 UTC and ended 24 d later following the pronounced decrease in average 0-50 m chlorophyll on January 8, 2011 at 00:00 UTC; it was comprised of 642 casts with an average cast duration of approximately 0.8 h (casts 462-1103). The post-dissipation period began following the pronounced decrease in chlorophyll on January 8, 2011 at 00:00 UTC and comprised 12 d and 285 casts (average cast duration of approximately 0.9 h; casts 1104-1388). The post-dissipation period ended on January 20, 2011 at 00:00 UTC (Figure 9).

Mooring Observations

As part of the Interannual Variability in the Ross Sea (IVARS) project, moorings were deployed at two locations in the southern Ross Sea during the austral summers of

2003-2004, 2004-2005, and 2005-2006 (Smith et al., 2011a). Of the two moorings, the

western mooring, *Callinectes* (Figure 7a; 77.000°S, 172.700°E), was bottom anchored in

approximately 600 m of water and was approximately 115 and 80 km from the center of

the 2010-2011 and 2012-2013 glider deployments, respectively. Dates of deployments

and retrievals for the *Callinectes* mooring over the three seasons (December 28, 2003 –

February 6, 2004, December 21, 2004 – January 29, 2005, and December 30, 2005 –

January 31, 2006), provided observations during the dissipation (December 14 – January

7) and post-dissipation (January 7-19) periods. During the 2004-2005 and 2005-2006

seasons, Seabird Microcat CTDs were placed at 24 m, which recorded temperature and

salinity values every 5 minutes. During all three seasons, Wet Labs ECO-FLSB

fluorometers were placed at 21, 23, and 21 m depth (respectively, 2003-2004, 2004-2005,

and 2005-2006); fluorescence values were recorded every 10 minutes. Both CTD and

fluorometer instruments were calibrated during mooring/instrumentation installation and

retrieval. More information on these moorings can be found in Smith et al. (2011a).

Wind Observations

Wind speeds and directions (hourly) were obtained from the Antarctic

Meteorological Research Center (AMRC) at the Space Science & Engineering Center,

University of Wisconsin at Madison (http://amrc.ssec.wisc.edu/). The center maintains an

extensive network of Automatic Weather Stations (AWS) across the Antarctic continent.

Two of the AMRC-AWSs, located east of Ross Island, are in the vicinity of the glider

deployments and are located on the Ross Ice Shelf. The first, Laurie II, (77.451°S,

170.760°E; anemometer height approximately 40 m above mean sea level) provided the

majority of wind speed and direction observations, while a second (Ferrell; 77.809°S, 170.818°E, approximately 35 km to the south of Laurie II; anemometer height approximately 45 m above mean sea level) was used when observations were not available from Laurie II (November 1, 2005 through January 6, 2006). Laurie II and Ferrell AWSs are approximately 180 and 200 km, respectively, from the center of the SG502, 2010-2011 glider deployment, and approximately 45 and 75 km, respectively, from the center of the SG503, 2012-2013 glider deployment (Figure 7a).

Satellite Observations

Chlorophyll *a* concentrations for the southwestern Ross Sea region were retrieved from the Ocean Color Web (http://oceancolor.gsfc.nasa.gov; NASA Ocean Biology Processing Group) as MODIS Aqua 1 km resolution Level 3 Standard Mapped Imagery. Sea ice concentrations for the same region were retrieved from the Universität Bremen SSMIS (http://www.iup.uni-bremen.de:8084/ssmis/index.html; SSMIS/DMSP data collected by the US Air Force Weather Agency) as 6.25km resolution images from the brightness temperature data derived from the DMSP SSMIS Passive Microwave sensors on the Nimbus 7 satellite (Spreen et al., 2008).

Statistical Analyses

Bootstrapped 95% confidence intervals of the means (n = 1000) were used to statistically compare variable averages between different temporal periods and deployment years. Significant differences for pairwise comparisons were assessed at the $\alpha = 0.05$ level.

To perform two sample hypothesis tests on variability in the non-normal, autocorrelated glider, mooring, and wind speed time series, bootstrapped data for the temporal periods and variables of interest were fit to an autoregressive integrated moving average (ARIMA) model to obtain a ratio of residual variance. This process was repeated 1000 times to construct a 95% confidence interval for the ratio of residual variances. If the 95% confidence interval did not contain 1, the null hypothesis of equal variance between groups was rejected, suggesting that the variances differed.

For the event-scale perturbation analyses and moving correlations, Pearson's linear correlation coefficients were calculated for glider and AWS variables. Correlation coefficients with p values ≤ 0.05 were considered statistically significant.

RESULTS

Overview of Glider Hydrographic and Biological Variables

Although the three glider deployments observed typical ranges for the measured water column properties (Dinniman et al., 2003; Orsi and Wiederwohl, 2009; Smith and Jones, 2015), there were significant differences (i.e., $p < 0.05$) between the two years (2010-2011 and 2012-2013) sampled by the gliders (Table 2). During the 2012-2013 accumulation, dissipation, and post-dissipation periods, sea surface (top 5 m) temperatures (SST), densities (SSD), and mixed layer depths (MLD) were significantly warmer, less dense, and shallower. Other properties varied across the three periods. Compared to SG502, 2010-2011, average chlorophyll at depths of 0-50 m for SG503, 2012-2013 was significantly greater during dissipation period, but was significantly lower during the post-dissipation period. Similarly, wind speeds were significantly weaker during the 2012-2013 accumulation and post-dissipation periods, but were significantly stronger during the 2012-2013 dissipation period (Table 2; Appendices A.1, A.2, A.3, A.4, A.5).

The overall surface seasonal trends (warming, freshening, decreasing densities, and diminishing wind speeds) are the dominant patterns observed during both years across the three periods. Exceptions to these trends were likely due to inter-annual/inter-seasonal differences in water column structure and wind forcing. MLDs were observed to shoal between the accumulation and dissipation periods during both years, but while the shoaling continues during the post-dissipation period during 2012-2013, there were slight

53

increases in MLD during 2010-2011. This difference in shoaling patterns was consistent with the observed winds during the post-dissipation period: there was a continued decrease in wind speed during 2012-2013, but an increase during 2010-2011. There is a slight increase in SSD observed during the 2012-2013 post-dissipation period as well, while decreases are observed during 2010-2011. Greater rates of change for SST and SSD (calculated slopes) were observed across the 2012-2013 periods. MLDs for 2010-2011 began deeper, and shoaled more rapidly through the dissipation periods than was observed in 2012-2013 (Table 2; Appendices A.1, A.2, A.3, A.5).

Overall variability (defined as residual variance) was greater for 2012-2013 compared with 2010-2011, with greater variability calculated for SST, SSD, and average 0-50 m chlorophyll across the three periods. However, shallow MLDs combined with the warm, less dense surface conditions and less variable wind speeds during 2012-2013, led to limited variability in MLDs during the 2012-2013 accumulation and post-dissipation periods. Variability in SST and SSD tended to be greatest during the dissipation periods, while variability in both wind speeds and MLDs generally decreased over the course of the three periods, with the exception of an increase in wind speed variability between the 2010-2011 dissipation and post-dissipation periods. Average 0-50 m chlorophyll variability was greatest during the 2012-2013 glider observations and, like SST and SSD, had the greatest variability during the dissipation period. Finally, bootstrapped 95% confidence intervals of residual variance indicated that there were significant differences in variability between all combinations of SST, SSD, MLD, average 0-50 m chlorophyll, or wind speeds between different temporal periods (Table 2; Appendices A.1, A.2, A.3, A.4, A.5).

54

Overview of Mooring Hydrographic and Biological Variables

The IVARS *Callinectes* mooring, located approximately 115 and 80 km from the centers of the 2010-11 and 2012-13 glider deployments respectively, provided two additional seasons of temperature and density observations and three additional seasons of fluorescence observations (covering the dissipation and post-dissipation periods) to assist in placing the 2012-2013 glider in a broader context. After filtering the glider data sets by the depths of the mooring instrumentation (temperature and density at 24 m, fluorescence at 21 or 23 m) and computing new period averages and residual variances, the 2012-2013 glider data maintained the characterization of being comparatively warmer and less dense. With only two sets of glider observations available from the accumulation period, the 2012-2013 accumulation period was significantly warmer than the SG503, 2010-2011 glider observations. During the 2012-2013 dissipation period, the average temperature at 24 m was $-0.82°C$, which was slightly warmer than the overall average for all four years ($-0.90°C$). By the post-dissipation period, however, it was significantly the warmest ($0.08°C$), indicating a rapid rate of warming between the two periods. Period averages for density at 24 m indicated that among the four seasons (grand averages: dissipation period, 27.685 kg m^{-3} and post-dissipation period, 27.626 kg m^{-3}), 2012-2013 remained significantly less dense during the dissipation (27.584 kg m^{-3}) and post-dissipation (27.515 kg m^{-3}) periods. Fluorescence values at 21 m for the two gliders and at 21, 23, and 21 m respectively for the three moorings, indicated that 2012-2013 was below average during the dissipation (1838.7 relative fluorescence units or RFU v. grand average of 1846.2 RFU) and post-dissipation (370.0 RFU v. grand average of 592.1

55

RFU) periods (Table 3; Appendices A.6, A.7, A.8). Lastly, observations from 2012-2013 generally had the greatest temperature, density, and fluorescence variability of the five seasons (with only slightly greater variability in fluorescence observed during the 2005-2006 dissipation and 2003-2004 post-dissipation periods; Table 3; Appendices A.6, A.7, A.8).

Overview of Glider and Mooring Seasonal Trends

By including the available raw fluorescence data from the three mooring seasons (2003-2006) and the two glider seasons (2010-2011, 2012-2013), it was observed that there were slight differences between seasons in the timings of key events within the seasonal progression of the phytoplankton bloom. Since observations of fluorescence during the accumulation and dissipation periods were limited, it was not possible to make comparisons regarding the timing of the bloom maxima. Fluorescence observations of the transition from bloom levels to post-bloom levels (between dissipation and post-dissipation periods) indicated that the switch of the five seasons all occurred within a period of 6 d (Table 3; Appendix A.8).

Event-Scale Perturbations: Wind-Mixed Layer Depth Coupling

The 2012-2013 accumulation period can be characterized as highly variable, including at least six event-scale perturbations in average 0-50 m chlorophyll within 12 d, and one strong wind event with a duration of 2 d (December 4-5, 2012; Table 2; Figure 8). With the exception of the one strong wind event, relatively calm conditions allowed MLDs to decrease, during which surface temperatures increased and densities decreased.

The water column structure during these calm periods facilitated phytoplankton growth and the accumulation of chlorophyll. Nevertheless, wind speeds were positively correlated with chlorophyll (r = 0.21 to 0.30; p < 0.001), and MLDs were negatively correlated with chlorophyll in the upper 30 m (r = −0.43 to −0.35; p < 0.001). A delay of 12-24 h between the onset of a wind event and the initiation of a decrease in upper 30 m chlorophyll appeared to result from delays in transferring the wind event's energy into changes to the upper water column structure (i.e., MLD increase). That is, during the accumulation period wind events typically began to affect mixed layer depths once wind speeds had nearly or fully reached the wind event's maximum velocity (Figures 10, 11, 16; Table 4).

Following the accumulation period, chlorophyll concentrations during the 2012-13 dissipation period remained variable, with several event-scale perturbations observed. Beginning with a large reduction of chlorophyll from 6.5 to 1.9 mg chlorophyll m^{-3} and a re-establishment back to 5.8 mg chlorophyll m^{-3} (a longer perturbation over the course of 4 d; December 14-18), the period included several rapid event-scale perturbations (December 18-22) nearly equal in magnitude to the initial December 14-18 perturbation, but with greater variation observed among depth bins. A lack of strong wind events early (December 14-23) allows the MLD to stay between 5 and 10 m and chlorophyll biomass to remain at approximately 70% of the seasonal maxima. Around December 23, there is a sharp reduction in average 0-50 m chlorophyll, which coincides with the observed December 23-25 wind event and the resulting MLD-chlorophyll disruption/dissipation (Table 2; Figure 8). Positive correlations that had been observed during the accumulation period between wind speed and chlorophyll in the upper 30 m and negative correlations

from 40 and 100 m (a product of out-of-phase wind and MLD-chlorophyll responses on the order of 12-24 h) appeared to reverse during the dissipation period, reflecting the increased temporal alignment (on the order of 2-12 h) between wind events and MLD-chlorophyll disruptions/dissipations. As a result, wind speed and chlorophyll display a weak negative correlation in the 10-20 m bin (r = −0.15; $p < 0.001$), but positive correlations between 30 and 100 m (r = 0.14 to 0.40; $p < 0.001$). Moving correlations suggest that the changes in correlation signs occurred on 9-11 December 2012, during the later stages of the accumulation period (Figures 12, 13, 16; Table 4; Appendix A.9).

The 2012-13 post-dissipation period has the least variability among all periods, and there are no remarkable event-scale perturbations in response to wind events during the span. Three strong wind events occur during this time, as well as the beginning of a fourth prolonged, strong wind event that concludes following the end of the post-dissipation period (Table 2; Figure 8). With low levels of biomass remaining in the upper 100 m following the dissipating effects of wind events and water column forcings upon chlorophyll, the four post-dissipation wind events have a greatly reduced effect on chlorophyll vertical distribution highlighted by the shift from positive correlations between 30 and 100 m (weakly negative near the surface) observed during the dissipation to weak, negative correlations (r = −0.31 to −0.15; p = < 0.001 to 0.019) across the majority of the water column (10-100 m) during the post-dissipation period (Figures 14, 15, 16; Table 4).

Event-Scale Perturbations: Vertical Fluxes

While wind events during the accumulation period were observed to affect

chlorophyll biomass after a 12-24 h delay, changes to chlorophyll were observed almost

immediately in response to changes to mixed layer depth. The December 4-5 wind event

influenced a December 5-6 excursion of the MLD from approximately 5-10 m depth to

60-80 m depth, where it remained for approximately 18 h. The initial responses in

chlorophyll biomass were limited to the upper 20 m of the water column and were

observed from 1200 to 2359 UTC (December 4), a 12 h period that was prior to the onset

of the MLD excursion. With the deepening of the MLD starting at 0000 UTC on

December 5, chlorophyll decreases were observed in the upper 40 m of the water column,

while chlorophyll increases were observed between 50 and 90 m. As a result, negative

correlations in the surface 40 m ($r = -0.43$ to -0.11; $p = < 0.001$ to 0.046) and weak

positive correlations between 50 and 80 m ($r = 0.12$ to 0.17; $p = 0.002$ to 0.038) were

observed between MLD and chlorophyll (Figures 10, 11, 16; Table 4).

During the dissipation period, correlation patterns over the upper 100 m between

MLD and chlorophyll did not display a sign change, but rather a magnitude change, due

to increased vertical fluxes. Again, as in the accumulation period, changes to chlorophyll

were observed to coincide with the excursion of the MLD, which following the onset of

the December 23-25 wind event, deepened to approximately 30 m for 12 h duration. It

then further deepened to approximately 40-75 m for 30 h as a successive wind event

began. While a reduction in chlorophyll had already occurred in the surface 10 m earlier

around December 15, these MLD excursions resulted in the prominent reduction of

chlorophyll between 10 and 30 m, and the appearance of chlorophyll between 40 and 100

m approximately 6-12 h prior to the onset of the MLD excursions on December 23. Correlations of MLD with chlorophyll between 10 and 30 m remain negative ($r = -0.26$ to -0.20; $p < 0.001$), and between 40-100 m are observed to become more strongly positive ($r = 0.15$ to 0.49; $p < 0.001$). The subsequent wind event on December 25-27 and those following on December 29-30 appear to continue to create disruptions in the mixing depth, which results in a continuation of elevated chlorophyll biomass at depth (between 30 and 90 m; December 25-31; Figures 12, 13, 16; Table 4).

The three strong wind events during the post-dissipation period did not appear to have an effect upon chlorophyll reductions or appearances in the upper 100 m likely due to the minimal response of the MLD to those wind events (typically, 5-25 m excursions observed per event). Chlorophyll biomass was maintained at a low level in the upper 10 m; bins between 10 and 100 m demonstrated decreasing chlorophyll over the course of the period (January 7-19). Period-wide trends (gradually increasing MLDs and decreasing chlorophyll) likely drive the negative correlations observed between 0 and 100 m ($r = -0.36$ to -0.14; $p = < 0.001$ to 0.019; Figures 14, 15, 16; Table 4).

2010-2011 Glider Observations of Event-Scale Perturbations

Observations of event-scale perturbations during the deployments of the SG502, 2010-2011 glider and the IVARS *Callinectes* 2003-2006 moorings (described in the next section) are useful to compare with the 2012-2013 glider observations. While there were no fluorescence observations in the Ross Sea Polynya during the accumulation period for the SG502, 2010-2011 glider or for the *Callinectes*, 2003-2006 moorings, the SG502, 2010-2011 glider did capture four minor event-scale perturbations in average 0-50 m

chlorophyll during the 24 d dissipation period. The first three of these events, occurring

on December 18, 25, and 30, 2010, were approximately 24 h in duration, with the fourth

event (January 5, 2011) being a sudden (6 h duration) biomass dissipation event. As a

result, the 2010-2011 dissipation period was ~50% less variable than the SG503, 2012-

2013 dissipation period as demonstrated by residual variances. Less wind variability was

also present, with three wind events (December 15, 25, and 31, 2010) observed during the

period each with durations of 2-3 d (Table 2; Figure 9).

The overall result of these wind events during the 2010-2011 dissipation period

appears to be minimal as correlations between wind speed and chlorophyll are weakly

negative between 10 and 90 m ($r = -0.15$ to -0.01; $p = < 0.001$ to 0.770, significant for

those r values less than approximately -0.08), which are reflective of the relative lack of

trending and high frequency variability in wind speed and chlorophyll across the

dissipation period. Wind events on December 15-17, 25-26, and 29-31 are observed to

result in excursions of MLDs to depth, with the December 15-17 wind event resulting in

an increase in the MLD from approximately 7 m to 50-55 m for 12 h before relaxing to

25 m and then (as wind speeds again increase) to 60 m for another 12 h. The latter two

wind events moderately increased MLDs from 10 to 30-50 m. While there was little to

observe regarding upper 50 m chlorophyll changes for the three wind events, it does

appear that elevated or increased chlorophyll between 40 and 90 m may have resulted

from the wind-MLD responses and vertical fluxes. Deeper positive correlations between

MLD and chlorophyll support this and are in agreement with similar observations from

the SG503, 2012-2013 glider. Across the water column, there is a positive correlation in

the 0-10 m bin ($r = 0.20$; $p < 0.001$), varied, weak correlations between 10 and 50 m ($r =$

−0.08 to 0.07; p = 0.044 to 0.566), and relatively stronger positive correlations between 50 and 100 m (r = 0.13 to 0.26; p = < 0.001 to 0.002; Figures 17, 18, 21; Table 5).

The SG502, 2010-2011 post-dissipation period (again similar to SG503, 2012-2013) has the least variability among the periods, and lacks remarkable event-scale perturbations in chlorophyll. Two wind events occur during the 12 d period, with the first on January 8, 2011 having a duration of 24 h, and the second with an extended duration of 8 d and sustained winds of 9-10 m s^{-1} (Table 2; Figure 9).

With less high frequency variability and low residual variability present during the SG502, 2010-2011 post-dissipation period, correlations between wind speed and chlorophyll, while weak and slightly positive in the surface 30 m (r = 0.04 to 0.06; p = 0.28 to 0.47), have strengthened to significant, negative correlations between 30 and 80 m (r = −0.28 to −0.13; p = < 0.001 to 0.03), and weak, negative correlations from 80 to 100 m (r = −0.10 to −0.05; p = 0.11 to 0.36). Patterns in the correlations between MLD and chlorophyll are similar with a weak, yet significant positive correlation in the 0-10 m bin (r = 0.15; p = 0.01), switching to negative correlations between 30 and 100 m (r = −0.28 to −0.12; p = < 0.001 to 0.04). The negative correlations occurring deeper than 30 m for both wind speed and MLD appear to be the product of the chlorophyll decreases from approximately 2 to approximately 1 mg Chl m^{-3} observed between 30 and 100 m on December 10. It is likely that the onset of the prolonged January 10-18 wind event is the causal factor (Figures 19, 20, 21; Tables 2, 5).

2003-2006 Mooring Observations of Event-Scale Perturbations

Observations of the dissipation and post-dissipation periods from the three seasons of IVARS *Callinectes* mooring deployments add a snapshot of the conditions and correlations between wind speed or temperature (at 24 m) and chlorophyll (at 21 or 23 m), which are thus comparable to the 20-30 m glider depth bin data. As the correlations from the two glider years have demonstrated, the 20-30 m depth bin often sits at an inflection point between patterns of significant, yet inverse, correlations among shallower and deeper strata. Thus, during the dissipation period for the three years of mooring observations, wind speed is both positively and negatively correlated with chlorophyll. Respectively over the three years, there is a positive correlation (r = 0.29; $p < 0.001$), a negative correlation (r = −0.39; $p < 0.001$), and a weak, non-significant negative correlation (r = −0.10; $p = 0.19$). Temperature data, available for the 2004-2005 and 2005-2006 seasons, were weakly (r = 0.07; $p = 0.17$) and strongly, negatively correlated (r = −0.78; $p < 0.001$; Figure 22).

During the post-dissipation period, variable trending appeared to drive several of the correlations as chlorophyll losses continue during continued upper water column warming. Variation in correlations continued, with wind speed and chlorophyll negatively correlated (r = −0.31; $p < 0.001$), positively correlated (r = 0.45; $p < 0.001$), and positively correlated (r = 0.12; $p = 0.03$), respectively for the 2003-2004, 2004-2005, and 2005-2006 mooring years. Temperature and chlorophyll were strongly, negatively correlated (r = −0.81 and −0.72; both $p < 0.001$; Figure 23).

2010-2011, 2012-2013 Glider Observations of Correlations between Average Temperature and Chlorophyll

While correlations between wind speed or MLD and chlorophyll appear to be driven strongly by individual wind events propagating changes through the water column, correlations between temperature and chlorophyll suggest the overarching influence of drivers that are cyclical or depth-independent. During the 2012-2013 accumulation period, there were strong temperature-chlorophyll correlations ($p < 0.001$) that persisted throughout the upper 100 m. Correlation coefficients ranged from 0.56 for the 10-20 m bin to 0.87 for the 90-100 m bin. The surface 0-10 m correlation coefficient was relatively weaker, yet significant ($p < 0.001$) at 0.28, likely due to increased influence from wind forcing, MLD fluctuations, and variability in diel photoinhibition of the fluorescence signal (Smith et al., 2011a; Kaufman et al., 2014; Figures 10, 11, 16; Table 4).

As the season progressed and chlorophyll began to dissipate throughout the upper 100 m of the water column, trends (such as the shift from increasing to decreasing chlorophyll biomass) and increased vertical fluxes resulted in correlational shifts that were depth-dependent. While temperature and chlorophyll had been strongly, positively correlated during the accumulation period when they both had been upwardly trending and vertical flux was minimal, a moving correlation suggests a switch to a negative correlation (r = −0.65 to −0.41; $p < 0.001$) in the upper 30 m around December 15-18 (Appendix A.9). Temperatures below 40 m during the dissipation remain significantly correlated with chlorophyll ($p < 0.001$), with the correlations strengthening with depth from r = 0.28 in the 40-50 m bin to r = 0.76 in the 80-90 m bin (Figures 12, 13, 16; Table 4).

A shift in the correlation patterns between temperature and chlorophyll continue during the post-dissipation period, as chlorophyll reductions are observed over a deeper range of the upper 100 m and the warming trend continues. With that, negative correlations between temperature and near surface chlorophyll deepened from 0-30 m to 10-60 m (r = −0.57 to −0.24; $p < 0.001$) between the dissipation and post-dissipation periods. Also, the deeper, positive correlations between temperature and chlorophyll during dissipation (r = 0.28 to 0.76; $p < 0.001$; 40-100 m) weakened considerably and were limited to 90-100 m (r = 0.22; $p < 0.001$). In the upper 10 m, temperature is positively correlated with chlorophyll (r = 0.27; $p < 0.001$), indicating the potential influence of atmospheric forcing near the conclusion of the phytoplankton summer season (Figures 14, 15, 16; Table 4). Lastly, moving correlations corroborate the depth dependent nature of these changes, with shifts from positive to negative correlation occurring later as depth increases (Appendix A.9).

Observations of temperature during the deployment of the SG502, 2010-2011 glider corroborate the SG503, 2012-2013 dissipation period observations, with negative correlations observed between 0 and 40 m (r = −0.62 to −0.18; $p < 0.001$), and positive correlations between 50 and 100 m (r = 0.19 to 0.60; $p < 0.001$; Figures 17, 18, 21; Table 5) during the 2010-2011 dissipation period. The progressive movement to depth of negative correlations between temperature and chlorophyll observed during SG503, 2012-2013 is not as apparent for the SG502, 2010-2011 glider observations. Temperature correlations with chlorophyll during the 2010-2011 post-dissipation are mostly weak, with negative correlations present between 10 and 40 m (r = 0.17 to 0.35; p = < 0.001 to

0.004), and a positive correlation present between 90 and 100 m (r = 0.19; $p < 0.001$;

Figures 19, 20, 21; Table 5).

DISCUSSION

Hydrographic and Biological Variability/Trends

Biological and hydrographic conditions in the southwestern Ross Sea, as documented by glider observations, moorings, and automatic weather station data, provided a broad view of the environmental conditions present across the five seasons of observations and demonstrate the substantial spatial and temporal variability in the region. By comparing the season of interest, 2012-2013, to the two 2010-2011 gliders, it was observed that during the 2012-2013 study, waters were warmer, less dense, and experienced shallow MLDs (Appendices A.1, A.2, A.3). By adding two additional mooring seasons, these conclusions were primarily upheld as 2012-2013 demonstrated above average temperatures and below average densities (Appendices A.6, A.7). As well, wind data indicated that the 2012-2013 study period had low average wind speeds (Appendix A.5). Since the observations driving these interpretations were obtained over relatively short, non-continuous periods (2003-2006 and 2010-2012), it remains uncertain what role long-term trends or patterns play in these conclusions. Previous studies (Stammerjohn et al., 2008; Bracegirdle and Kolstad, 2010; Jacobs and Giulivi, 2010; Smith et al., 2014b) have demonstrated that the Ross Sea continental shelf is experiencing trends in increasing ice concentrations, decreased open ice duration, and decreased salinities. Therefore, it is possible that the 2012-2013 overall trends may be partially attributable to the larger forcings observed across the entire Ross Sea sector.

While forcings may be somewhat uniform on the continental shelf scale, it is well understood that environmental conditions across the relatively vast Ross Sea continental shelf (986,000 km^2; DiTullio and Smith, 1996; Arrigo et al., 1998a; Smith et al., 2000), as well as the relatively small glider and mooring study areas in the southwestern Ross Sea (63,000 km^2; Smith et al., 2011a; Kaufman et al., 2014) demonstrate high levels of spatial and temporal variability. Satellite ocean color observations illustrate the variability inherent in the Ross Sea (Figure 24). Considering the cruise tracks of the two gliders (the long out-and-back transect taken by the SG502, 2010-2011 glider and the spatially-restricted radiator pattern taken by the SG503, 2012-2013 glider), the mode of variability measured by each can be assumed to be dominated by spatial and temporal variability, respectively.

In the Ross Sea, this variability may be caused by a variety of factors such as ice, tides or currents, vertical or horizontal advection, stratification, and seasonality or location. During the 2010-2011 glider observations, the long out-and-back transect, completed over 28 d and covering ~400 km, was characterized by 1) relatively low variability for measurements of SST, SSD, and average 0-50 m chlorophyll, 2) relatively moderate excursions of the observed event-scale perturbations, and 3) a flat trend in average 0-50 chlorophyll. In contrast, the 2012-2013 glider observations, where the re-occupation of a limited (25x50 km) study area, were characterized by 1) relatively high variability, 2) pronounced excursions in the observed event-scale perturbations, and 3) a downward trend to a post-bloom level between the dissipation and post-dissipation periods. Different combinations of factors, in addition to the design of the glider cruise tracks, are likely to have resulted in these contrasting summaries of the two seasons. For

68

example, differences in the proximity to ice between the two locations likely have a great effect on the observed differences in variability. The 2012-2013 glider operated adjacent to and sometimes into an ice field, which especially during the accumulation and dissipation periods had an effect on the observed rapid excursions in average chlorophyll above and below the overall de-trended mean. Ice fields typically add a great deal of variability to the vertical stratification of a water column, as melting ice injects lowered salinity water into the surface, changing stratification, which thus leads to variability in chlorophyll measured by the glider (Figure 25; Smith and Jones, 2015). Additionally, the 2012-2013 glider operated in close proximity to Ross Island and the Ross Ice Shelf (ca. 25 km from the center of the glider deployment and as close as ca. 8.4 km; Figure 7), features that along with rapid changes in bathymetry and currents (Dinniman et al., 2007), contribute to the greater observed variability during the 2012-2013 season.

Event-Scale Perturbations: Wind-Mixed Layer Depth Coupling

During the 2012-2013 accumulation period (December 1-14), disturbances to water column structure driven by wind events had the greatest capacity to effect changes in chlorophyll. Changes resulting from turbulent wind mixing typically propagate from the surface to a depth determined by the speed, duration, and direction of a wind event. Wind mixing events, like those observed during the 2012-2013 glider deployment, resulted in measureable changes to mixed layer depths, and in modifications of the temperature and density of waters in the upper 100 m. For example, wind events occurring on December 4-5 and two wind events occurring in quick succession on December 23-26 (durations of ~48-96 h), resulted in MLD increases from ~5-10 m to

~25-80 m, where they remained for ca. 36-72 h (slightly shorter than wind events and with a lag; Figures 10, 11, 12, 13, 16; Table 4). Indications of turbulent mixing were also apparent as temperature changes during periods of increased MLDs, where noticeable increases in temperature at depths between 30 and 90 m were observed during the later December 23-26 mixing event. Deeper MLDs (60-80 m) were required to increase temperatures between 70 and 90 m (Figures 12, 13, 16; Table 4). In contrast, limited turbulent mixing during relatively calm periods, such as those observed over the first two days of December and at the end of the accumulation period (December 12-13), promoted the shoaling of MLDs to shallower than 15 m (Figures 10, 11, 16; Table 4). By limiting deep mixing and maintaining phytoplankton in the well-lit, nutrient-replete surface layer, shallow and stable MLDs generate periods (hours to days) that allow biomass to accumulate and growth to proceed under irradiance-saturated conditions (Smith and Donaldson, 2015).

The delay between the onset of a wind event and the resulting changes to the mixed layer were on the order of 12-24 h during the accumulation period (Figures 10, 11, 16; Table 4). Therefore, the temporal alignment of accumulated biomass (following calm, shallow MLD periods) and the deepening of MLDs (in response to wind energy inputs) produced significant correlations in the upper 30 m between wind speed or MLD with chlorophyll (respectively $r = 0.21$ to 0.30 and $r = -0.43$ to -0.35; $p < 0.001$; Figure 10, 16; Table 4). However, between 40 and 100 m, these correlations switched signs and magnitudes, with wind speed and chlorophyll negatively correlated ($r = -0.51$ to -0.21; $p < 0.001$) and MLD and chlorophyll positively correlated between 50 and 80 m ($r = 0.12$ to 0.17; $p = 0.011$ to 0.002; Figures 10, 11, 16; Table 4).

70

The contrasting observations of the correlations between wind speed with chlorophyll and MLD with chlorophyll, and the change in correlational sign that occurs at the inflection point at 40 m are both the result two inter-related processes. First, the temporal uncoupling between a wind event and the resultant mixing response or MLD excursion, on the order of 12-24 h, leads to the differences in signs between wind speed and MLD correlations. Importantly, the timing between MLD excursions and chlorophyll responses experiences little to no changes, thus maintaining the correlations of MLD with chlorophyll between the accumulation and the dissipation period. Second, the resultant mixing effects of the wind event (as indicated by increased MLDs) have depth-dependent influences on chlorophyll. Chlorophyll is reduced in shallow waters and appears in deeper waters as a result of the MLD excursions to depth with little delay, which indicates the influence of mixing or vertical advection upon chlorophyll biomass to depth. During the accumulation period, this is most apparent in the biomass increases between 40 and 80 m (December 5-7) following the prolonged wind event (Figures 10, 11, 16; Table 4).

With the arrival of the bloom maxima and the transition to the bloom dissipation period, changes in wind speeds, MLDs, and chlorophyll caused shifts in the correlations between those variables. The most changed of the correlations (Figure 12, 13, 16; Table 4) were wind speed and chlorophyll, with a negative correlation between 10 and 20 m (r = −0.15; p < 0.001), and positive correlations between 30 and 100 m (r = 0.14 to 0.40; p < 0.001) during the dissipation. This reflects a shift in the delay between the onset of a wind event and the resulting response in the MLD, which shortens from 12-24 h during the accumulation period (December 1-14, 2012) to 2-12 h during the dissipation period

71

(December 14, 2012 – January 7, 2013). This is illustrated by the prominent wind events during the dissipation period, which (with little delay) affect the vertical distribution of chlorophyll. Following a calm period on December 14-22 with variable yet high chlorophyll biomass in the upper 40 m, wind events from December 23-27 quickly drive average chlorophyll concentrations from 4-8 mg chlorophyll m^{-3} to 1.5-3 mg chlorophyll m^{-3} (Figure 12, 13, 16; Table 4). With the tighter temporal coupling between wind events and a response in MLD, the effect of the increased winds on chlorophyll is now rapid. Compared with the accumulation results, the dissipation correlations suggest that wind events typically cause phytoplankton biomass to be quickly removed out of surface waters shallower than 20-40 m and subsequently appear in waters between 50 and 100 m (Figures 12, 13, 16; Table 4). Moving correlation analyses suggest that this shift in the signs of the wind speed with chlorophyll correlations occurred just prior to the time of the bloom maxima (December 9-13; Appendix A.9).

While the correlations between wind speed and chlorophyll changed from the accumulation to the dissipation period due to changes in timing, there are minimal changes for the correlations between MLD and chlorophyll moving into the dissipation period, as changes in chlorophyll remain tightly coupled to MLD. Significant, negative correlations near the surface weakened (10 to 30 m; r = -0.26 to -0.20; $p < 0.001$), while significant correlations at depth strengthened (40 to 100 m; r = 0.15 to 0.49; $p < 0.001$; Figures 12, 13, 16; Table 4). Generally, the underlying mechanism of shoaled MLDs encouraging biomass buildup and minimal mixing to depth, and increased MLDs allowing deeper mixing to carry phytoplankton biomass to depths and stimulate aggregate formation appears to hold from the accumulation through the dissipation

72

period, leaving the correlation pattern largely intact. During the dissipation period, this pattern is most apparent during the MLD excursions from 5-10 m to 70-75 m that occurred on December 23-26, 2012. The decline of chlorophyll between 10 and 40 m on December 22 results in chlorophyll appearances between 50 and 90 m (Figures 12, 13, 16; Table 4).

As illustrated by a period of low wind speeds and stable, shallow MLDs (December 14-22, 2012), the coupling of wind events and MLD excursions with chlorophyll changes may not always be the case when noting the variability in chlorophyll observed between 10 and 50 m. Nevertheless, while little change is noted in MLDs during this low wind period, a short duration (8-12 h) increase in wind speed on December 18, 2012 appears to have an effect on chlorophyll and drive chlorophyll reductions (10-20 m) and appearance (30-50 m) occurring on December 19 (Figures 12, 13, 16; Table 4).

By the post-dissipation period (January 7-19, 2013), reductions of chlorophyll across the upper 100 m caused the correlations of wind speed and MLD with chlorophyll to weaken. That is, with chlorophyll biomass largely at post-bloom levels, three wind events (January 10, 12-13, and 14-15) and limited MLD excursions have a minimal effect upon chlorophyll vertical distribution. With the end of the growing season approaching (Smith et al., 2011a), trends of increasing wind events, the associated deepening of the MLD, and decreasing chlorophyll appear to be the driving factors in a switch to negative correlations for both wind speed and MLD (Figures 14, 15, 16; Table 4).

Among several factors that may lead to variability in shallow chlorophyll biomass, these observations suggest strongly that vertical stratification may play one of

the greater roles in influencing the variability observed in the upper 100 m of the water column over the 2012-2013 season. Observations of seasonal changes to the temporal coupling between wind events and MLD excursions illustrate that alternating calm and perturbation periods rework vertical stratification, so that mid-season wind events are more effective at rapidly deepening mixing and shunting chlorophyll biomass to depth (Smith and Jones, 2015). Contributions to accumulation and dissipation period perturbations may also be the result of the glider proximity to an ice field (Figure 25), where meltwater increases stability and has profound effects on phytoplankton biomass. Lastly, changes to the temporal coupling between wind events and MLD excursions may be due to the observations of shifting wind direction over the course of the accumulation and dissipation periods (Figure 26). Wind directions during the accumulation period are typically from the southwest with an average direction of 222°. From the early through the late dissipation period, the wind direction shifts to the south and eventually to the east-southeast with an average direction of 167°. The shift is likely due to seasonal changes in regional and global circulation patterns, yet the local topography (Ross Island and Ross Ice Shelf to the south of the 2012-2013 glider) likely also affects wind directions in the glider study area (Dinniman et al., 2007).

Event-Scale Perturbations: Vertical Fluxes

The disappearance of biomass in surface waters and its appearance in waters between 40 and 100 m is unlikely to be fully explained by wind induced mixing and resulting MLD excursions alone, due to the relatively shallow nature of the observed effects of wind mixing (MLDs increasing to 25-80 m; Figure 8c). While a strong wind

74

event, like the one observed December 4-5, 2012, caused the MLD to increase sharply from approximately 5 to 75 m and decreasing back to 5 m, the timing and nature of the disappearance of chlorophyll shallower than 40 to 50 m and the appearance of chlorophyll between 50 and 90 m suggests the potential for wind-induced turbulent mixing causing aggregate formation and vertical flux (Waniek, 2003; Burd and Jackson, 2009). That is, particle-particle interaction was enhanced by turbulence, and resulted in the formation of larger particles (or aggregates) that had significant numbers of chlorophyll-containing cells. These larger particles also sank faster, and were then observed at depth. For example, chlorophyll disappearances between 0 and 30 m preceded the MLD increases and are aligned temporally with the maximal wind speeds on December 4, 2012. Within 12 h, biomass appeared at 70 to 90 m prior to the influence of the MLD at those depths (Figures 10, 11). Together, this suggests that vertical biomass displacement may be explained by water movement (the result of wind/MLD events), coupled with aggregate formation and vertical flux (the result of wind derived turbulence).

The overall abundance of aggregates is therefore a function of production and loss processes that are influenced by several environmental factors such as particle stickiness and frequency of particle interaction (Burd and Jackson, 2009). Depending on the complex interplay of these factors, aggregate formation and increased particle sizes may proceed. On the other hand, wind-driven turbulence may also cause aggregate or particle disintegration; where subsequently smaller particles may slow the rates of vertical fluxes and the movement of biomass to depth. Coincident with slower sinking rates, increased remineralization of smaller particles might also occur.

Several of the factors involved in the processes of aggregate formation are dependent upon the biological characteristics of the particle, which are dictated by the species involved in the aggregate formation and the condition of the particles. The majority of biomass reductions in the surface waters and rapid appearances in waters deeper than 40-50 m occurred during the dissipation period from December 14, 2012 until January 7, 2013. Spring biomass during this time is typically dominated by *Phaeocystis antarctica* (Smith and Gordon, 1997; Arrigo et al., 1999). Research efforts have suggested that the colonial form of *Phaeocystis* contributes greatly to aggregate formation and subsequent, rapid vertical flux to depth (DiTullio et al., 2000; Smith et al., 2011b). With differences in the carbon to chlorophyll ratios between *Phaeocystis* and diatom species, observations of POC:Chl during the study periods suggest low POC:Chl ratios were present (*Phaeocystis*-dominated blooms) during the accumulation and dissipation periods (Figure 27). Therefore, it is likely that aggregate processes on *Phaeocystis*-dominated blooms during the dissipation period likely played a role in the rapid vertical flux of biomass to depth.

2010-2011 Glider Observations of Event-Scale Perturbations

An overall comparison of the correlations from the 2012-2013 data to those of the previous 2010-2011 observations revealed similar patterns in MLD and temperature, but a different wind speed pattern. During the 2010-2011 dissipation period (December 15, 2010 to January 8, 2011), wind speeds were slower and less variable (average of 3.5 m s^{-1}; residual variance of 4.9 m s^{-1}; Table 2), and average 0-50 m chlorophyll was lower and less variable than the 2012-2013 data (respective averages of 3.21 and 3.34 mg

chlorophyll m^{-3} and residual variances of 0.63 and 1.32 mg chlorophyll m^{-3}; Table 2).

Weak, mostly negative correlations between wind speed and chlorophyll (r = -0.11 to

0.05; p = < 0.001 to 0.77) appeared to result from the observed relatively low levels of

variability, minimal changes in wind speeds and chlorophyll (Figure 9a, 9b), and the

minimized response (in comparison to 2012-2013) in chlorophyll to wind-event forcing.

It should be noted that wind speeds prior to the 2010-2011 dissipation period were some

of the strongest recorded and had the highest average wind speed of the five years of

observations, which likely had an influence on conditions observed during the dissipation

(Figure 9b; Appendix A.5). Nevertheless, some evidence for the flux of aggregates and

chlorophyll to depth was observed late in the period (January 4-7), as chlorophyll losses

in the upper 40 m (from ~2 to 0.5 mg chlorophyll m^{-3}) and the maintenance of

chlorophyll in waters between 60 and 100 m (from ~2.5 to 2 mg chlorophyll m^{-3}; Figures

17, 18, 21; Table 5).

A lack of response in chlorophyll to wind-event forcing also affected the strengths

of the correlations between MLDs and chlorophyll during the 2010-2011 dissipation

period. For example, between December 15 and 18, 2010, there was an excursion of

MLD from ~5 m to ~60 m, yet the responses in chlorophyll were minimal. Nevertheless,

0-100 m correlations maintained a muted, yet similar pattern when compared to 2012-

2013 with a negative correlation between 20 and 30 m (r = −0.08; p = 0.04), and positive

correlations between 50 and 100 m (r = 0.13 to 0.26; p = < 0.001 to 0.002; Figures 17, 18,

21; Table 5). However, the correlations between temperature and chlorophyll were

largely similar to those observed during 2012-2013, as a warming temperature trend

combined with marginal chlorophyll reductions, creating negative correlations in the

upper 40 m (r = −0.62 to −0.18; $p < 0.001$), and covariance of the two variables creating positive correlations between 50 and 100 m (r = 0.19 to 0.60; $p < 0.001$; Figures 17, 18, 21; Table 5).

During the post-dissipation period (January 8-20, 2011), correlation patterns and underlying mechanics were similar to those observed during 2012-2013, albeit slightly weaker or less coupled. As was the case during the 2012-2013 post-dissipation, the long-duration wind event (January 10-18) produced a modest deepening in MLD. With minimal changes observed in chlorophyll in the upper 30 m, correlations between wind speed or MLD and chlorophyll are weak (respectively r = 0.04 to 0.06 and r = −0.07 to 0.15; $p = 0.28$ to 0.47 and $p = 0.01$ to 0.85; Figures 19, 20, 21; Table 5). At depths greater than 40 m, the reduction of any remaining chlorophyll following the onset of the long-duration wind event (January 10) drove negative correlations between wind speed and MLD with chlorophyll (respectively r = −0.28 to −0.05 and r = −0.28 to −0.12; $p = $ < 0.001 to 0.36 and $p = $ < 0.001 to 0.04; Figures 19, 20, 21; Table 5). Lastly, correlations between temperature and chlorophyll during the post-dissipation period are unexpectedly positive between 10 and 40 m (r = 0.17 to 0.35; $p = $ < 0.001 to 0.004). When compared to the negative correlations observed during the 2012-2013 post-dissipation driven by increases in temperature with chlorophyll disappearances in the surface, it appears that chlorophyll was beginning to increase in near-surface waters (January 11-20) likely the result of a secondary bloom event (Figures 19, 20, 21; Table 5).

2003-2006 Mooring Observations of Event-Scale Perturbations

Limited observations from the 2003-2006 IVARS Callinectes moorings provide

additional correlations, but by aligning with the depth where many of the correlations

change sign with depth the results may be confounding or unhelpful. That is, the depths

of the mooring CTDs (24 m) and fluorometers (21 or 23 m) were adjacent or aligned with

changes in correlational signs occurring either in the 20-30, 30-40, or 40-50 m bins. This

is likely due to limits on the influence of surface wind forcing upon chlorophyll changes

to a depth of 20-50 m. As a result, mooring correlations (respectively 2003-2004, 2004-

2005, 2005-2006) during the dissipation period for wind speed (r = 0.29, -0.39, -0.10; p

= < 0.001, < 0.001, 0.19) and temperature (r = n/a, 0.07, -0.78; p = n/a, 0.17, < 0.001),

expressed a wide range of relationships. During the post-dissipation period, correlations

(respectively for the three seasons) for wind speed (r = -0.31, 0.45, 0.12; p = < 0.001,

< 0.001, 0.03) were variable, although temperature (r = n/a, -0.81, -0.72; p = n/a,

< 0.001, < 0.001) displayed a strong negative relationship for the two seasons of data,

which agrees with the observations of negative correlations observed during the 2012-

2013 post-dissipation period (Figures 22, 23).

Correlations between Average Temperature and Chlorophyll

Strong, significant correlations between temperature and chlorophyll during the

accumulation period are complex and not easily understood. Observations during the

2012-2013 accumulation period indicate that positive correlations between temperature

and chlorophyll in the surface 30 m (r = 0.28 to 0.67; p < 0.001) could partially be the

product of the co-occurrence of increased biomass typically present during calm, shallow

79

MLDs periods and warming of shallow MLDs through surface heat inputs. The co-occurrence of two periodic patterns (diel fluorescence cycles in surface phytoplankton due to photochemical quenching and diurnal solar radiation heating) may also explain a component of the positive correlation present in the surface 30 m (Figure 28a). Observations of chlorophyll and temperature from the upper 30 m are indeed cyclic and patterns approximately align with local mid-day/UTC mid-night, but ample variability in surface waters appears to modify the pattern (Figures 10, 11). It has been shown in other oceanic systems that chlorophyll accumulations assist in energy (heat) capture and result in modest temperature increases (Lewis et al., 1983; Siegel et al., 1995), but it is unclear if this effect is occurring in the Ross Sea. Wind events (generally from the south, making them cold) tend to disrupt this pattern and drive surface cooling and decreased biomass. However, because these interpretations have the strongest effects in the surface 30 m of the water column (the approximate depth of the euphotic zone), other factors likely contribute to the strong, positive correlations between 0 and 100 m.

Ocean color satellite imagery has clearly demonstrated the presence of micro- to mesoscale variability in chlorophyll fluorescence measured to the first optical depth of $1/k$ meters (e.g., Arrigo and McClain, 1994), where k is the attenuation coefficient (typically 0.04 to 0.16 m^{-1} in the Ross Sea, which equates to an optical depth of ~6-25 m). Together with highly variable spatial observations of fluorescence (DiTullio et al., 2000; Smith et al., submitted), this suggests high spatial variability in the southwestern Ross Sea, including the regions of the glider and mooring observations, that occurs in addition to the known temporal variability. Thus during the 2012-2013 study period, the highly variable hydrographic and biological conditions formed a patchy mosaic of

environments (on the order of hours and several km) that were supportive of growth and/or biomass accumulation (relatively warm temperatures and shallow, strong MLDs) and others that were not (relatively cooler temperatures, deeper MLDs). As there is a great deal of agreement in the variations in temperature and chlorophyll across the upper 100 m during the 2012-2013 accumulation period (e.g., temperature increases in near surface 10 m bins were reflected in deeper 10 m bins, etc.), this suggests that patchiness is fairly homogenous across the upper 100 m and plays a role in driving the strong positive correlation between temperature and chlorophyll. While I have no data on vertical fluxes, based on the data of Kaufman et al. (2014) it is likely that when the processes of wind-driven aggregate formation and vertical flux act upon a patch supportive of elevated growth/biomass accumulation, it may promote elevated biomass conditions in the waters beneath the patch. Observations of the small-scale elevated patches diminished in magnitude with depth, suggesting that those aggregates and cells were being rapidly remineralized. Without full water column particulate matter profiles, it is impossible to quantify the amounts being delivered to the sediments.

The vertical synchrony between temperature and chlorophyll also suggests that tidal fluctuations, or perhaps internal waves, may have an influence on the strong co-variance and correlation between temperature and chlorophyll in the upper 100 m by driving the vertical displacement of isotherms and chlorophyll in synchrony. Maximum amplitudes of tides in the Ross Sea may be up to 3 m, with studies suggesting the greatest current speeds occurring over the continental shelf break, over shallow banks, or near ice shelves (Padman et al., 2003, 2009; Johnson and Van Woert, 2006). While the cyclic nature of temperature and chlorophyll appears to be dominated by a 24-h period,

substantial variability exists in the pattern over the course of the study period. With a dearth of available tidal height data for the Ross Sea, future analysis would be needed to investigate this potential linkage.

Throughout the dissipation period and partially into the post-dissipation period, increases in temperature are observed as a result of inputs of heat into surface waters. Heat inputs, in the form of solar radiation at the ocean surface, removal of insulating ice layers, shoaling of warm MCDW from depth, warmer air temperatures, and reduced wind speeds are known to promote temperature increases in the surface waters of the Ross Sea (Orsi and Wiederwohl, 2009; Smith et al., 2011a). The observed shifts across the upper 50 m of the water column from strong, positive correlations (r = 0.28 to 0.72; $p < 0.001$) during the accumulation period, to primarily negative correlations (r = −0.65 to 0.28; $p < 0.001$) appear to be the result of continued warming in concert with the reduction of chlorophyll in surface waters (Figures 12, 13, 16; Table 4). Warming is apparent in the upper 20 m (increases from approximately −1.0 to 0.5°C in the 0-10 m bin), while it is also visible at depths to 70 m, albeit with a delay (increases from approximately −1.8 to −0.8°C in the 60-70 m bin; Figures 12, 13).

By the post-dissipation period chlorophyll has further declined in the surface 10 m and continues to dissipate at depths from 10 to 100 m (Figures 14, 15).Waters continue to warm early in the period and then stabilize in the later part of the post-dissipation period. Correlations between temperature and chlorophyll remained similar to those observed during the dissipation period, but the depth of the negative correlation has deepened from 0 to 30 m (r = −0.41 to −0.65; $p < 0.001$) to 10 to 60 m depth (r = −0.57 to −0.24; $p < 0.001$) and a positive correlation appeared in the 0-10 m bin (r = 0.27; $p < 0.001$;

Figures 14, 15, 16; Table 4). The movement of negative correlations to depth is likely the result of both dissipating phytoplankton biomass via flux to depth and the continued warming of those waters (Figure 28b, 28c, 28d). With little biomass remaining in the surface 10 m and temperatures relatively stable, the positive correlation is likely the result of factors similar to those found during the accumulation period that cause covariance between the two variables.

SUMMARY AND CONCLUSIONS

With event-scale perturbations in phytoplankton biomass occurring over short spatial and temporal time spans, the utility of a high-resolution autonomous glider cannot be understated. Hydrographic and biological observations in the southwestern Ross Sea from two seasons of glider observations and three seasons of mooring observations have demonstrated that a complex interplay of variables induce responses in chlorophyll fluorescence. Differences in the variability, timing, and trends of chlorophyll demonstrated that the 2012-2013 variability was greater than the average of the five seasons, while the timing of the key transition from bloom to post-bloom levels were within a relatively limited 6 d window. Over the course of a season, perturbations or responses in chlorophyll were heavily influenced by the degree of temporal coupling between wind events and the depth of mixing (MLD), with greater delays observed early in the season that shortened following the transition from biomass maximum to biomass dissipation. Furthermore, by leading to aggregate formation and vertical flux of biomass material, physical forcing factors also contributed to observed perturbations through the reductions of biomass in surface layers and the appearance in deeper layers, with the rapid flux of material to depths below the mixed layer suggesting that MLD excursions alone could not explain these changes. It was less clear how the strong correlations between temperature and chlorophyll played an influence, through the correlational shift across the season can be attributed in part to the overall trend of chlorophyll biomass reduction with continued warming, in addition to the physical wind mixing and biological

84

turbulent aggregate formation processes. Further research on short-term, event-scale

perturbations of phytoplankton biomass is warranted to gather additional data on the

mechanisms driving these processes.

REFERENCES

Abrahamsen, E.P., 2014. Sustaining observations in the polar oceans. Philosophical Transactions of the Royal Society Series A 372, 20130337. doi:10.1098/rsta.2013.0337

Ainley, D.G., Ballard, G., Jones, R.M., Jongsomjit, D., Pierce, S.D., Smith, W.O., Veloz, S.D., 2015. Trophic cascades in the western Ross Sea, Antarctica: revisited. Marine Ecology Progress Series 534, 1–16. doi:10.3354/meps11394

Arrigo, K.R., 2014. Sea ice ecosystems. Annual Review of Marine Science 6, 439–467. doi:10.1146/annurev-marine-010213-135103

Arrigo, K.R., DiTullio, G.R., Dunbar, R.B., Robinson, D.H., Van Woert, M.L., Worthen, D.L., Lizotte, M.P., 2000. Phytoplankton taxonomic variability in nutrient utilization and primary production in the Ross Sea. Journal of Geophysical Research 105, 8827–8846.

Arrigo, K.R., McClain, C.R., 1994. Spring Phytoplankton Production in the Western Ross Sea. Science 266, 261–263. doi:10.1126/science.266.5183.261

Arrigo, K.R., Robinson, D.H., Worthen, D.L., Dunbar, R.B., DiTullio, G.R., Van Woert, M.L., Lizotte, M.P., 1999. Phytoplankton Community Structure and the Drawdown of Nutrients and CO_2 in the Southern Ocean. Science 283, 365–367. doi:10.1126/science.283.5400.365

Arrigo, K.R., Robinson, D.H., Worthen, D.L., Schieber, B., Lizotte, M.P., 1998a. Bio-optical properties of the southwestern Ross Sea. Journal of Geophysical Research 103, 21683–21695.

Arrigo, K.R., van Dijken, G.L., 2003. Phytoplankton dynamics within 37 Antarctic coastal polynya systems. Journal of Geophysical Research 108, 1–18. doi:10.1029/2002JC001739

Arrigo, K.R., van Dijken, G.L., 2004. Annual changes in sea-ice, chlorophyll *a*, and primary production in the Ross Sea, Antarctica. Deep Sea Research Part II 51, 117–138. doi:10.1016/j.dsr2.2003.04.003

Arrigo, K.R., van Dijken, G.L., Long, M.C., 2008. Coastal Southern Ocean: A strong anthropogenic CO_2 sink. Geophysical Research Letters 35, 1–6. doi:10.1029/2008GL035624

Arrigo, K.R., Weiss, A.M., Smith, W.O., 1998b. Physical forcing of phytoplankton
dynamics in the southwestern Ross Sea. Journal of Geophysical Research 103,
1007–1021.

Arrigo, K.R., Worthen, D.L., Schnell, A., Lizotte, M.P., 1998c. Primary production in
Southern Ocean waters. Journal of Geophysical Research 103, 15587–15600.

Asper, V.L., Smith, W.O., 1999. Particle fluxes during austral spring and summer in the
southern Ross Sea, Antarctica. Journal of Geophysical Research 104, 5345–5359.

Banse, K., 1996. Low seasonality of low concentrations of surface chlorophyll in the
Subantarctic water ring: underwater irradiance, iron, or grazing? Progress in
Oceanography 37, 241–291. doi:10.1016/S0079-6611(96)00006-7

Boss, E.S., Pegau, W.S., 2001. Relationship of light scattering at an angle in the
backward direction to the backscattering coefficient. Applied Optics 40, 5503–5507.

Boyd, P.W., 2002. Environmental Factors Controlling Phytoplankton Processes in the
Southern Ocean. Journal of Phycology 38, 844–861.

Bracegirdle, T.J., Kolstad, E.W., 2010. Climatology and variability of Southern
Hemisphere marine cold-air outbreaks. Tellus A 62, 202–208. doi:10.1111/j.1600-
0870.2009.00431.x

Burd, A.B., Jackson, G.A., 2009. Particle Aggregation. Annual Review of Marine
Science 1, 65–90. doi:10.1146/annurev.marine.010908.163904

Curry, B., Lee, C.M., Petrie, B., Moritz, R.E., Kwok, R., 2014. Multiyear Volume, Liquid
Freshwater, and Sea Ice Transports through Davis Strait, 2004–10*. Journal of
Physical Oceanography 44, 1244–1266. doi:10.1175/JPO-D-13-0177.1

Dinniman, M.S., Klinck, J.M., Smith, W.O., 2003. Cross-shelf exchange in a model of
the Ross Sea circulation and biogeochemistry. Deep Sea Research Part II 50, 3103–
3120. doi:10.1016/j.dsr2.2003.07.011

Dinniman, M.S., Klinck, J.M., Smith, W.O., 2007. Influence of sea ice cover and
icebergs on circulation and water mass formation in a numerical circulation model
of the Ross Sea, Antarctica. Journal of Geophysical Research 112, 1–13.
doi:10.1029/2006JC004036

DiTullio, G.R., Grebmeier, J.M., Arrigo, K.R., Lizotte, M.P., Robinson, D.H., Leventer,
A.R., Barry, J.P., Van Woert, M.L., Dunbar, R.B., 2000. Rapid and early export of
Phaeocystis antarctica blooms in the Ross Sea, Antarctica. Nature 404, 595–598.
doi:10.1038/35007061

DiTullio, G.R., Smith, W.O., 1996. Spatial patterns in phytoplankton biomass and
pigment distributions in the Ross Sea. Journal of Geophysical Research 101, 18467–

18477. doi:10.1029/96JC00034

Dunbar, R.B., Leventer, A.R., Mucciarone, D.A., 1998. Water column sediment fluxes in the Ross Sea, Antarctica: Atmospheric and sea ice forcing. Journal of Geophysical Research 103, 30741–30759. doi:10.1029/1998JC900001

El-Sayed, S.Z., Biggs, D.C., Holm-Hansen, O., 1983. Phytoplankton standing crop, primary productivity, and near-surface nitrogenous nutrient fields in the Ross Sea, Antarctica. Deep Sea Research Part A 30, 871–886.

Eriksen, C.C., Osse, T.J., Light, R.D., Wen, T., Lehman, T.W., Sabin, P.L., Ballard, J.W., Chiodi, A.M., 2001. Seaglider: a long-range autonomous underwater vehicle for oceanographic research. IEEE Journal of Oceanic Engineering 26, 424–436. doi:10.1109/48.972073

Garçon, V.C., Oschlies, A., Doney, S.C., McGillicuddy, D.J., Waniek, J.J., 2001. The role of mesoscale variability on plankton dynamics in the North Atlantic. Deep Sea Research Part II 48, 2199–2226. doi:10.1016/S0967-0645(00)00183-1

Gardner, W.D., Richardson, M.J., Smith, W.O., 2000. Seasonal patterns of water column particulate organic carbon and fluxes in the Ross Sea, Antarctica. Deep Sea Research Part II 47, 3423–3449.

Glenn, S.M., Jones, C., Twardowski, M.S., Bowers, L., Kerfoot, J., Kohut, J.T., Webb, D., Schofield, O.M., 2008. Glider observations of sediment resuspension in a Middle Atlantic Bight fall transition storm. Limnology and Oceanography 53, 2180–2196. doi:10.4319/lo.2008.53.5_part_2.2180

Glenn, S.M., Schofield, O.M., Kohut, J.T., McDonnell, J., Ludescher, R., Seidel, D., Aragon, D., Haskins, T., Handel, E., Haldeman, C., Heifetz, I., Kerfoot, J., Lemus, E., Lictenwalner, S., Ojanen, L., Roarty, H., Carvalho, F., Lopez, A., Martin, A., Jones, C., Webb, D., Miller, J., Lewis, M., McLean, S., Martins, A., Barrera, C., Ramos, A., Fanjul, E., 2011. The Trans-Atlantic Slocum Glider Expeditions: A Catalyst for Undergraduate Participation in Ocean Science and Technology. Marine Technology Society Journal 45, 52–67. doi:10.4031/MTSJ.45.1.12

Jacobs, S.S., Giulivi, C.F., 2010. Large Multidecadal Salinity Trends near the Pacific–Antarctic Continental Margin. Journal of Climate 23, 4508–4524. doi:10.1175/2010JCLI3284.1

JGOFS, 1996. Protocols for the Joint Global Ocean Flux Study (JGOFS) Core Measurements, IOC SCOR Rpt. 19. Bergen, Norway.

Johnson, E.S., Van Woert, M.L., 2006. Tidal currents of the Ross Sea and their time stability. Antarctic Science 18, 141–154. doi:10.1017/S0954102006000137

Johnson, K.S., Coletti, L.J., 2002. In situ ultraviolet spectrophotometry for high

resolution and long-term monitoring of nitrate, bromide and bisulfide in the ocean. Deep Sea Research Part I 49, 1291–1305. doi:10.1016/S0967-0637(02)00020-1

Kaufman, D.E., Friedrichs, M.A.M., Smith, W.O., Queste, B.Y., Heywood, K.J., 2014. Biogeochemical Variability in the Southern Ross Sea as Observed by a Glider Deployment. Deep Sea Research Part I 92, 93–106.

L'Héveéder, B., Mortier, L., Testor, P., Lekien, F., 2013. A Glider Network Design Study for a Synoptic View of the Oceanic Mesoscale Variability. Journal of Atmospheric and Oceanic Technology 30, 1472–1493. doi:10.1175/JTECH-D-12-00053.1

Lewis, M.R., Cullen, J.J., Platt, T., 1983. Phytoplankton and thermal structure in the upper ocean: Consequences of nonuniformity in chlorophyll profile. Journal of Geophysical Research 88, 2565–2570. doi:10.1029/JC088iC04p02565

Long, M.C., Dunbar, R.B., Tortell, P.D., Smith, W.O., Mucciarone, D.A., Ditullio, G.R., 2011. Vertical structure, seasonal drawdown, and net community production in the Ross Sea, Antarctica. Journal of Geophysical Research: Oceans 116, 1–19. doi:10.1029/2009JC005954

Mahadevan, A., D'Asaro, E.A., Lee, C.M., Perry, M.J., 2012. Eddy-driven stratification initiates North Atlantic spring phytoplankton blooms. Science 337, 54–58.

McGillicuddy, D.J., Sedwick, P.N., Dinniman, M.S., Arrigo, K.R., Bibby, T.S., Greenan, B.J.W., Hofmann, E.E., Klinck, J.M., Smith, W.O., Mack, S.L., Marsay, C.M., Sohst, B.M., van Dijken, G.L., 2015. Iron supply and demand in an Antarctic shelf ecosystem. Geophysical Research Letters 42, 8088–8097. doi:10.1002/2015GL065727

Mignot, A., Ferrari, R., Mork, K.A., 2015. Spring bloom onset in the Nordic Seas. Biogeosciences Discussions 12, 13631–13673. doi:10.5194/bgd-12-13631-2015

Miles, T.N., Seroka, G.N., Kohut, J.T., Schofield, O.M., Glenn, S.M., 2015. Glider observations and modeling of sediment transport in Hurricane Sandy. Journal of Geophysical Research: Oceans 120, 1771–1791. doi:10.1002/2014JC010474

Morel, A., 1974. Optical properties of pure water and pure sea water. Optical Aspects of Oceanography 1.

Mrvaljevic, R.K., Black, P.G., Centurioni, L.R., Chang, Y.T., D'Asaro, E. a., Jayne, S.R., Lee, C.M., Lien, R.C., Lin, I.I., Morzel, J., Niiler, P.P., Rainville, L., Sanford, T.B., 2013. Observations of the cold wake of Typhoon Fanapi (2010). Geophysical Research Letters 40, 316–321. doi:10.1029/2012GL054282

Nelson, D.M., DeMaster, D.J., Dunbar, R.B., Smith, W.O., 1996. Cycling of organic carbon and biogenic silica in the Southern Ocean: Estimates of water-column and sedimentary fluxes on the Ross Sea continental shelf. Journal of Geophysical

Research 101, 18519–18532.

Orsi, A.H., Wiederwohl, C.L., 2009. A recount of Ross Sea waters. Deep Sea Research Part II 56, 778–795. doi:10.1016/j.dsr2.2008.10.033

Padman, L., Erofeeva, S., Joughin, I., 2003. Tides of the Ross Sea and Ross Ice Shelf cavity. Antarctic Science 15, 31–40. doi:10.1017/S0954102003001032

Padman, L., Howard, S.L., Orsi, A.H., Muench, R.D., 2009. Tides of the northwestern Ross Sea and their impact on dense outflows of Antarctic Bottom Water. Deep Sea Research Part II 56, 818–834. doi:10.1016/j.dsr2.2008.10.026

Parkinson, C.L., Cavalieri, D.J., 2012. Antarctic sea ice variability and trends, 1979-2010. Cryosphere 6, 871–880. doi:10.5194/tc-6-871-2012

Peloquin, J.A., Smith, W.O., 2007. Phytoplankton blooms in the Ross Sea, Antarctica: Interannual variability in magnitude, temporal patterns, and composition. Journal of Geophysical Research 112, 1–12. doi:10.1029/2006JC003816

Pinkerton, M.H., Bradford-Grieve, J.M., 2014. Characterizing foodweb structure to identify potential ecosystem effects of fishing in the Ross Sea, Antarctica. ICES Journal of Marine Science 71, 1542–1553.

Piterbarg, L., Taillandier, V., Griffa, A., 2014. Investigating frontal variability from repeated glider transects in the Ligurian Current (North West Mediterranean Sea). Journal of Marine Systems 129, 381–395. doi:10.1016/j.jmarsys.2013.08.003

Queste, B.Y., 2013. Hydrographic Observations of Oxygen and Related Physical Variables in the North Sea and Western Ross Sea Polynya. University of East Anglia.

Queste, B.Y., Fernand, L., Jickells, T.D., Heywood, K.J., Hind, A.J., 2015a. Drivers of summer oxygen depletion in the central North Sea. Biogeosciences Discussions 12, 8691–8722. doi:10.5194/bgd-12-8691-2015

Queste, B.Y., Heywood, K.J., Smith, W.O., Kaufman, D.E., Jickells, T.D., Dinniman, M.S., 2015b. Observations of dissolved oxygen dynamics during a phytoplankton bloom in the Ross Sea polynya. Antarctic Science 1–11. doi:10.1017/S0954102014000881

Riser, S.C., Johnson, K.S., 2008. Net production of oxygen in the subtropical ocean. Nature 451, 323–325. doi:10.1038/nature06441

Rudnick, D.L., Davis, R.E., Eriksen, C.C., Fratantoni, D.M., Perry, M.J., 2004. Underwater Gliders for Ocean Research. Marine Technology Society Journal 38, 73–84. doi:10.4031/002533204787522703

Sedwick, P.N., DiTullio, G.R., Mackey, D.J., 2000. Iron and manganese in the Ross Sea, Antarctica: Seasonal iron limitation in Antarctic shelf waters. Journal of Geophysical Research 105, 11321–11336. doi:10.1029/2000JC000256

Sedwick, P.N., Marsay, C.M., Sohst, B.M., Aguilar-Islas, A.M., Lohan, M.C., Long, M.C., Arrigo, K.R., Dunbar, R.B., Saito, M.A., Smith, W.O., DiTullio, G.R., 2011. Early season depletion of dissolved iron in the Ross Sea polynya: Implications for iron dynamics on the Antarctic continental shelf. Journal of Geophysical Research 116, 1–19. doi:10.1029/2010JC006553

Siegel, D.A., Ohlmann, J.C., Washburn, L., Bidigare, R.R., Nosse, C.T., Fields, E., Zhou, Y., 1995. Solar radiation, phytoplankton pigments and the radiant heating of the equatorial Pacific warm pool. Journal of Geophysical Research 100, 4885–4891. doi:10.1029/94JC03128

Smith, W.O., Ainley, D.G., Arrigo, K.R., Dinniman, M.S., 2014a. The Oceanography and Ecology of the Ross Sea. Annual Review of Marine Science 6, 469–487. doi:10.1146/annurev-marine-010213-135114

Smith, W.O., Asper, V.L., Tozzi, S., Liu, X., Stammerjohn, S.E., 2011a. Surface layer variability in the Ross Sea, Antarctica as assessed by in situ fluorescence measurements. Progress in Oceanography 88, 28–45. doi:10.1016/j.pocean.2010.08.002

Smith, W.O., Comiso, J.C., 2008. Influence of sea ice on primary production in the Southern Ocean: A satellite perspective. Journal of Geophysical Research 113, 1–19. doi:10.1029/2007JC004251

Smith, W.O., Dennett, M.R., Mathot, S., Caron, D.A., 2003a. The temporal dynamics of the flagellated and colonial stages of *Phaeocystis antarctica* in the Ross Sea. Deep Sea Research Part II 50, 605–617. doi:10.1016/S0967-0645(02)00586-6

Smith, W.O., Dinniman, M.S., Hofmann, E.E., Klinck, J.M., 2014b. The effects of changing winds and temperatures on the oceanography of the Ross Sea in the 21st century. Geophysical Research Letters 41, 1624–1631.

Smith, W.O., Dinniman, M.S., Klinck, J.M., Hofmann, E.E., 2003b. Biogeochemical climatologies in the Ross Sea, Antarctica: Seasonal patterns of nutrients and biomass. Deep Sea Research Part II 50, 3083–3101. doi:10.1016/j.dsr2.2003.07.010

Smith, W.O., Dinniman, M.S., Tozzi, S., DiTullio, G.R., Mangoni, O., Modigh, M., Saggiomo, V., 2010. Phytoplankton photosynthetic pigments in the Ross Sea: Patterns and relationships among functional groups. Journal of Marine Systems 82, 177–185. doi:10.1016/j.jmarsys.2010.04.014

Smith, W.O., Donaldson, K., 2015. Photosynthesis–irradiance responses in the Ross Sea,

Antarctica: a meta-analysis. Biogeosciences 12, 3567–3577. doi:10.5194/bg-12-3567-2015

Smith, W.O., Goetz, K.T., Kaufman, D.E., Queste, B.Y., Asper, V.L., Costa, D.P., Dinniman, M.S., Friedrichs, M.A.M., Hofmann, E.E., Heywood, K.J., Klinck, J.M., Kohut, J.T., Lee, C.M., 2014c. Multiplatform, Multidisciplinary Investigations of the Impacts of Modified Circumpolar Deep Water in the Ross Sea, Antarctica. Oceanography 27, 180–185.

Smith, W.O., Gordon, L.I., 1997. Hyperproductivity of the Ross Sea (Antarctica) polynya during austral spring. Geophysical Research Letters 24, 233–236. doi:10.1029/96GL03926

Smith, W.O., Jones, R.M., 2015. Vertical mixing, critical depths, and phytoplankton growth in the Ross Sea. ICES Journal of Marine Science 72, 1–9. doi:10.1093/icesjms/fsu234

Smith, W.O., Marra, J., Hiscock, M.R., Barber, R.T., 2000. The seasonal cycle of phytoplankton biomass and primary productivity in the Ross Sea, Antarctica. Deep Sea Research Part II 47, 3119–3140.

Smith, W.O., Nelson, D.M., 1985. Phytoplankton Bloom Produced by a Receding Ice Edge in the Ross Sea: Spatial Coherence with the Density Field. Science 227, 163–166.

Smith, W.O., Nelson, D.M., DiTullio, G.R., Leventer, A.R., 1996. Temporal and spatial patterns in the Ross Sea: Phytoplankton biomass, elemental composition, productivity and growth rates. Journal of Geophysical Research 101, 18455–18465. doi:10.1029/96JC01304

Smith, W.O., Sakshaug, E., 1990. Polar Phytoplankton, in: Smith, W.O. (Ed.), Polar Oceanography Part B: Chemistry, Biology, and Geology. Academic Press, San Diego, CA, pp. 477–525.

Smith, W.O., Shields, A.R., Dreyer, J.C., Peloquin, J.A., Asper, V.L., 2011b. Interannual variability in vertical export in the Ross Sea: Magnitude, composition, and environmental correlates. Deep Sea Research Part I 58, 147–159. doi:10.1016/j.dsr.2010.11.007

Smith, W.O., Shields, A.R., Peloquin, J.A., Catalano, G., Tozzi, S., Dinniman, M.S., Asper, V.L., 2006. Interannual variations in nutrients, net community production, and biogeochemical cycles in the Ross Sea. Deep Sea Research Part II 53, 815–833. doi:10.1016/j.dsr2.2006.02.014

Smith, W.O., Tozzi, S., Long, M.C., Sedwick, P.N., Peloquin, J.A., Dunbar, R.B., Hutchins, D.A., Kolber, Z., DiTullio, G.R., 2013. Spatial and temporal variations in

variable fluoresence in the Ross Sea (Antarctica): Oceanographic correlates and bloom dynamics. Deep Sea Research Part I 79, 141–155. doi:10.1016/j.dsr.2013.05.002

Spreen, G., Kaleschke, L., Heygster, G., 2008. Sea ice remote sensing using AMSR-E 89-GHz channels. Journal of Geophysical Research: Oceans 113, 1–14. doi:10.1029/2005JC003384

Stammerjohn, S.E., Martinson, D.G., Smith, R.C., Yuan, X., Rind, D., 2008. Trends in Antarctic annual sea ice retreat and advance and their relation to El Niño–Southern Oscillation and Southern Annular Mode variability. Journal of Geophysical Research 113, 1–20. doi:10.1029/2007JC004269

Stramski, D., Reynolds, R.A., Kahru, M., Mitchell, B.G., 1999. Estimation of Particulate Organic Carbon in the Ocean from Satellite Remote Sensing. Science 285, 239–242. doi:10.1126/science.285.5425.239

Stramski, D., Reynolds, R.A., Mitchell, B.G., 1998. Relationship Between the Backscattering Coefficient, Beam Attenuation Coefficient and Particulate Organic Matter Concentrations in the Ross Sea. Proceedings of Ocean Optics 1–10.

Thompson, A.F., Heywood, K.J., Schmidtko, S., Stewart, A.L., 2014. Eddy transport as a key component of the Antarctic overturning circulation. Nature Geoscience 7, 879–884. doi:10.1038/NGEO2289

Thomson, R.E., Fine, I. V., 2003. Estimating mixed layer depth from oceanic profile data. Journal of Atmospheric and Oceanic Technology 20, 319–329.

Waniek, J.J., 2003. The role of physical forcing in initiation of spring blooms in the northeast Atlantic. Journal of Marine Systems 39, 57–82. doi:10.1016/S0924-7963(02)00248-8

Worby, A.P., Geiger, C.A., Paget, M.J., Van Woert, M.L., Ackley, S.F., DeLiberty, T.L., 2008. Thickness distribution of Antarctic sea ice. Journal of Geophysical Research: Oceans 113, 1–14. doi:10.1029/2007JC004254

Table 2: Overview of variables measured by the three gliders and automatic weather stations during the accumulation (December 1 - 14), dissipation (December 14 - January 7), and post-dissipation (January 7-19) periods. Values are averages and values in parentheses are ARIMA model residual variances. SST = sea surface temperature; SSS = sea surface salinity; SSD = sea surface density; MLD = mixed layer depth; Chl = chlorophyll.

Variable - Data Set	Accumulation	Dissipation	Post-Dissipation
SST - SG502, 2010-11 [°C]	n/a	-0.72 (0.11)	0.14 (0.10)
SST - SG503, 2010-11 [°C]	-1.72 (0.03)	-0.69 (0.19)	-0.16 (0.02)
SST - SG503, 2012-13 [°C]	-1.14 (0.17)	-0.04 (0.33)	0.70 (0.18)
SSS - SG502, 2010-11 [unitless]	n/a	34.403 (0.007)	34.367 (0.007)
SSS - SG503, 2010-11 [unitless]	34.510 (0.007)	34.461 (0.005)	34.419 (0.004)
SSS - SG503, 2012-13 [unitless]	34.409 (0.011)	34.131 (0.060)	34.222 (0.010)
SSD - SG502, 2010-11 [kg m^{-3}]	n/a	27.681 (0.003)	27.604 (0.003)
SSD - SG503, 2010-11 [kg m^{-3}]	27.787 (0.005)	27.709 (0.004)	27.651 (0.002)
SSD - SG503, 2012-13 [kg m^{-3}]	27.687 (0.007)	27.408 (0.045)	27.442 (0.009)
MLD - SG502, 2010-11 [m]	n/a	22.0 (220.3)	22.1 (154.5)
MLD - SG503, 2010-11 [m]	82.3 (1931.7)	21.5 (237.3)	29.8 (150.2)
MLD - SG503, 2012-13 [m]	21.7 (616.9)	16.3 (331.6)	13.4 (58.2)
Avg 0-50 m Chl - SG502, 2010-11 [mg Chl m^{-3}]	n/a	3.21 (0.63)	1.28 (0.07)
Avg 0-50 m Chl - SG503, 2012-13 [mg Chl m^{-3}]	4.79 (1.27)	3.34 (1.32)	1.12 (0.10)
Wind Speed - 2010-11 [m s^{-1}]	8.4 (14.7)	3.5 (4.9)	5.4 (9.3)
Wind Speed - 2012-13 [m s^{-1}]	4.1 (11.0)	3.8 (9.2)	3.2 (6.6)
Wind Direction - 2010-11 [°]	216 (2459)	186 (6079)	197 (2974)
Wind Direction - 2012-13 [°]	222 (4424)	167 (8199)	193 (9271)

Table 3: Overview of variables measured by the *Callinectes* moorings and by the gliders filtered to the same depths during the accumulation (December 1-14), dissipation (December 14 - January 7), and post-dissipation (January 7-19) periods. Values are averages and values in parentheses are ARIMA model residual variances.

Variable - Data Set	Accumulation	Dissipation	Post-Dissipation
Temperature at 24 m - *Callinectes*, 2004-05 [°C]	n/a	−0.79 (0.13)	−0.44 (0.07)
Temperature at 24 m - *Callinectes*, 2005-06 [°C]	n/a	−0.70 (0.18)	−0.11 (0.10)
Temperature at 24 m - SG502, 2010-11 [°C]	n/a	−1.13 (0.10)	−0.09 (0.08)
Temperature at 24 m - SG503, 2010-11 [°C]	−1.77 (0.02)	−1.06 (0.18)	−0.28 (0.04)
Temperature at 24 m - SG503, 2012-13 [°C]	−1.46 (0.05)	−0.82 (0.28)	0.08 (0.20)
Density at 24 m - *Callinectes*, 2004-05 [kg m^{-3}]	n/a	27.723 (4.6E-04)	27.697 (1.1E-04)
Density at 24 m - *Callinectes*, 2005-06 [kg m^{-3}]	n/a	27.685 (3.8E-04)	27.632 (7.3E-04)
Density at 24 m - SG502, 2010-11 [kg m^{-3}]	n/a	27.710 (1.3E-03)	37.628 (1.2E-03)
Density at 24 m - SG503, 2010-11 [kg m^{-3}]	27.791 (6.2E-03)	27.726 (2.5E-03)	27.658 (2.0E-03)
Density at 24 m - SG503, 2012-13 [kg m^{-3}]	27.721 (1.5E-03)	27.584 (1.3E-02)	27.515 (2.3E-03)
Fluorescence at 21 m - *Callinectes*, 2003-04 [RFU]	n/a	2031 (2.75E+05)	860 (1.21E+05)
Fluorescence at 23 m - *Callinectes*, 2004-05 [RFU]	n/a	1553 (3.83E+05)	430 (4.22E+04)
Fluorescence at 21 m - *Callinectes*, 2005-06 [RFU]	n/a	2314 (1.29E+06)	831 (4.77E+04)
Fluorescence at 21 m - SG502, 2010-11 [RFU]	n/a	1495 (3.75E+05)	469 (4.10E+04)
Fluorescence at 21 m - SG503, 2012-13 [RFU]	2429 (4.33E+05)	1839 (1.12E+06)	370 (5.02E+04)

Table 4: Pearson product-moment correlation coefficients and test p-values between wind speed, mixed layer depth, or average 0-50 m chlorophyll with average 0-50 m chlorophyll during SG503, 2012-2013 for the accumulation (December 1-14), dissipation (December 14 - January 7), and post-dissipation (January 7-19) periods.

Variable (Depth Bin)	Accumulation r value	p	Dissipation r value	p	Post-Dissipation r value	p
Wind Speed (0-10 m)	0.238	0.000	0.030	0.471	0.060	0.313
Wind Speed (10-20 m)	0.304	0.000	−0.150	0.000	−0.227	0.000
Wind Speed (20-30 m)	0.208	0.000	−0.062	0.135	−0.305	0.000
Wind Speed (30-40 m)	0.062	0.278	0.144	0.001	−0.252	0.000
Wind Speed (40-50 m)	−0.205	0.000	0.322	0.000	−0.138	0.019
Wind Speed (50-60 m)	−0.462	0.000	0.397	0.000	−0.189	0.001
Wind Speed (60-70 m)	−0.490	0.000	0.395	0.000	−0.153	0.009
Wind Speed (70-80 m)	−0.514	0.000	0.323	0.000	−0.203	0.001
Wind Speed (80-90 m)	−0.449	0.000	0.288	0.000	−0.226	0.000
Wind Speed (90-100 m)	−0.392	0.000	0.204	0.000	−0.254	0.000
Mixed Layer Depth (0-10 m)	−0.398	0.000	0.025	0.547	−0.170	0.004
Mixed Layer Depth (10-20 m)	−0.426	0.000	−0.264	0.000	−0.321	0.000
Mixed Layer Depth (20-30 m)	−0.346	0.000	−0.204	0.000	−0.339	0.000
Mixed Layer Depth (30-40 m)	−0.114	0.046	0.006	0.883	−0.363	0.000
Mixed Layer Depth (40-50 m)	0.041	0.467	0.154	0.000	−0.359	0.000
Mixed Layer Depth (50-60 m)	0.145	0.011	0.344	0.000	−0.355	0.000
Mixed Layer Depth (60-70 m)	0.173	0.002	0.360	0.000	−0.328	0.000
Mixed Layer Depth (70-80 m)	0.118	0.038	0.480	0.000	−0.293	0.000
Mixed Layer Depth (80-90 m)	0.082	0.149	0.485	0.000	−0.239	0.000
Mixed Layer Depth (90-100 m)	−0.029	0.615	0.372	0.000	−0.139	0.019
Average Temperature (0-10 m)	0.281	0.000	−0.441	0.000	0.271	0.000
Average Temperature (10-20 m)	0.585	0.000	−0.651	0.000	−0.339	0.000
Average Temperature (20-30 m)	0.671	0.000	−0.413	0.000	−0.574	0.000
Average Temperature (30-40 m)	0.708	0.000	−0.062	0.135	−0.571	0.000
Average Temperature (40-50 m)	0.718	0.000	0.283	0.000	−0.427	0.000
Average Temperature (50-60 m)	0.702	0.000	0.510	0.000	−0.237	0.000
Average Temperature (60-70 m)	0.787	0.000	0.594	0.000	−0.085	0.150
Average Temperature (70-80 m)	0.846	0.000	0.726	0.000	−0.001	0.988
Average Temperature (80-90 m)	0.867	0.000	0.757	0.000	0.059	0.321
Average Temperature (90-100 m)	0.869	0.000	0.716	0.000	0.220	0.000

Table 5: Pearson product-moment correlation coefficients and test *p*-values between wind speed, mixed layer depth, or average 0-50 m chlorophyll with average 0-50 m chlorophyll during SG502, 2010-2011 for the accumulation (December 2-15), dissipation (December 15 - January 8), and post-dissipation (January 8-20) periods.

Variable (Depth Bin)	Accumulation		Dissipation		Post-Dissipation	
	r value	*p*	r value	*p*	r value	*p*
Wind Speed (0-10 m)	n/a	n/a	0.050	0.236	0.064	0.284
Wind Speed (10-20 m)	n/a	n/a	−0.012	0.770	0.055	0.355
Wind Speed (20-30 m)	n/a	n/a	−0.148	0.000	0.043	0.465
Wind Speed (30-40 m)	n/a	n/a	−0.112	0.007	−0.282	0.000
Wind Speed (40-50 m)	n/a	n/a	−0.066	0.113	−0.213	0.000
Wind Speed (50-60 m)	n/a	n/a	−0.089	0.033	−0.185	0.002
Wind Speed (60-70 m)	n/a	n/a	−0.049	0.244	−0.151	0.011
Wind Speed (70-80 m)	n/a	n/a	−0.081	0.054	−0.129	0.029
Wind Speed (80-90 m)	n/a	n/a	−0.089	0.033	−0.096	0.106
Wind Speed (90-100 m)	n/a	n/a	−0.060	0.149	−0.055	0.357
Mixed Layer Depth (0-10 m)	n/a	n/a	0.200	0.000	0.148	0.012
Mixed Layer Depth (10-20 m)	n/a	n/a	0.039	0.345	0.011	0.851
Mixed Layer Depth (20-30 m)	n/a	n/a	−0.084	0.044	−0.071	0.229
Mixed Layer Depth (30-40 m)	n/a	n/a	−0.024	0.565	−0.276	0.000
Mixed Layer Depth (40-50 m)	n/a	n/a	0.070	0.096	−0.247	0.000
Mixed Layer Depth (50-60 m)	n/a	n/a	0.186	0.000	−0.164	0.005
Mixed Layer Depth (60-70 m)	n/a	n/a	0.219	0.000	−0.162	0.006
Mixed Layer Depth (70-80 m)	n/a	n/a	0.260	0.000	−0.166	0.005
Mixed Layer Depth (80-90 m)	n/a	n/a	0.170	0.000	−0.151	0.011
Mixed Layer Depth (90-100 m)	n/a	n/a	0.127	0.002	−0.119	0.044
Average Temperature (0-10 m)	n/a	n/a	−0.517	0.000	0.095	0.110
Average Temperature (10-20 m)	n/a	n/a	−0.616	0.000	0.352	0.000
Average Temperature (20-30 m)	n/a	n/a	−0.410	0.000	0.321	0.000
Average Temperature (30-40 m)	n/a	n/a	−0.179	0.000	0.169	0.004
Average Temperature (40-50 m)	n/a	n/a	0.068	0.104	−0.070	0.237
Average Temperature (50-60 m)	n/a	n/a	0.191	0.000	−0.073	0.217
Average Temperature (60-70 m)	n/a	n/a	0.357	0.000	−0.017	0.769
Average Temperature (70-80 m)	n/a	n/a	0.477	0.000	−0.010	0.860
Average Temperature (80-90 m)	n/a	n/a	0.552	0.000	0.087	0.143
Average Temperature (90-100 m)	n/a	n/a	0.605	0.000	0.194	0.001

Figure 5: Conceptual representation of bloom progression in the southern Ross Sea. Irradiance (dotted purple line) increases to a seasonal maximum on December 21. Sea ice cover (dotted black line) decreases rapidly beginning in early November and reach a minimum in February. Similarly, mixed layer depths (orange line) decrease rapidly beginning in early November and become shallowest in January. Chlorophyll concentrations (green line) increase rapidly in November, with a maximum in December, and an extremely rapid decrease in early January. Initial spring increases in chlorophyll are primarily due to the growth and accumulation of the haptophyte, *Phaeocystis antarctica* (red line), whereas summer increases are typically due to the growth and accumulation of diatoms (blue line). All variables are representative and plotted on a relative scale from 0-100%. Modified from Smith et al. (2014a).
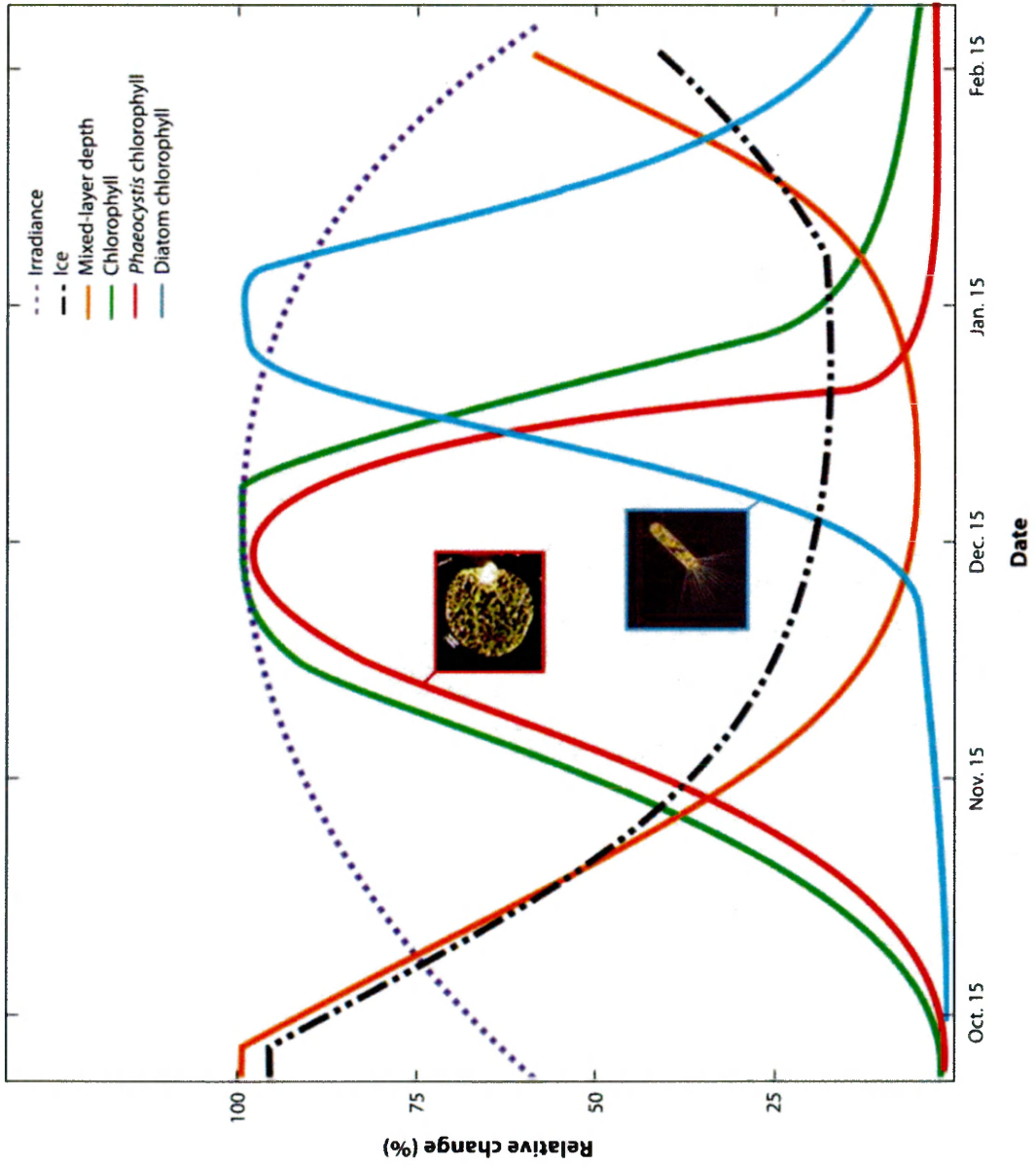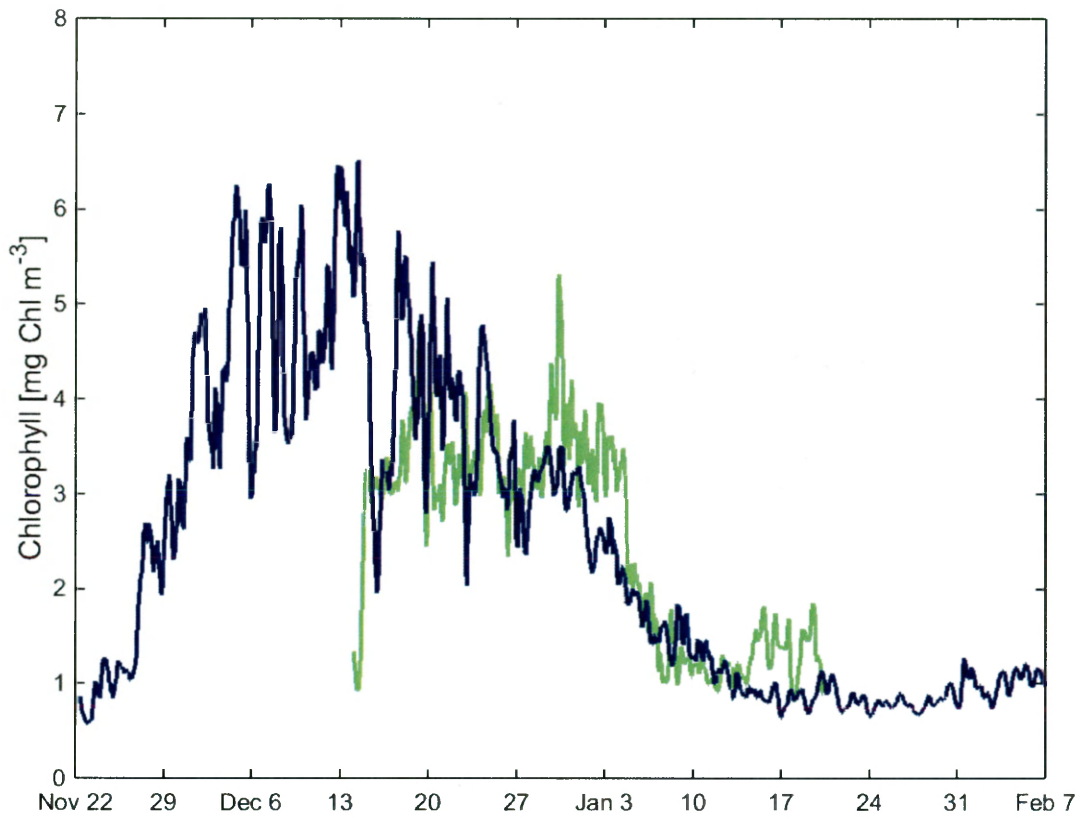
Figure 6: Climatology for chlorophyll *a* (Chl) over two seasons, 2010-2011 (green line) and 2012-2013 (blue line). Glider chlorophyll *a* values have been averaged over the top 50 m of the water column.

Figure 7: (a) Seaglider locations for SG502, 2010-2011 (green line), SGSG503 2010-2011 (light blue line), and SG503, 2012-2013 (dark blue line). Major features and instrumentation are marked: A. McMurdo Sound, B. Central Basin, C. Crary Bank, D. Pennell Bank, E. Ross Bank, F. Ross Island, G. Cape Crozier, H. Ross Ice Shelf, I. *Callinectes* Mooring, J. Laurie II AWS, and K. Ferrell AWS. Bathymetry data (in meters) retrieved from the Bedmap2 data set (Fretwell et al., 2013). Gray shading indicates topography above sea level. Figure and figure script adapted from Kaufman et al., (2014). **(b)** Close-up of SG503_2012 (dark blue line) locations.
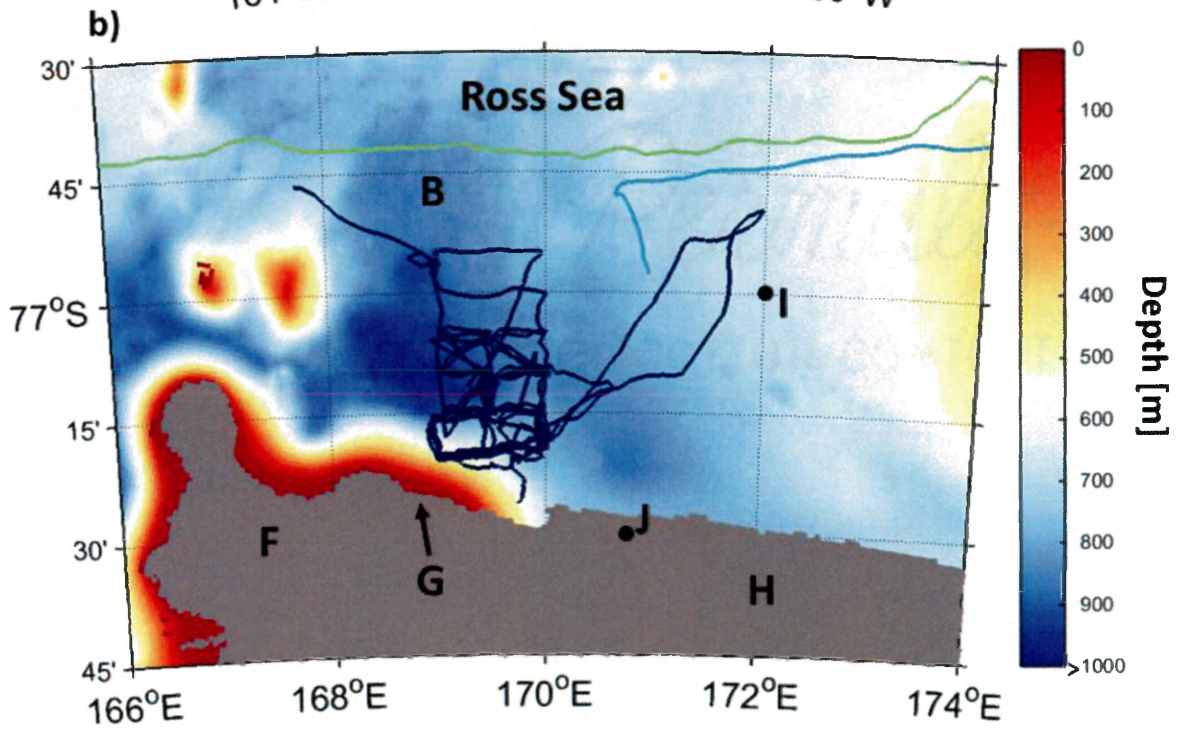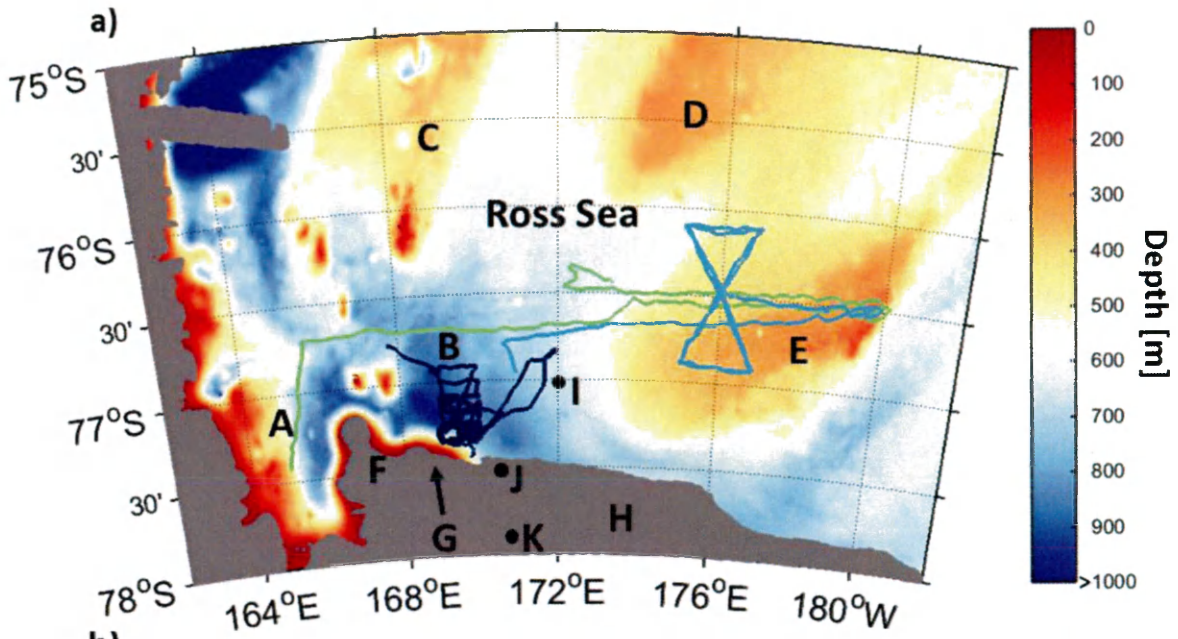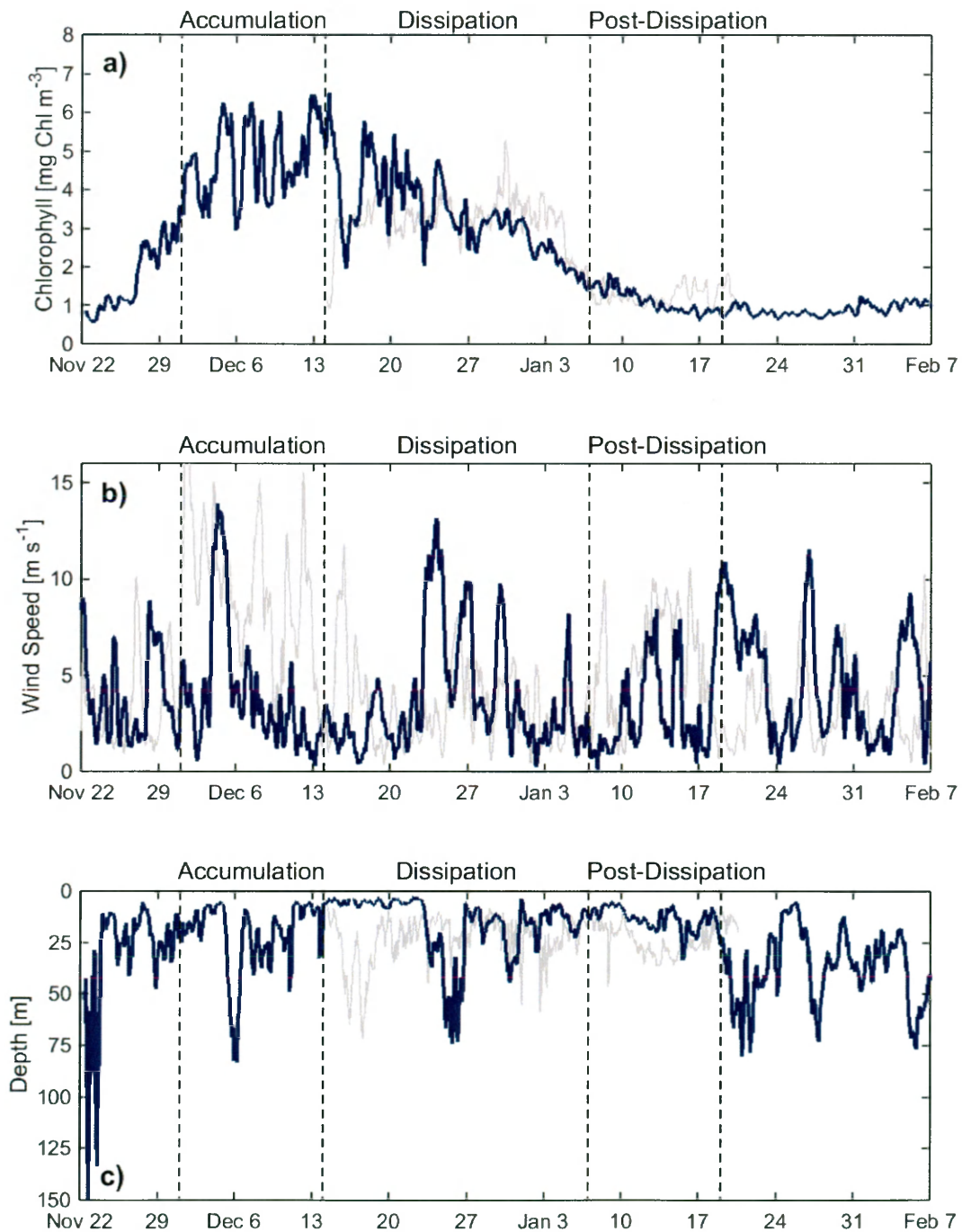
Figure 8: (**a**) Average 0-50 m chlorophyll, (**b**) wind speed, and (**c**) mixed layer depth for SG503, 2012-2013 are shown as dark blue lines. SG502, 2010-2011 is shown in the background as gray lines (see text for SG502, 2010-2011 period definitions). Accumulation (December 1-14), dissipation (December 14 – January 7), and post-dissipation periods (January 7-19) are indicated by vertical, dashed lines.

103
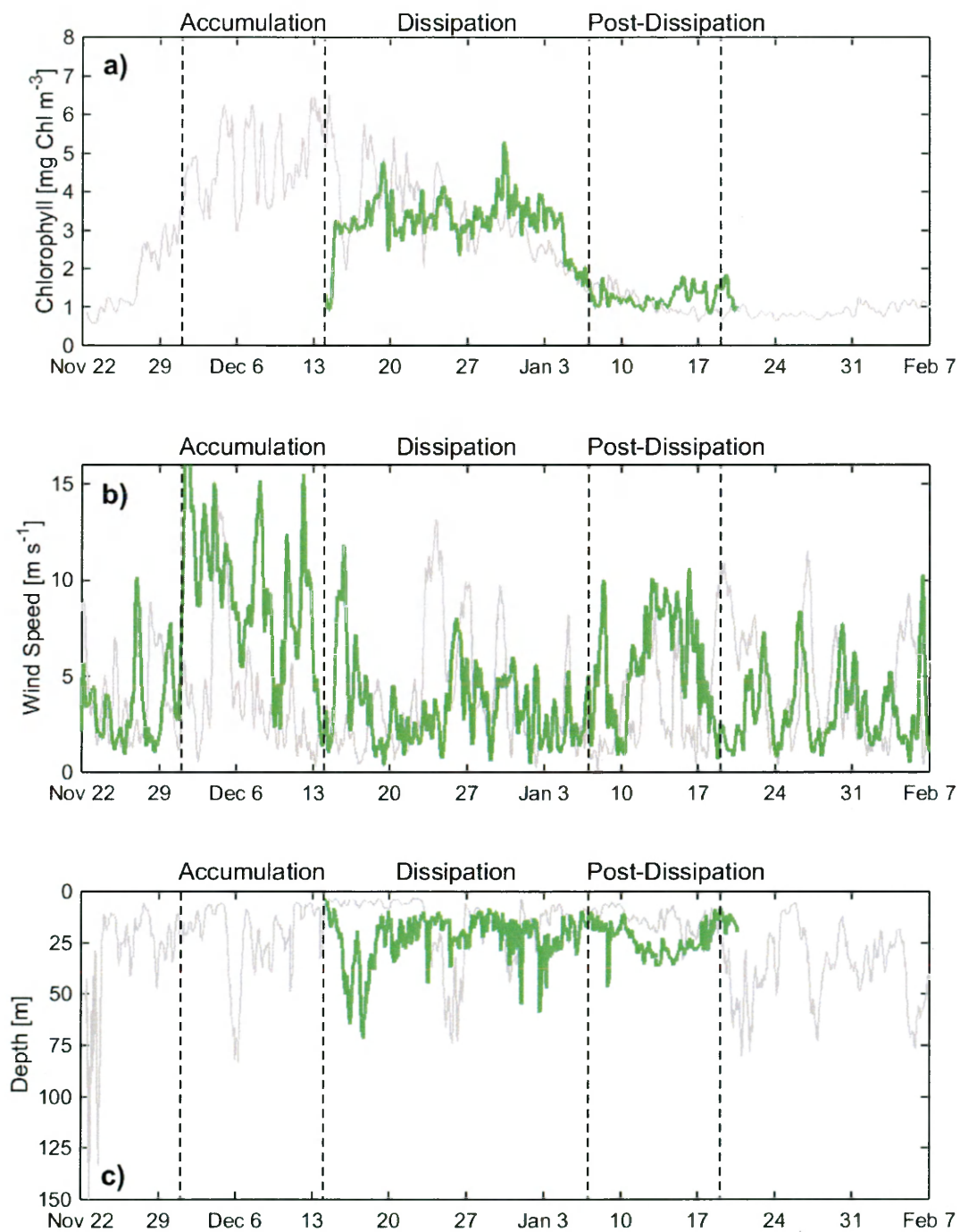
Figure 9: (**a**) Average 0-50 m chlorophyll, (**b**) wind speed, and (**c**) mixed layer depth for SG502, 2010-2011 are shown as green lines. SG503, 2012-2013 is shown in the background as gray lines. Accumulation (December 1-14), dissipation (December 14 – January 7), and post-dissipation periods (January 7-19) are indicated by vertical, dashed lines.
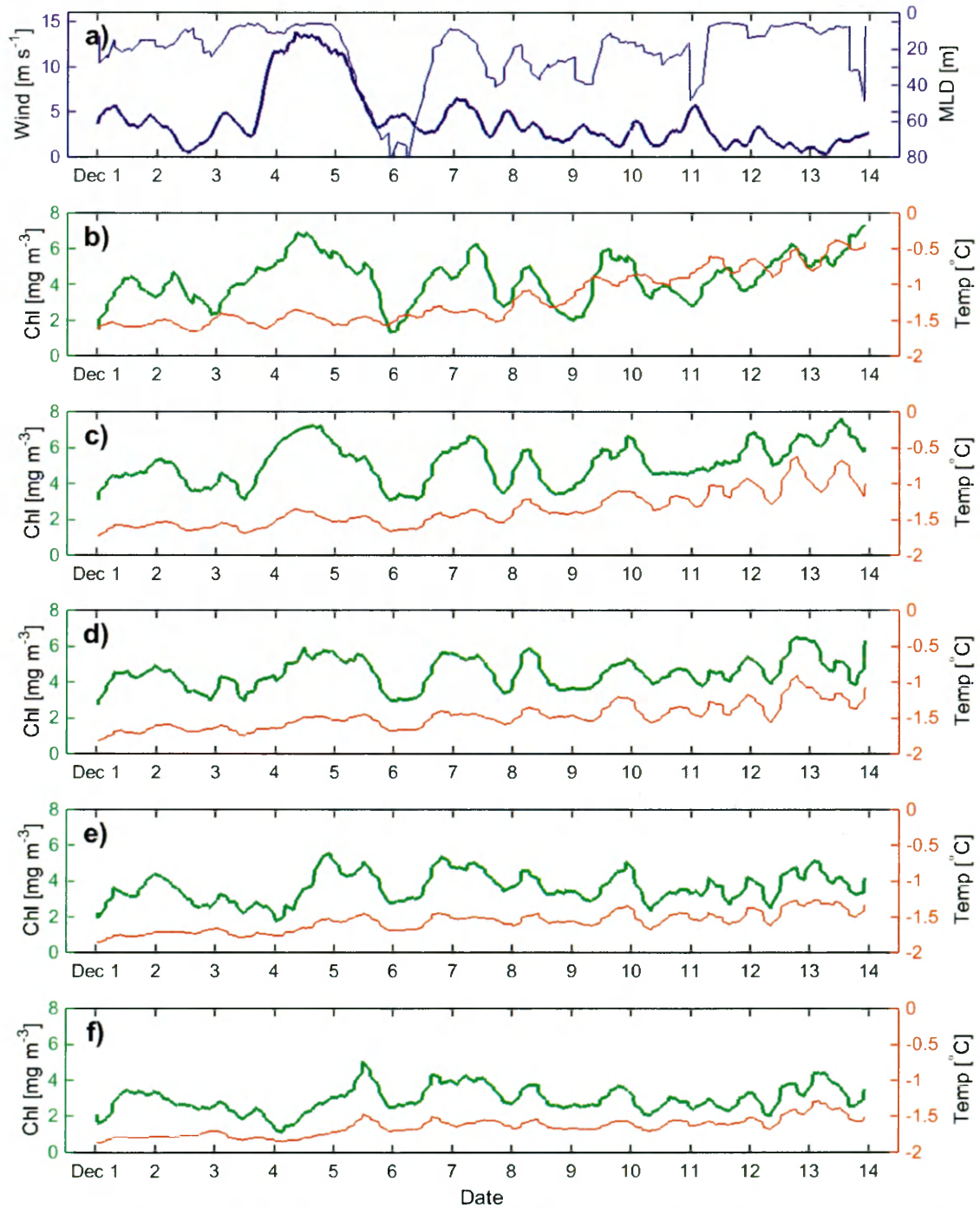
Figure 10: Glider observations of chlorophyll (Chl) and temperature (Temp) in short-term events during the accumulation period (December 1-14) for SG503, 2012-2013. (**a**) Wind speed (thick purple line) and MLD (thin purple line). Panels (**b**) through (**f**) display average 10 m chlorophyll (thick green line) and temperature (thin orange line) in 0-10, 10-20, 20-30, 30-40, and 40-50 m bins.

105
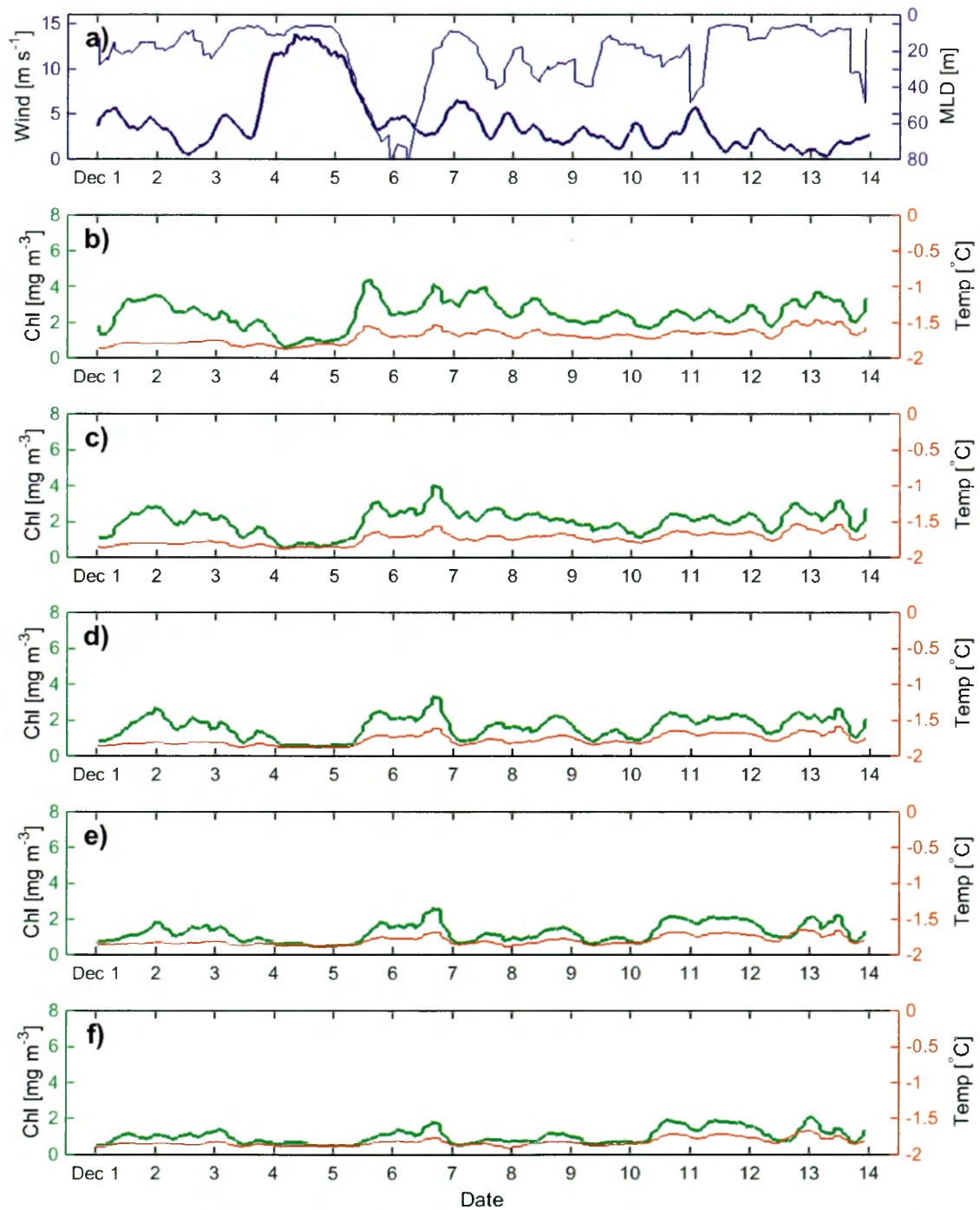
Figure 11: Glider observations of chlorophyll (Chl) and temperature (Temp) in short-term events during the accumulation period (December 1-14) for SG503, 2012-2013. (**a**) Wind speed (thick purple line) and MLD (thin purple line). Panels (**b**) through (**f**) display average 10 m chlorophyll (thick green line) and temperature (thin orange line) in 50-60, 60-70, 70-80, 80-90, and 90-100 m bins.
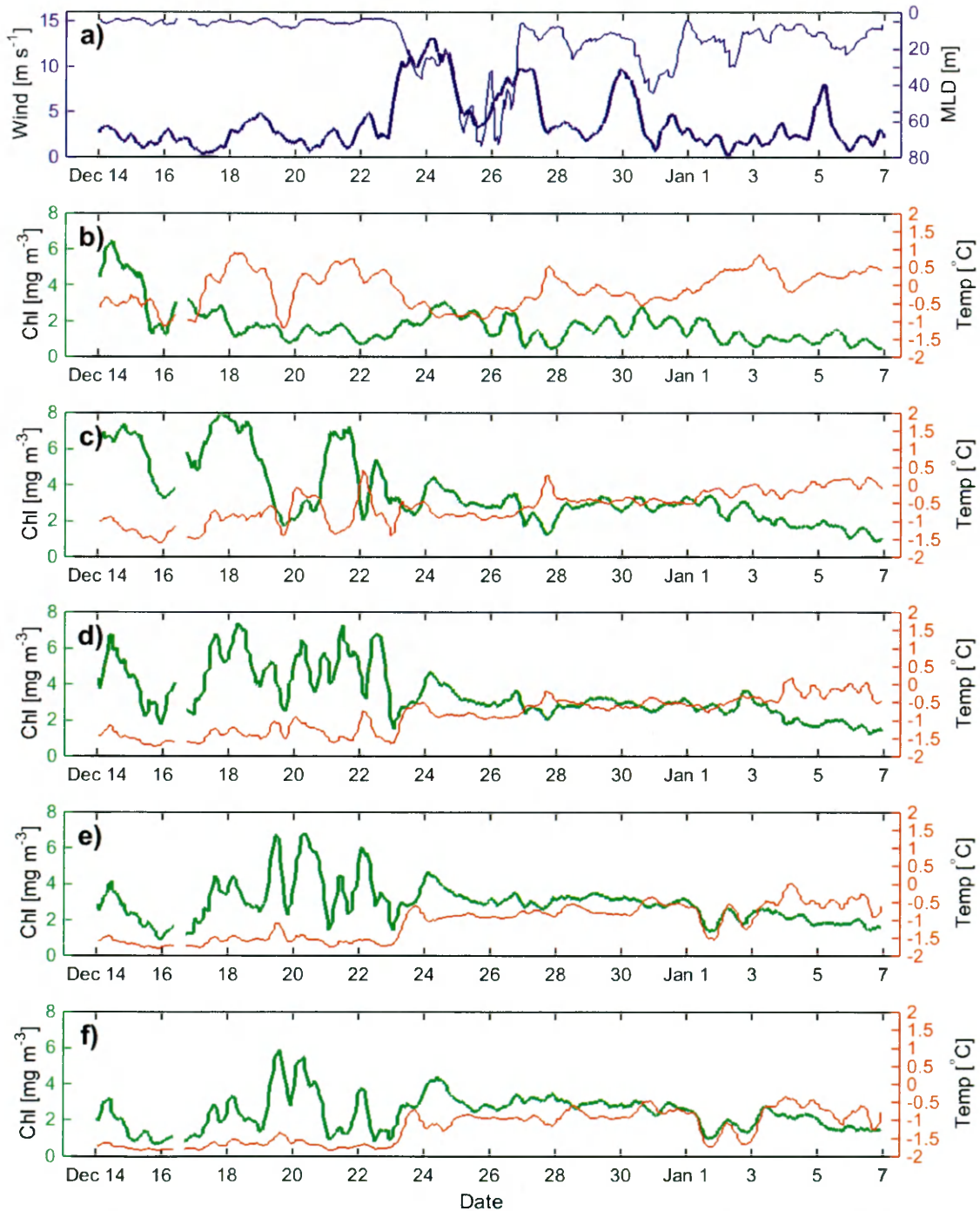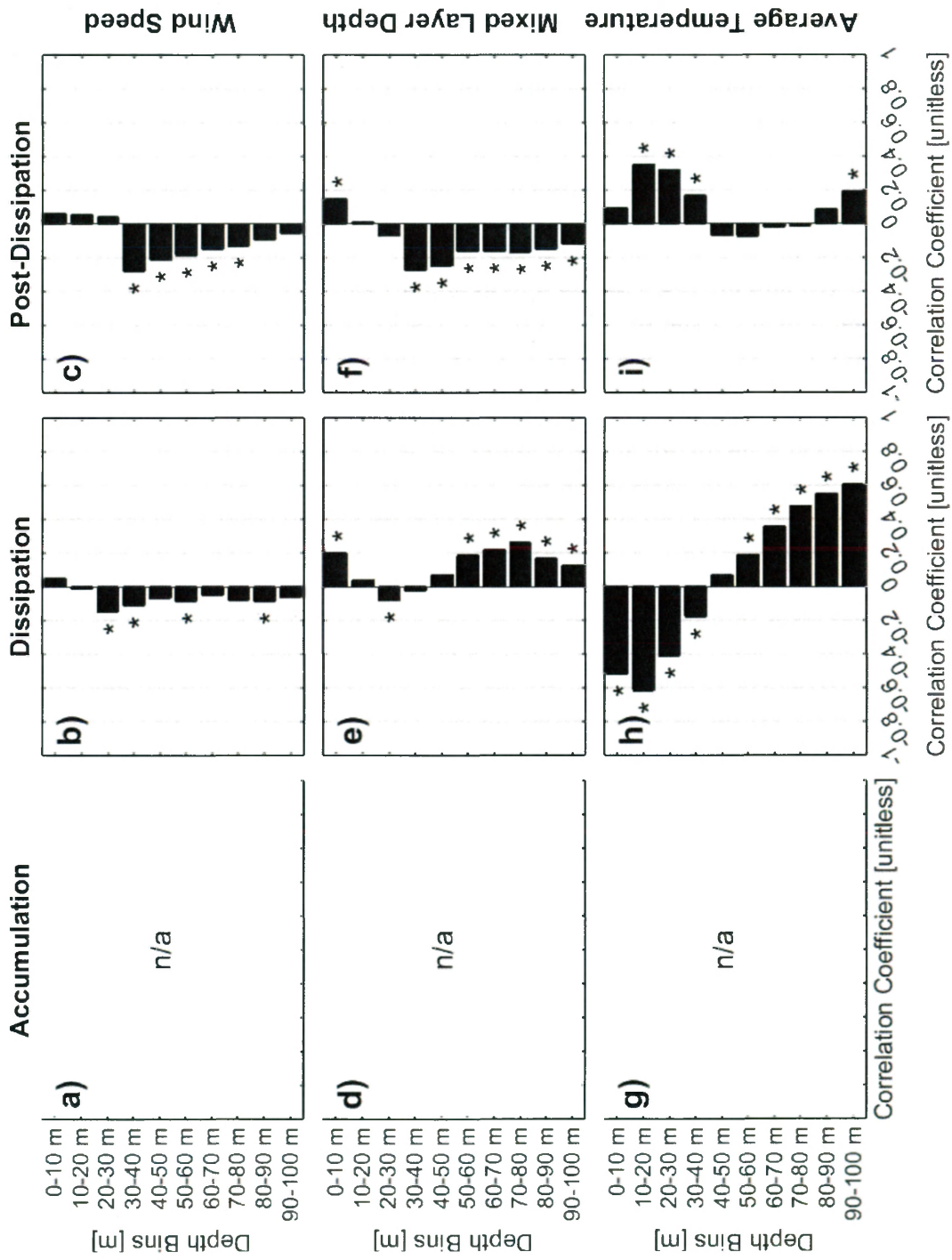
Figure 12: Glider observations of chlorophyll (Chl) and temperature (Temp) in short-term events during the dissipation period (December 14 – January 7) for SG503, 2012-2013. (**a**) Wind speed (thick purple line) and MLD (thin purple line). Panels (**b**) through (**f**) display average 10 m chlorophyll (thick green line) and temperature (thin orange line) in 0-10, 10-20, 20-30, 30-40, and 40-50 m bins.
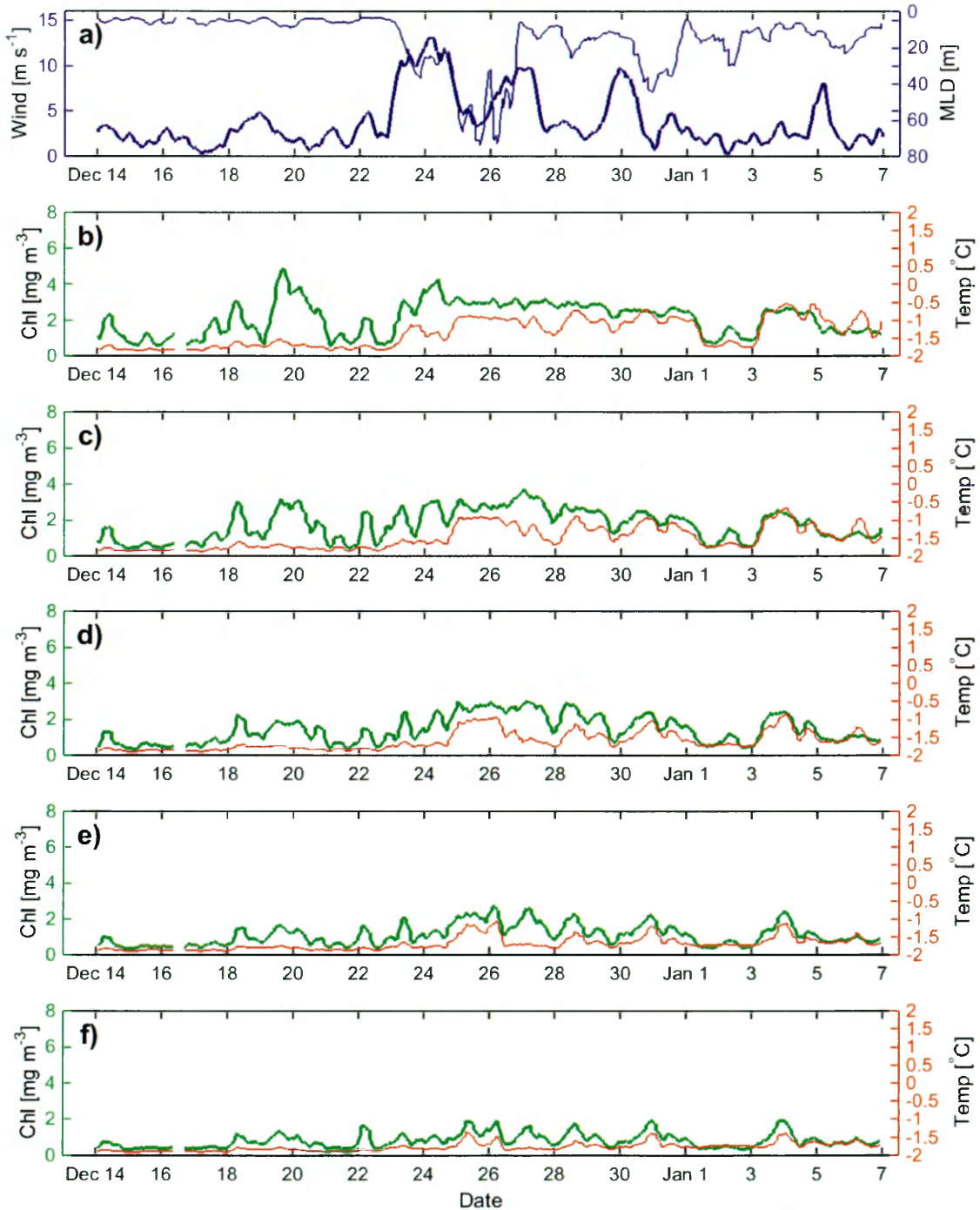
Figure 13: Glider observations of chlorophyll (Chl) and temperature (Temp) in short-term events during the dissipation period (December 14 – January 7) for SG503, 2012-2013. (**a**) Wind speed (thick purple line) and MLD (thin purple line). Panels (**b**) through (**f**) display average 10 m chlorophyll (thick green line) and temperature (thin orange line) in 50-60, 60-70, 70-80, 80-90, and 90-100 m bins.

108
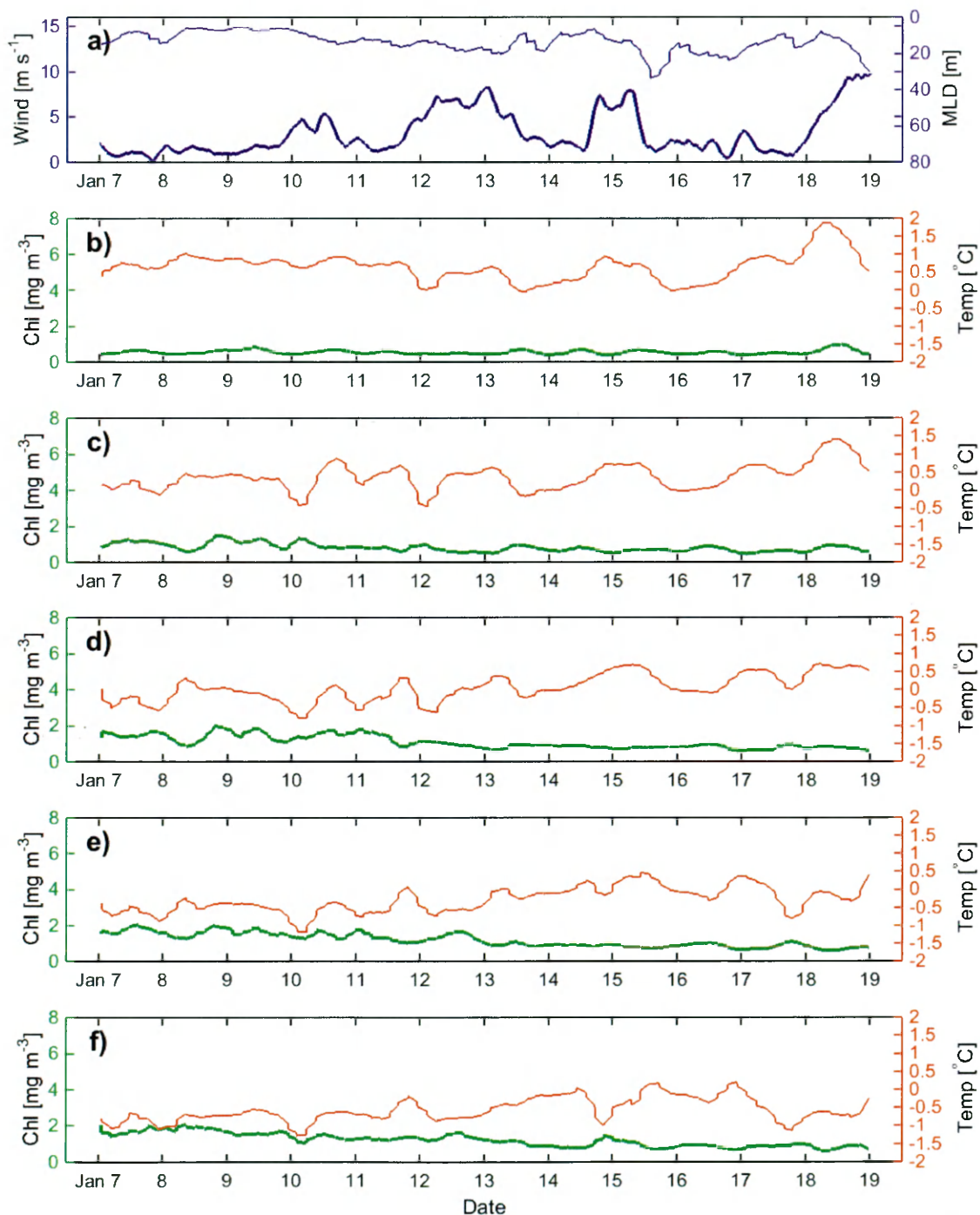
Figure 14: Glider observations of chlorophyll (Chl) and temperature (Temp) in short-term events during the post-dissipation period (January 7-19) for SG503, 2012-2013. (**a**) Wind speed (thick purple line) and MLD (thin purple line). Panels (**b**) through (**f**) display average 10 m chlorophyll (thick green line) and temperature (thin orange line) in 0-10, 10-20, 20-30, 30-40, and 40-50 m bins.
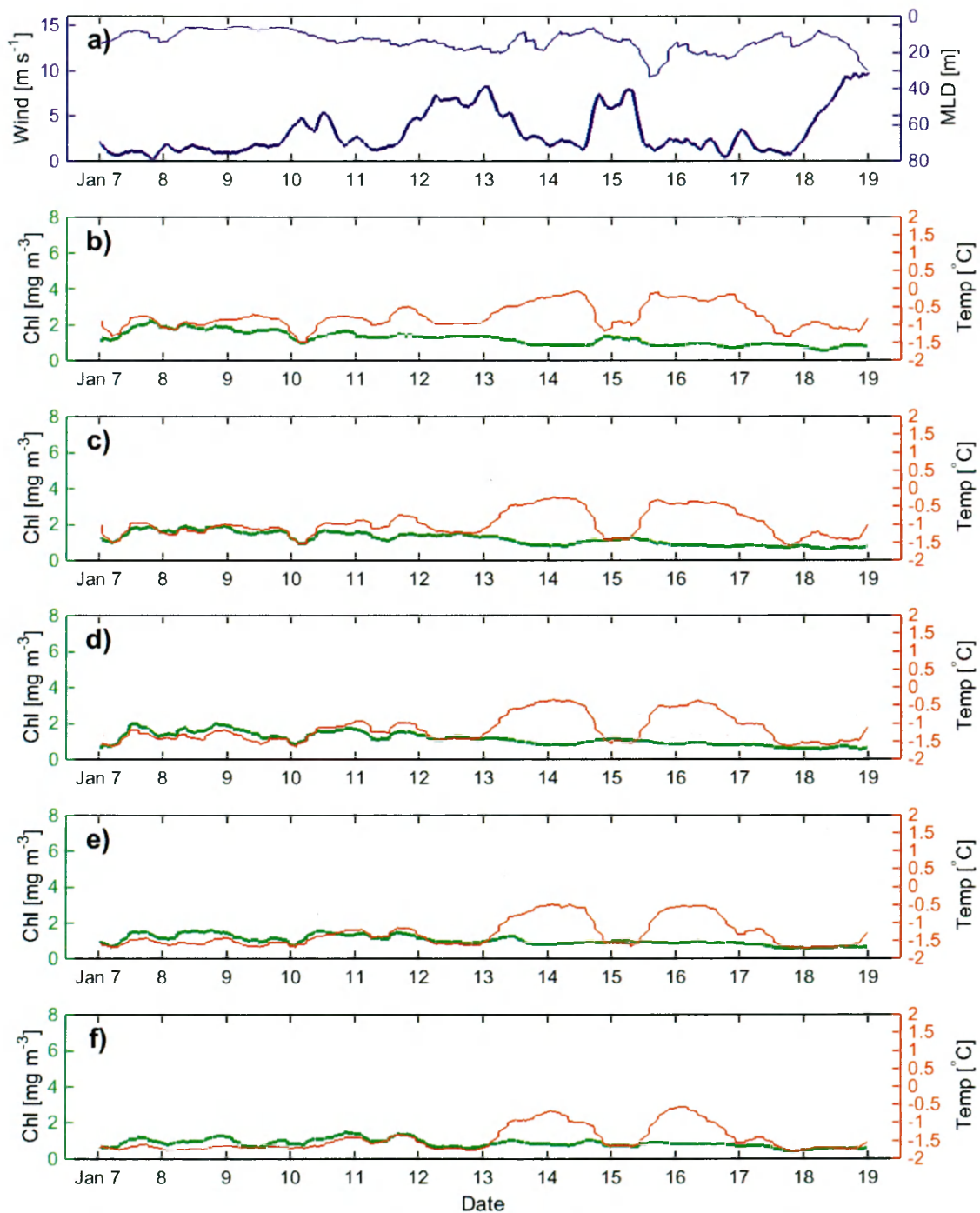
Figure 15: Glider observations of chlorophyll (Chl) and temperature (Temp) in short-term events during the post-dissipation period (January 7-19) for SG503, 2012-2013. (**a**) Wind speed (thick purple line) and MLD (thin purple line). Panels (**b**) through (**f**) display average 10 m chlorophyll (thick green line) and temperature (thin orange line) in 50-60, 60-70, 70-80, 80-90, and 90-100 m bins.

Figure 16: Pearson product-moment correlation coefficients for SG503, 2012-2013 between wind speed and average 10 m chlorophyll during the (**a**) accumulation, (**b**) dissipation, and (**c**) post-dissipation periods, between mixed layer depth and 10 m chlorophyll during the (**d**) accumulation, (**e**) dissipation, and (**f**) post-dissipation periods, and between 10 m temperature and 10 m chlorophyll during the (**g**) accumulation, (**h**) dissipation, and (**i**) post-dissipation periods. Temporal periods are defined as: accumulation (December 1-14), dissipation (December 14 – January 7), and post-dissipation (January 7-19). Stars indicate significance at the $p < 0.05$ level.
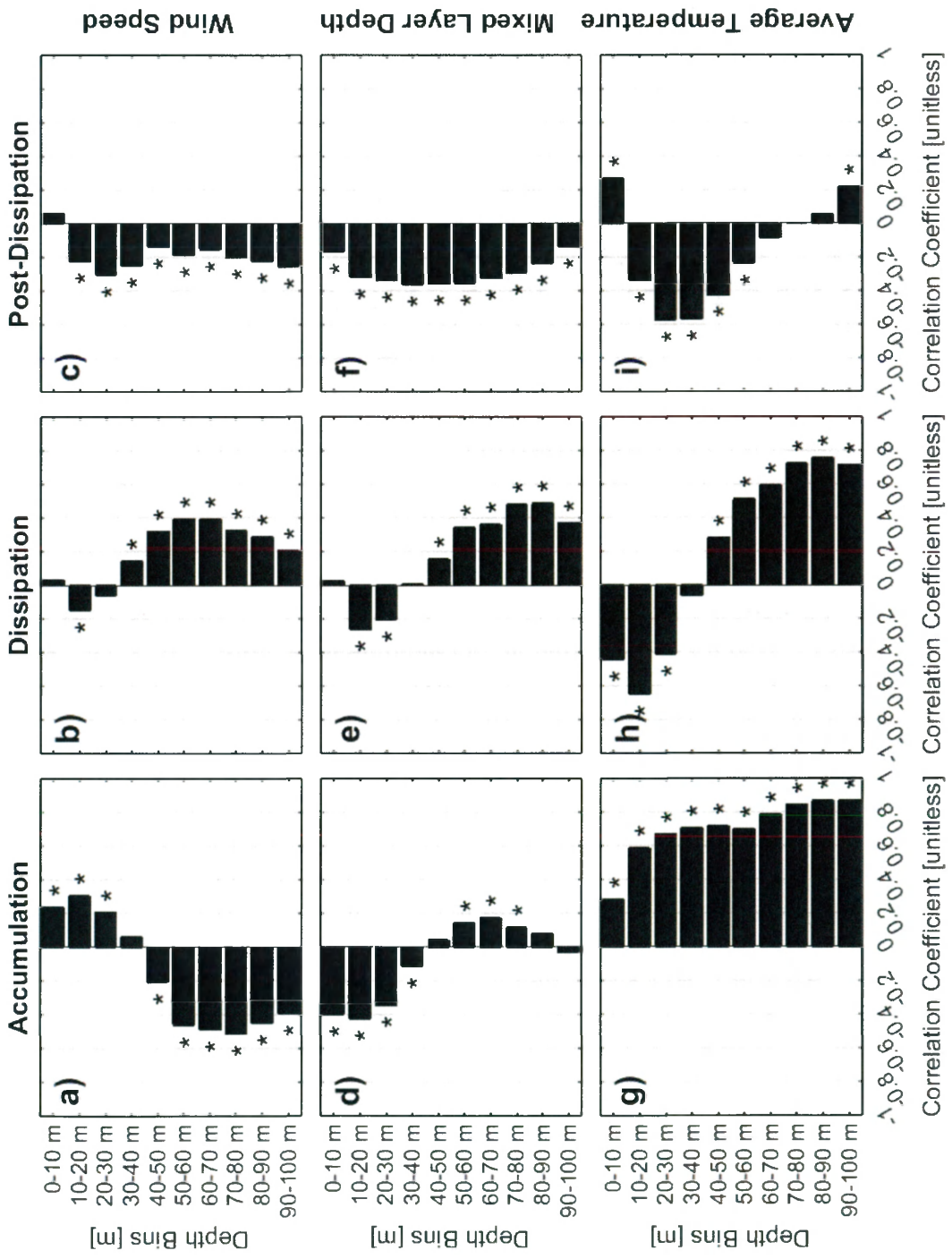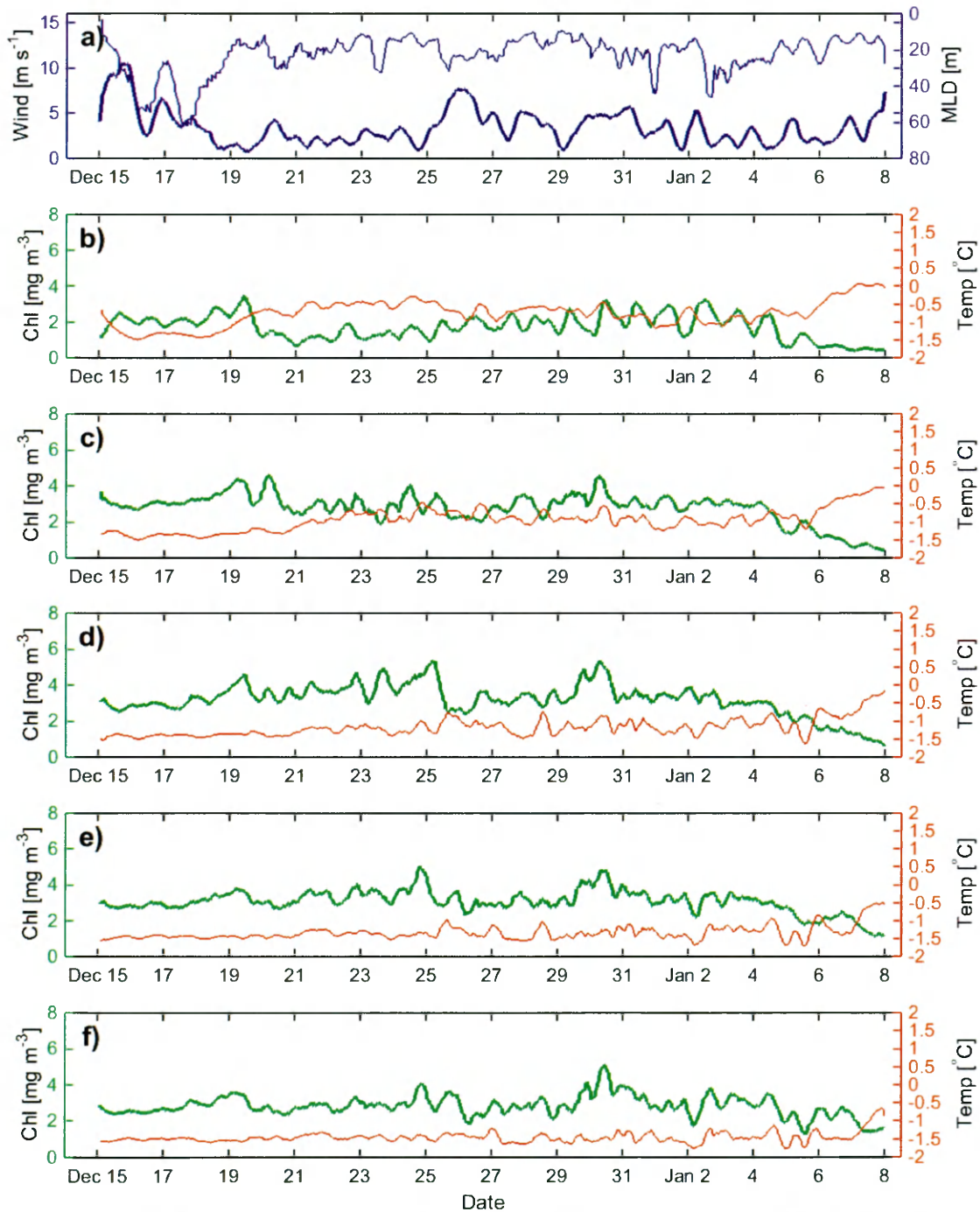
Figure 17: Glider observations of chlorophyll (Chl) and temperature (Temp) in short-term events during the dissipation period (December 15 – January 8) for SG502, 2010-2011. (**a**) Wind speed (thick purple line) and MLD (thin purple line). Panels (**b**) through (**f**) display average 10 m chlorophyll (thick green line) and temperature (thin orange line) in 0-10, 10-20, 20-30, 30-40, and 40-50 m bins.
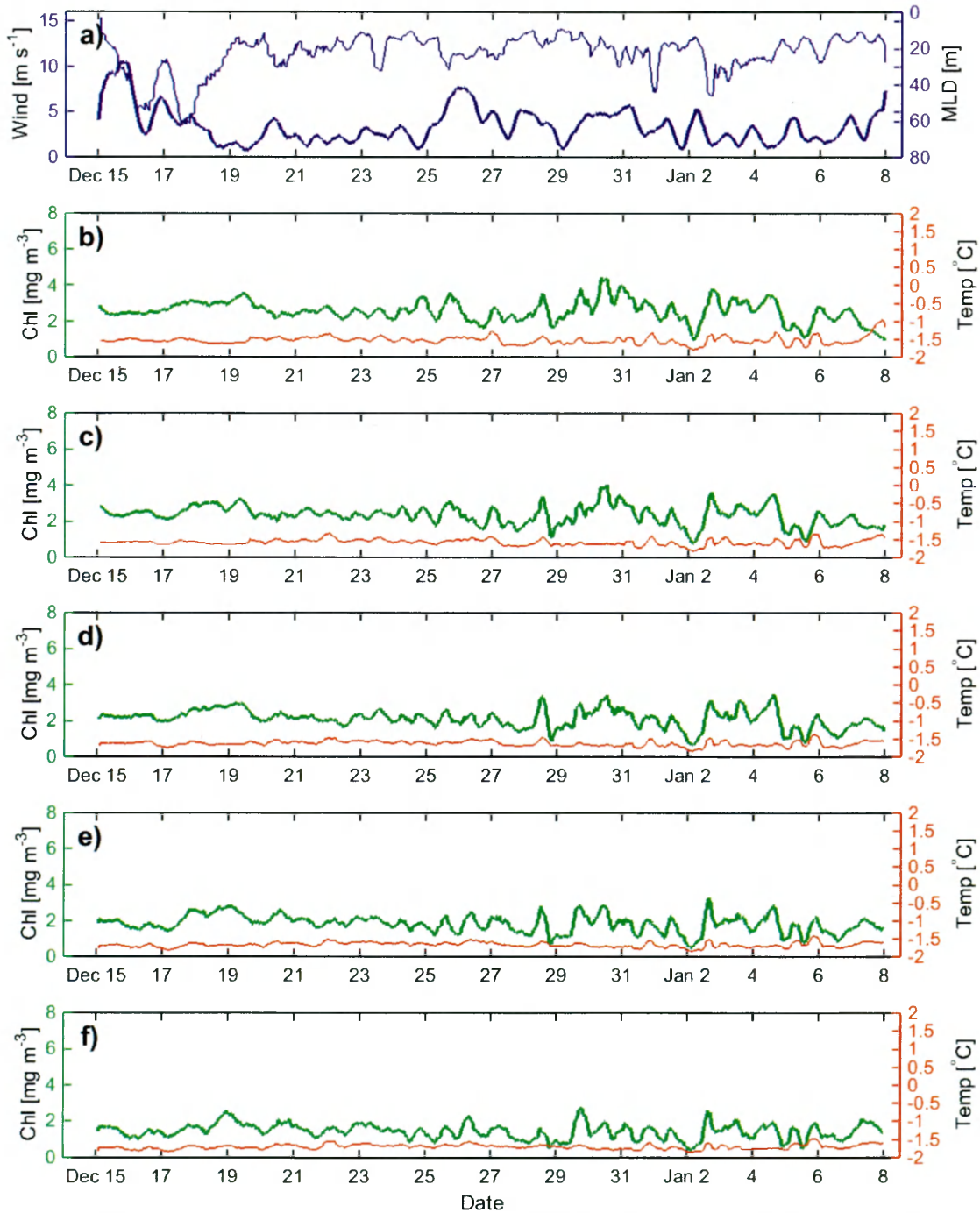
Figure 18: Glider observations of chlorophyll (Chl) and temperature (Temp) in short-term events during the dissipation period (December 15 – January 8) for SG502, 2010-2011. (**a**) Wind speed (thick purple line) and MLD (thin purple line). Panels (**b**) through (**f**) display average 10 m chlorophyll (thick green line) and temperature (thin orange line) in 50-60, 60-70, 70-80, 80-90, and 90-100 m bins.
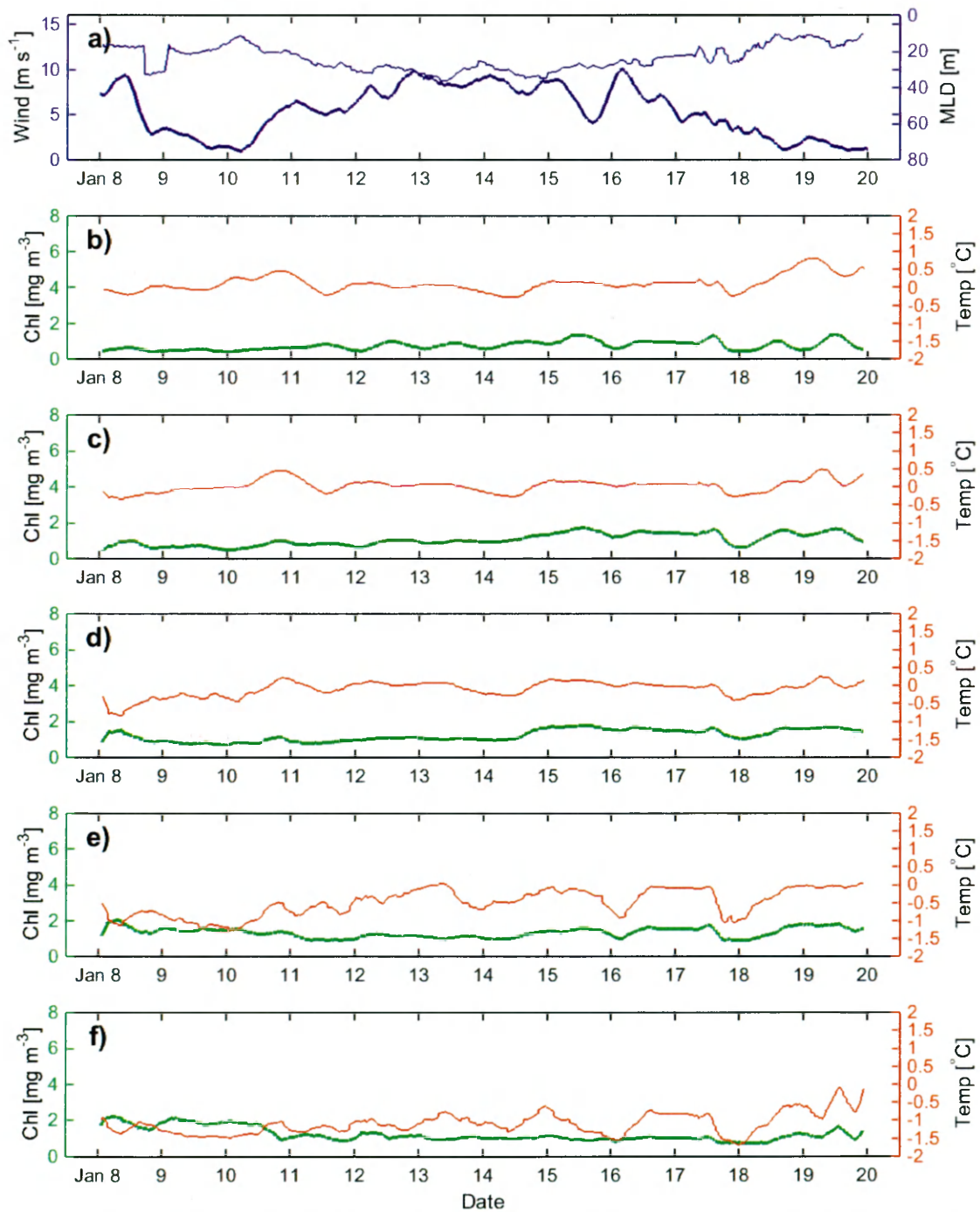
Figure 19: Glider observations of chlorophyll (Chl) and temperature (Temp) in short-term events during the post-dissipation period (January 8-20) for SG502, 2010-2011. (**a**) Wind speed (thick purple line) and MLD (thin purple line). Panels (**b**) through (**f**) display average 10 m chlorophyll (thick green line) and temperature (thin orange line) in 0-10, 10-20, 20-30, 30-40, and 40-50 m bins.
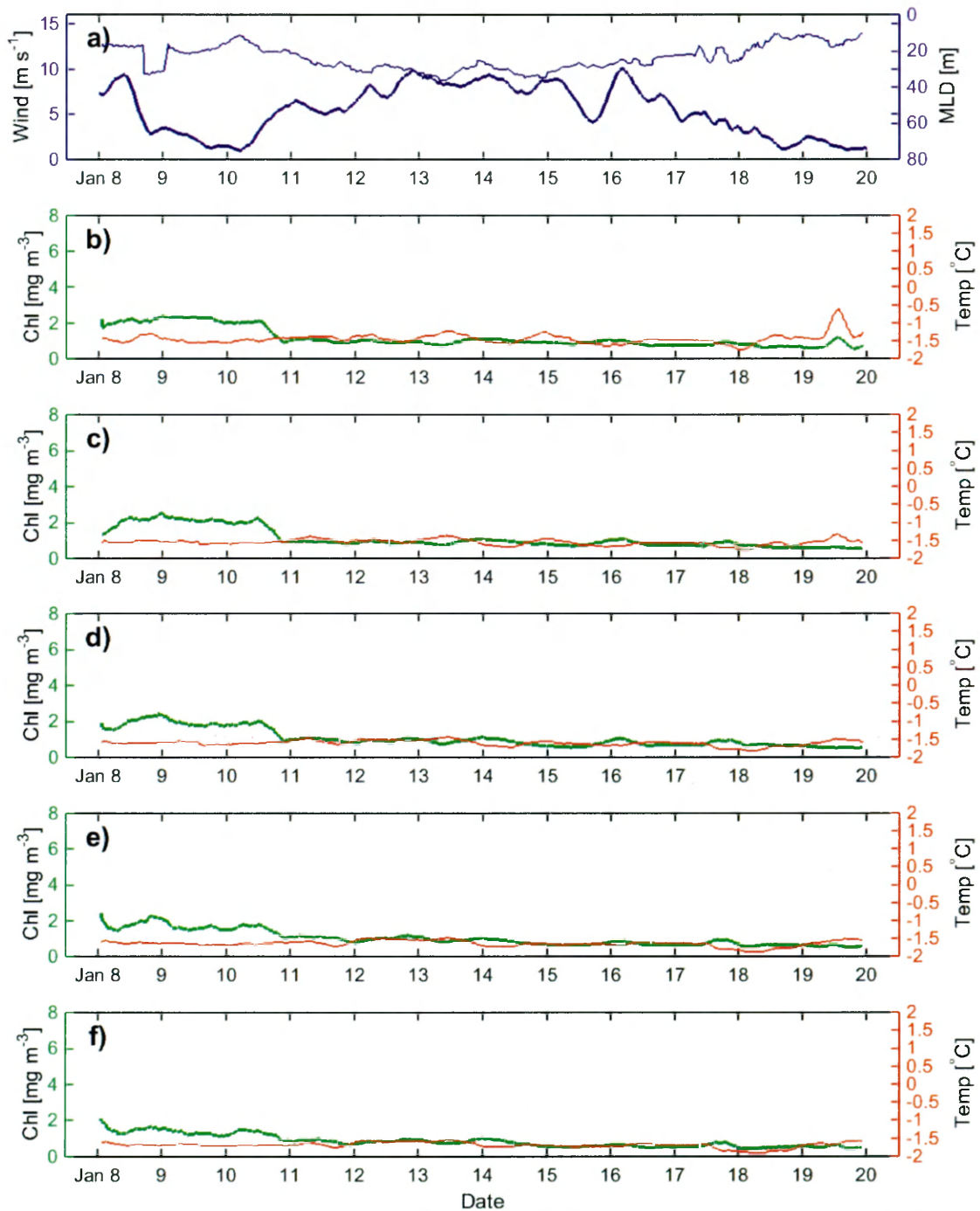
Figure 20: Glider observations of chlorophyll (Chl) and temperature (Temp) in short-term events during the post-dissipation period (January 8-20) for SG502, 2010-2011. (**a**) Wind speed (thick purple line) and MLD (thin purple line). Panels (**b**) through (**f**) display average 10 m chlorophyll (thick green line) and temperature (thin orange line) in 50-60, 60-70, 70-80, 80-90, and 90-100 m bins.

116

Figure 21: Pearson product-moment correlation coefficients for SG502, 2010-2011 between wind speed and average 10 m chlorophyll during the (**a**) accumulation, (**b**) dissipation, and (**c**) post-dissipation periods, between mixed layer depth and 10 m chlorophyll during the (**d**) accumulation, (**e**) dissipation, and (**f**) post-dissipation periods, and between 10 m temperature and 10 m chlorophyll during the (**g**) accumulation, (**h**) dissipation, and (**i**) post-dissipation periods. Temporal periods are defined as: dissipation (December 15 – January 8) and post-dissipation (January 8-20). Stars indicate significance at the $p < 0.05$ level.

Figure 22: Mooring observations of short-term events during the dissipation period (December 14 – January 7) for the IVARS *Callinectes* mooring from 2003-2006. Mooring observations of (**a**) wind speed (thick purple line) and (**b**) fluorescence at 21 m (thick green line) during 2003-2004; of (**c**) wind speed (thick purple line) and (**d**) fluorescence at 23 m (thick green line) and temperature at 24 m (thin orange line) during 2004-2005; of (**e**) wind speed (thick purple line) and (**f**) fluorescence at 21 m (thick green line) and temperature at 24 m (thin orange line) during 2005-2006.
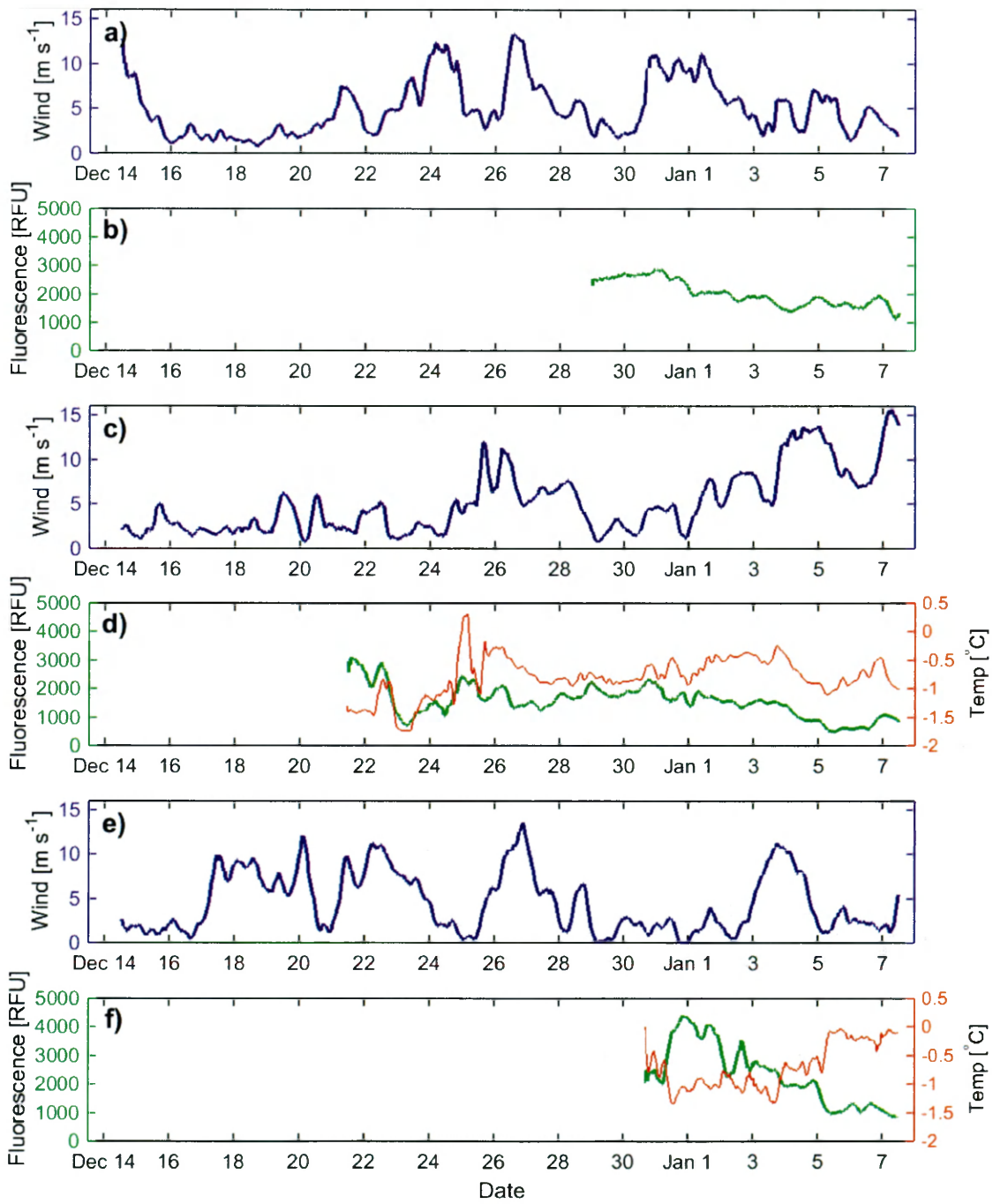
Figure 23: Mooring observations of short-term events during the post-dissipation period (January 7-19) for the IVARS *Callinectes* mooring from 2003-2006. Mooring observations of (**a**) wind speed (thick purple line) and (**b**) fluorescence at 21 m (thick green line) during 2003-2004; of (**c**) wind speed (thick purple line) and (**d**) fluorescence at 23 m (thick green line) and temperature at 24 m (thin orange line) during 2004-2005; of (**e**) wind speed (thick purple line) and (**f**) fluorescence at 21 m (thick green line) and temperature at 24 m (thin orange line) during 2005-2006.
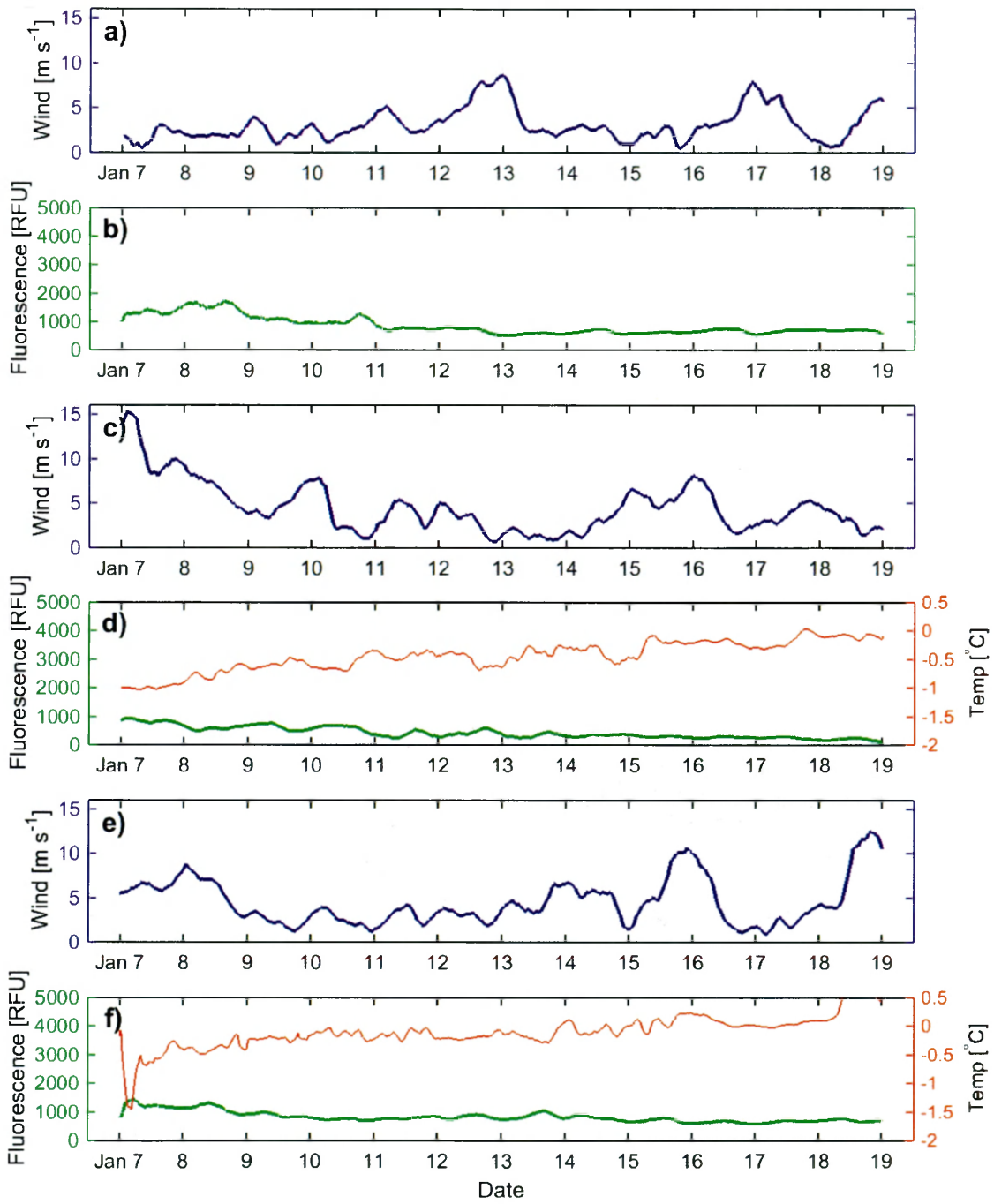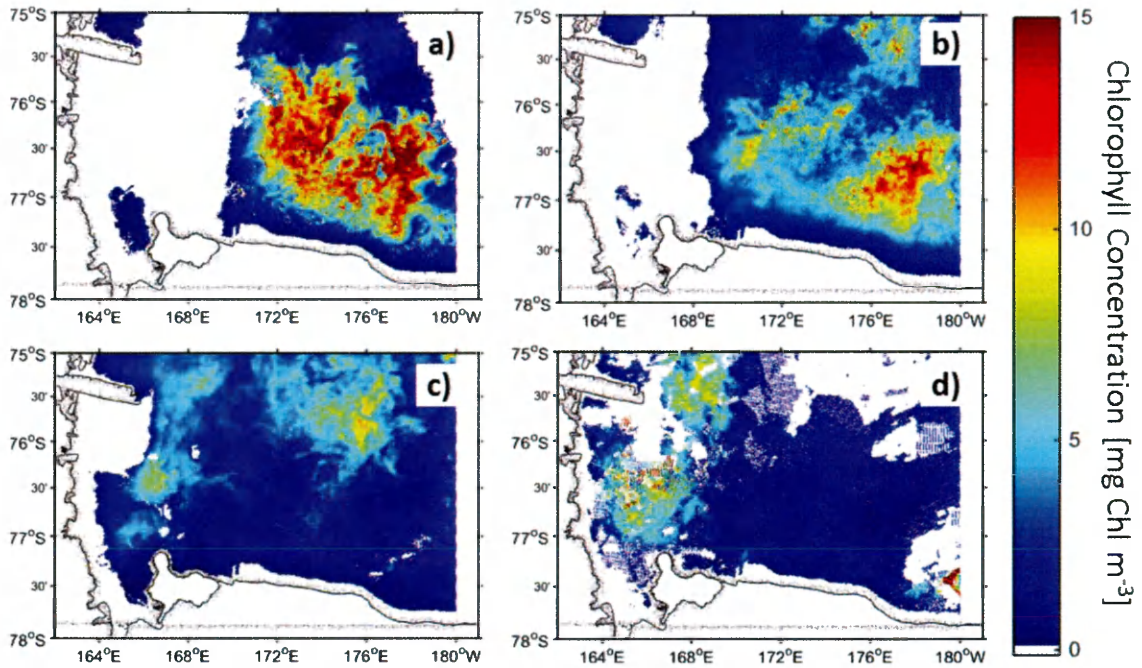
Figure 24: Monthly mean surface chlorophyll *a* concentration for the period of glider deployment: (**a**) November 2012, (**b**) December 2012, (**c**) January 2013, and (**d**) February 2013. Data from the MODIS Aqua satellite.

December 2, 2012

December 28, 2012

Figure 25: MODIS Aqua true color satellite imagery showing the ice field for December 2, 2012 and December 28, 2012. The red box indicates the location of the SG503, 2012-2013 glider study area.
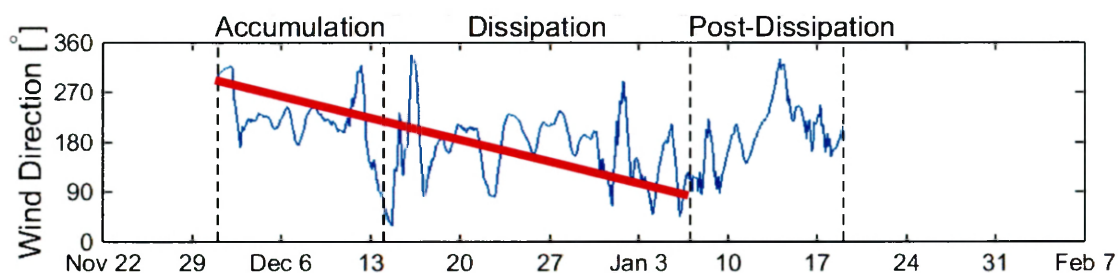
Figure 26: Wind direction as measured by the Laurie II AWS anemometer for the SG503, 2012-2013 season. Accumulation (December 1-14), dissipation (December 14 – January 7), and post-dissipation periods (January 7-19) are indicated by vertical, dashed lines. A red line indicates the trend in wind direction from southwest to south-southeast over the course of the accumulation and dissipation periods.
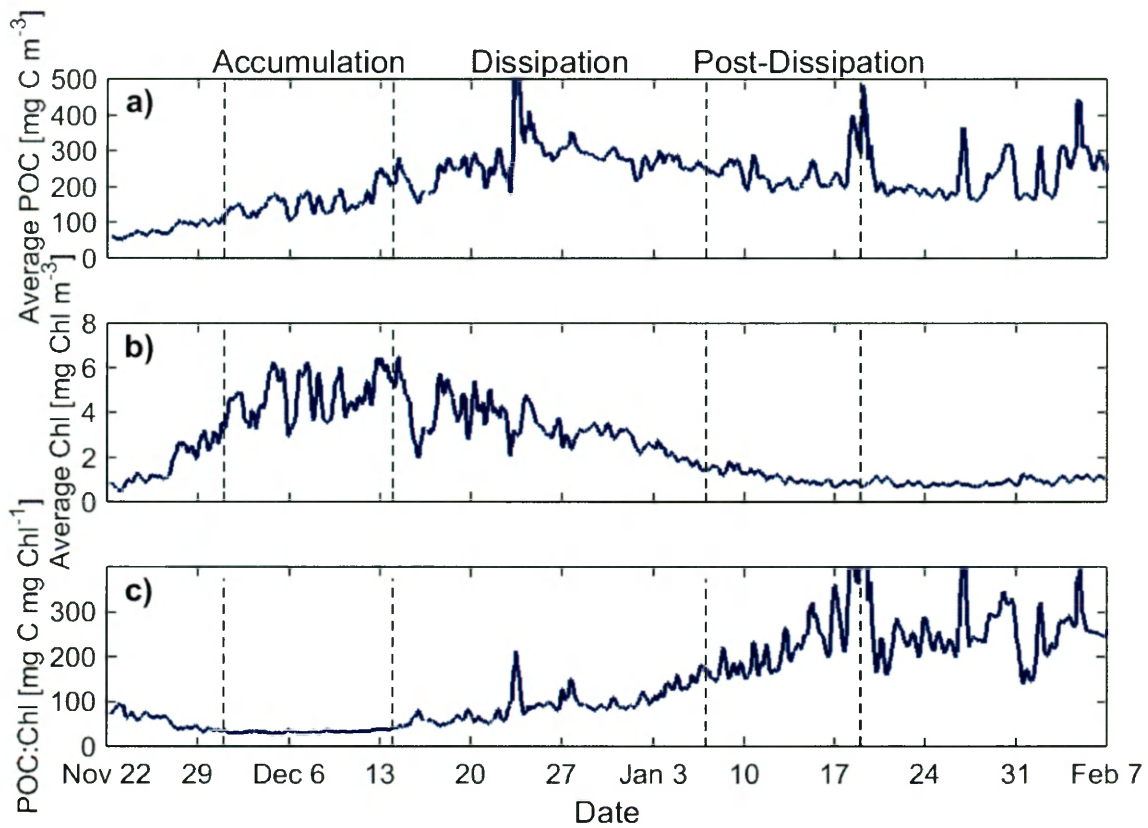
Figure 27: (**a**) Average 0-50 m POC, (**b**) average 0-50 m chlorophyll, and (c) the ratio of the two variables, POC:Chl for SG503, 2012-2013 are shown as dark blue lines. Accumulation (December 1-14), dissipation (December 14 – January 7), and post-dissipation periods (January 7-19) are indicated by vertical, dashed lines.

Figure 28: Vertical sections for SG503, 2012-2013 glider fluorescence with temperature contours (every 0.2°C) for the (**a**) accumulation (December 1-14), (**b**) the first half of the dissipation (December 14-26), (**c**) the second half of the dissipation (December 26 – January 7), and (**d**) the post-dissipation (Jan 7-19) periods. X-axis is days from glider launch (November 22).
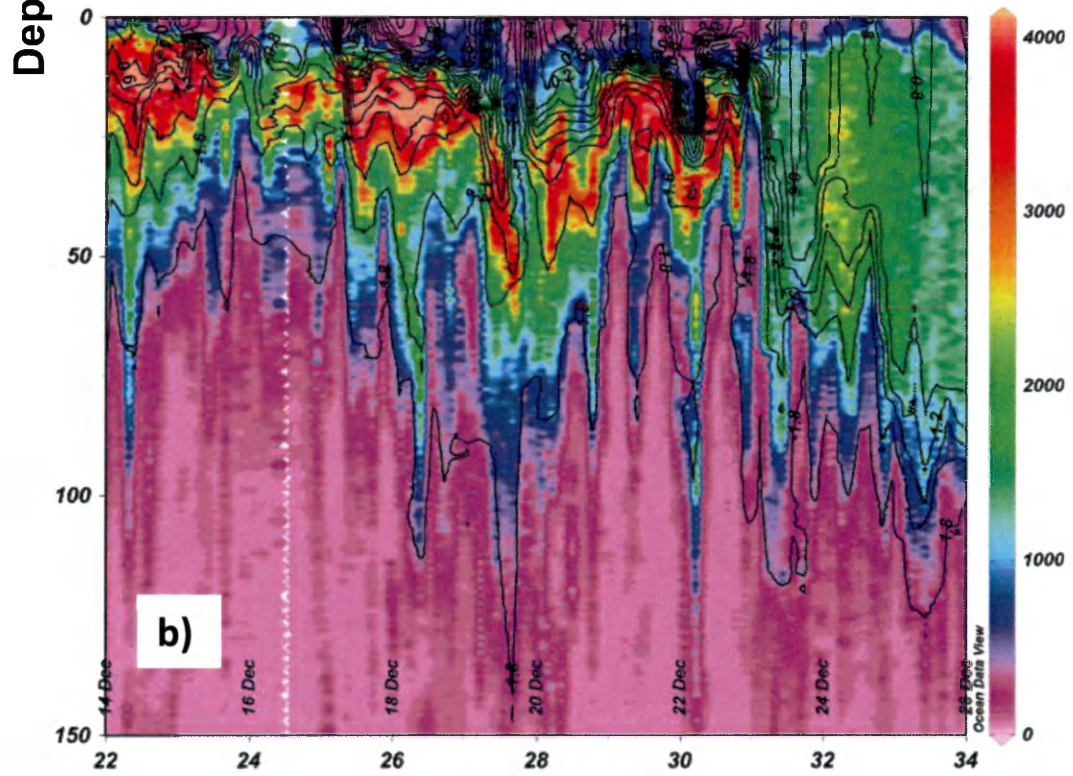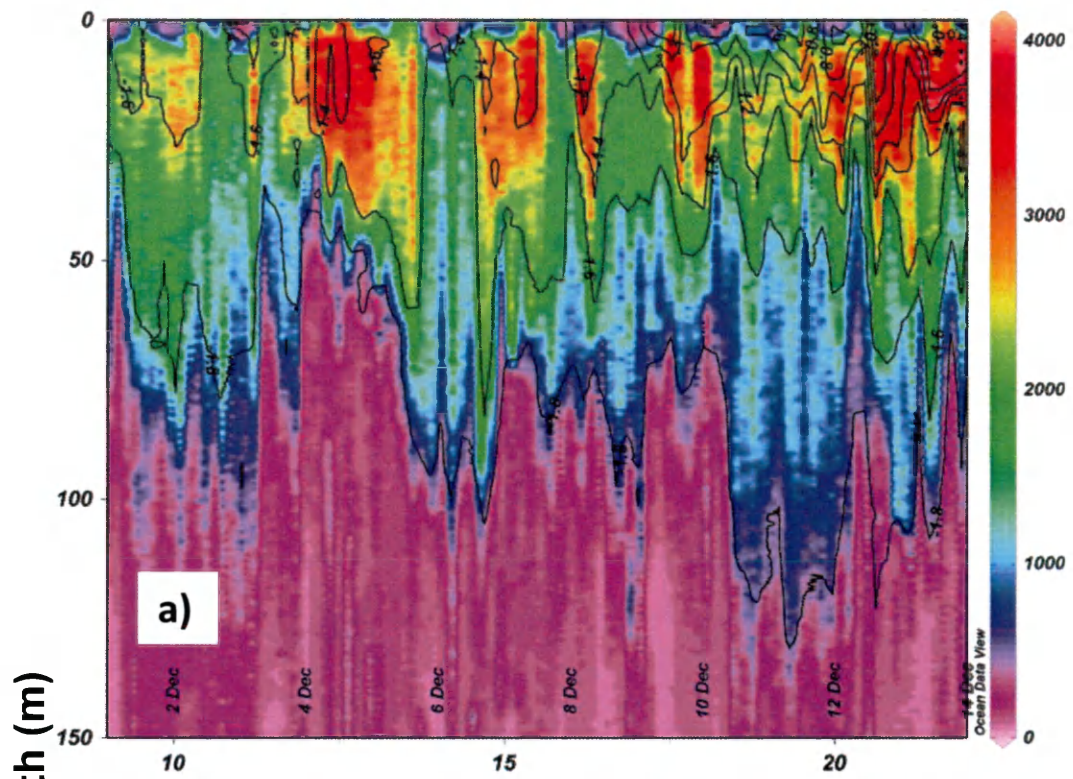
Time (days since November 22)

129

APPENDIX

Appendix A.1: (**a**) Sea surface temperature (SST) for SG502 (2010-2011; green line), SG503 (2010-2011; light blue line), and SG503 (2012-2013; dark blue line). Accumulation (December 1-14), dissipation (December 14 – January 7), and post-dissipation (January 7-19) periods are delineated by vertical, dashed lines. (**b**) Summary statistics for SST are displayed for the three gliders during the three temporal periods. Averages are shown as black dots; one standard deviation both above and below the average are shown as black bars; individual data points are displayed as small points.
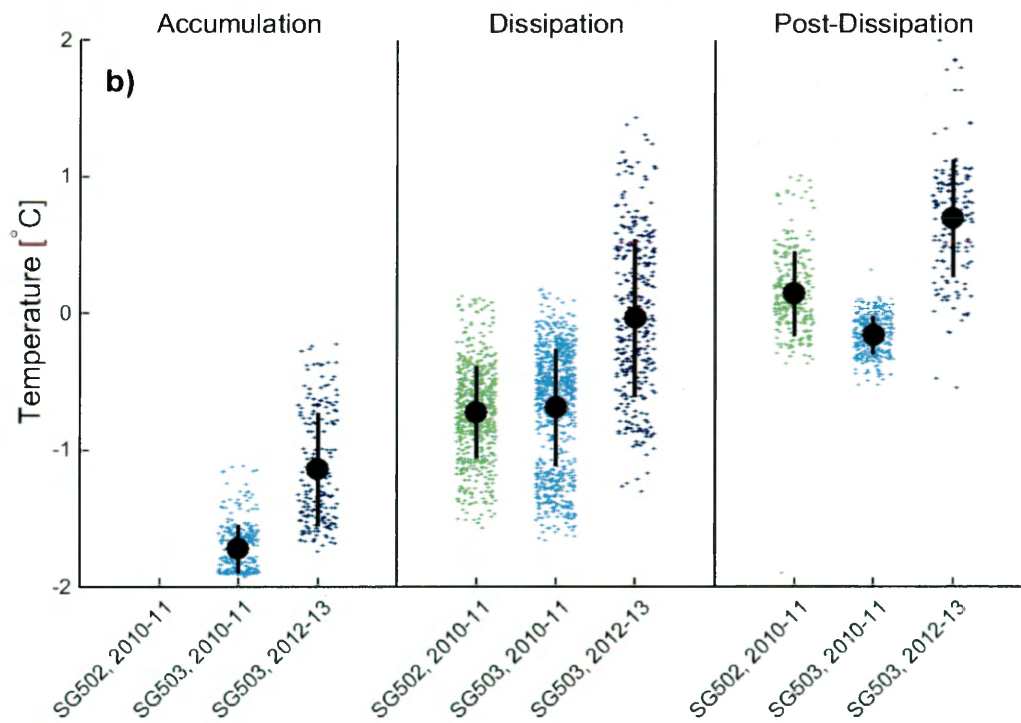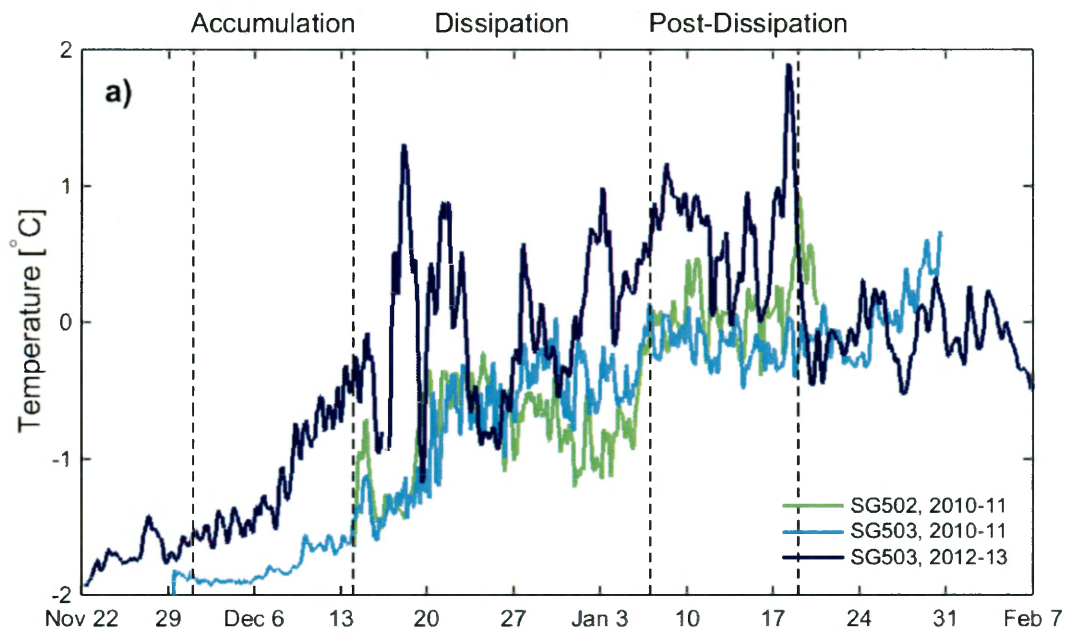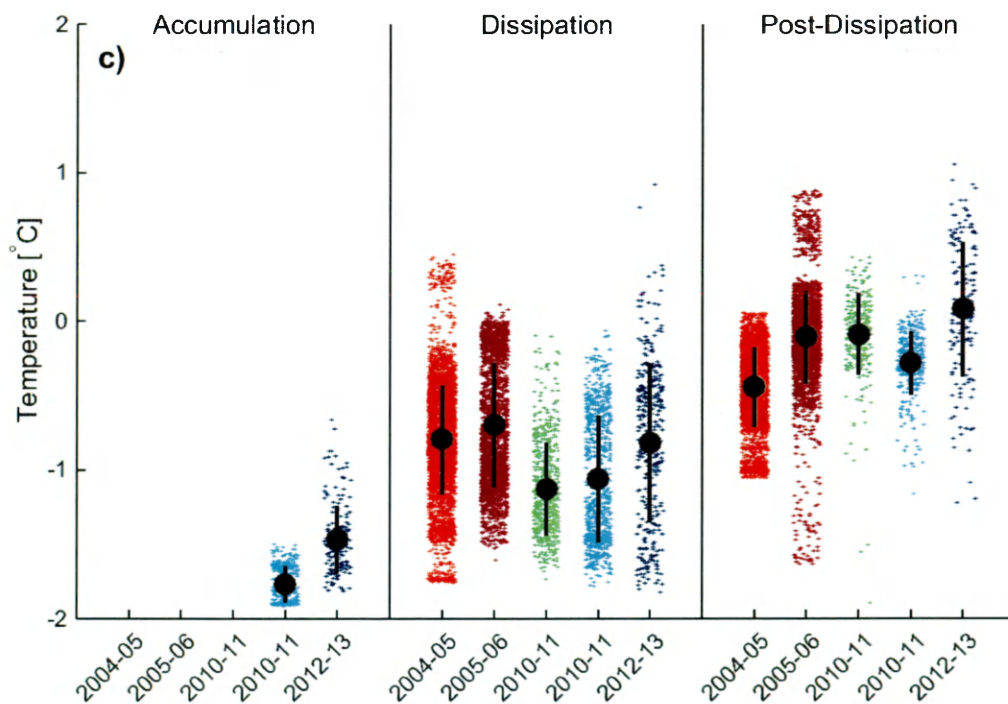
Appendix A.2: (**a**) Sea surface density (SSD) for SG502 (2010-2011; green line), SG503 (2010-2011; light blue line), and SG503 (2012-2013; dark blue line). Accumulation (December 1-14), dissipation (December 14 – January 7), and post-dissipation (January 7-19) periods are delineated by vertical, dashed lines. (**b**) Summary statistics for SSD are displayed for the three gliders during the three temporal periods. Averages are shown as black dots; one standard deviation both above and below the average are shown as black bars; individual data points are displayed as small points.
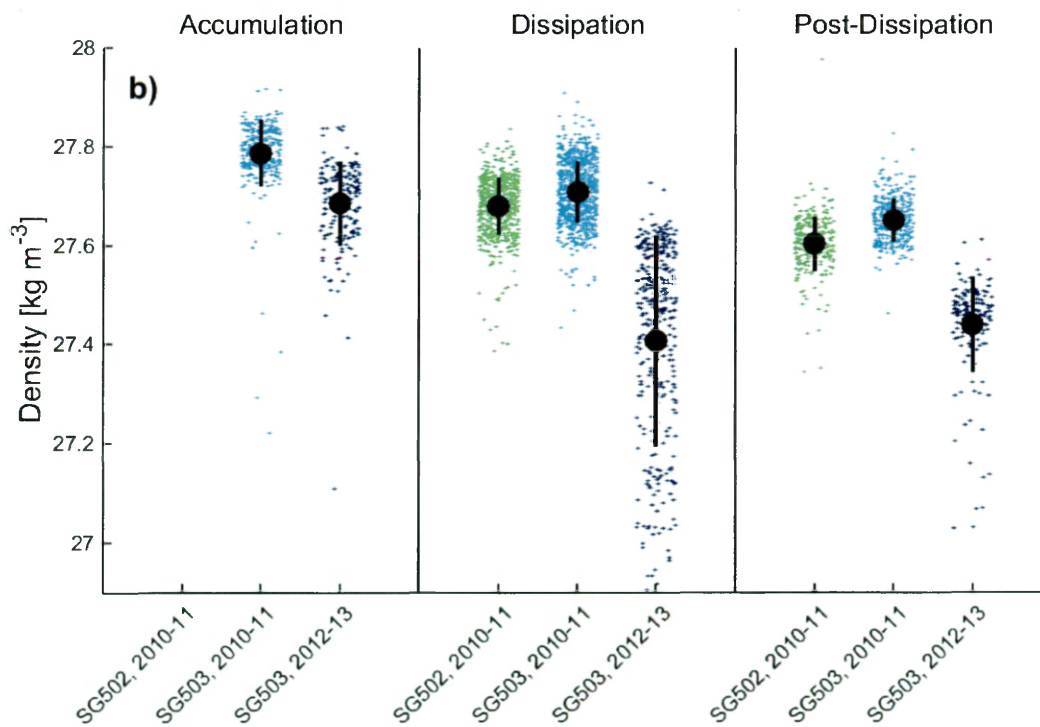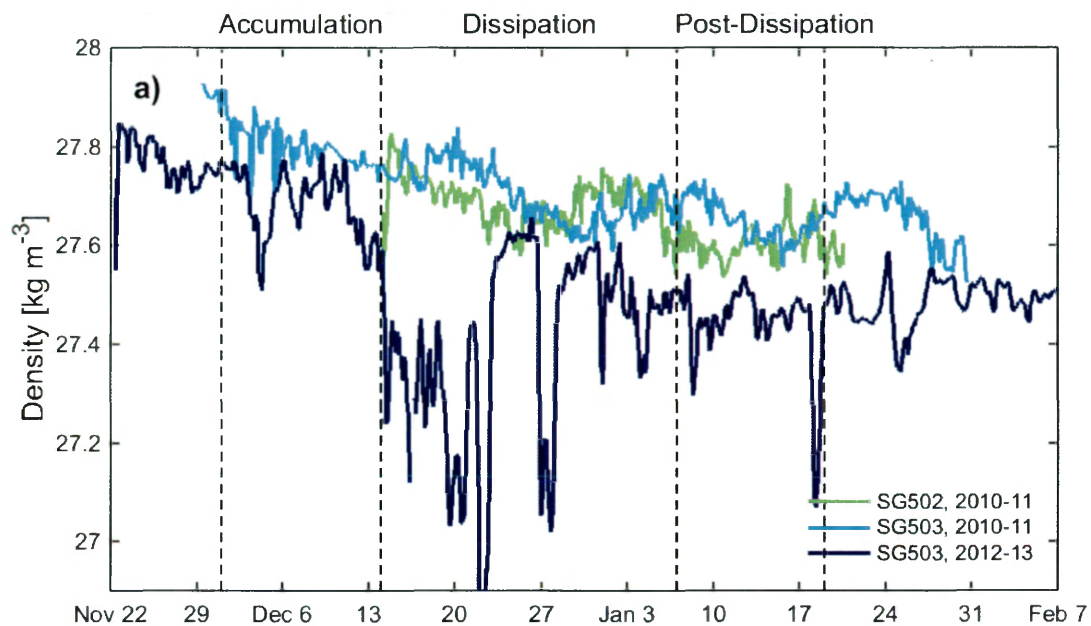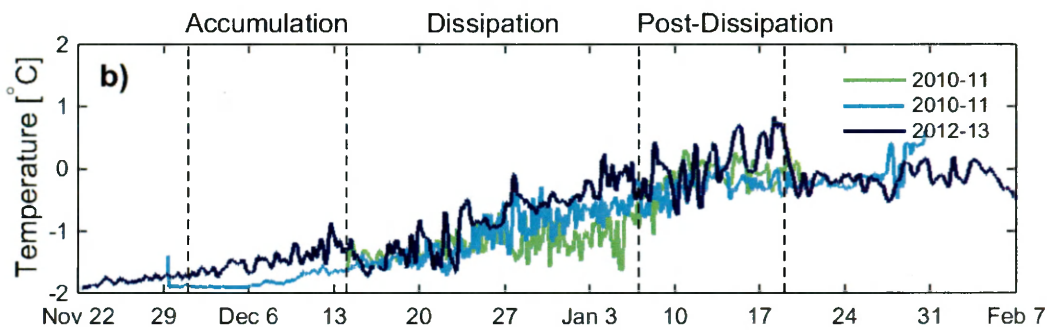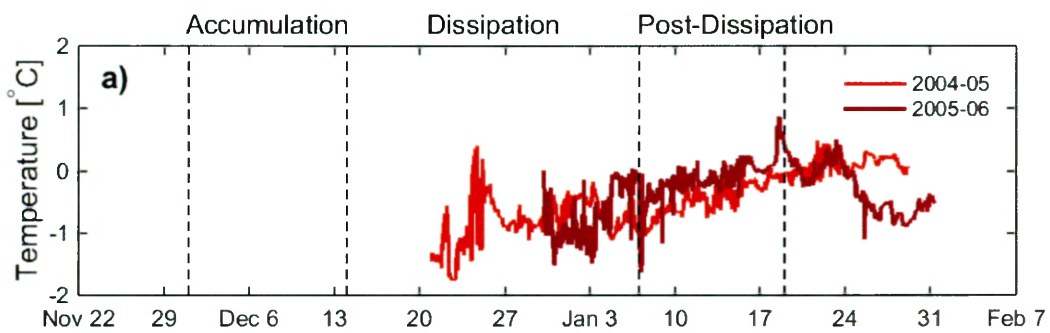
Appendix A.3: (**a**) Mixed layer depths (MLD) for SG502 (2010-2011; green line), SG503 (2010-2011; light blue line), and SG503 (2012-2013; dark blue line). Accumulation (December 1-14), dissipation (December 14 – January 7), and post-dissipation (January 7-19) periods are delineated by vertical, dashed lines. (**b**) Summary statistics for MLD are displayed for the three gliders during the three temporal periods. Averages are shown as black dots; one standard deviation both above and below the average are shown as black bars; individual data points are displayed as small points.
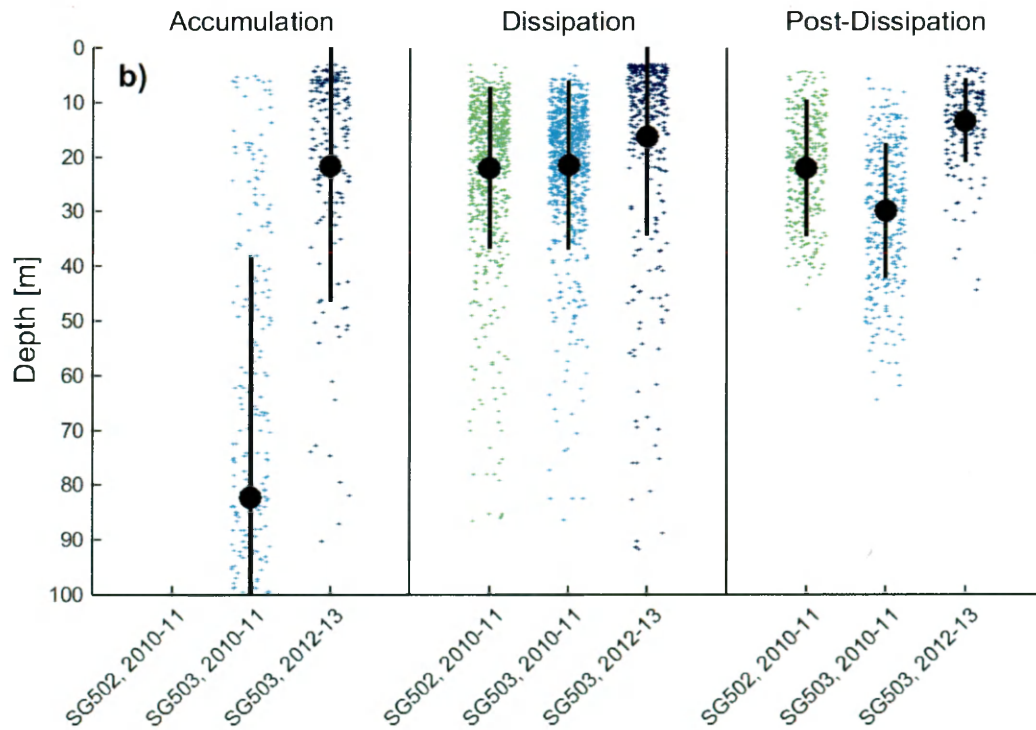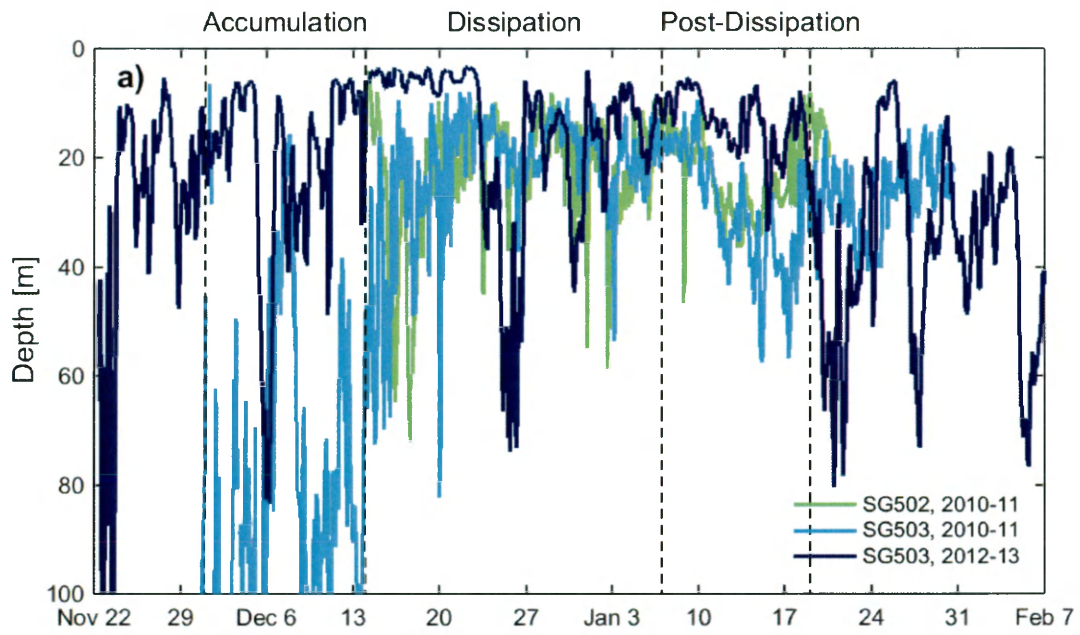
Appendix A.4: (**a**) Average 0-50 m chlorophyll for SG502 (2010-2011; green line) and SG503 (2012-2013; dark blue line). Accumulation (December 1-14), dissipation (December 14 – January 7), and post-dissipation (January 7-19) periods are delineated by vertical, dashed lines. (**b**) Summary statistics for average 0-50 m chlorophyll are displayed for the two gliders during the three temporal periods. Averages are shown as black dots; one standard deviation both above and below the average are shown as black bars; individual data points are displayed as small points.
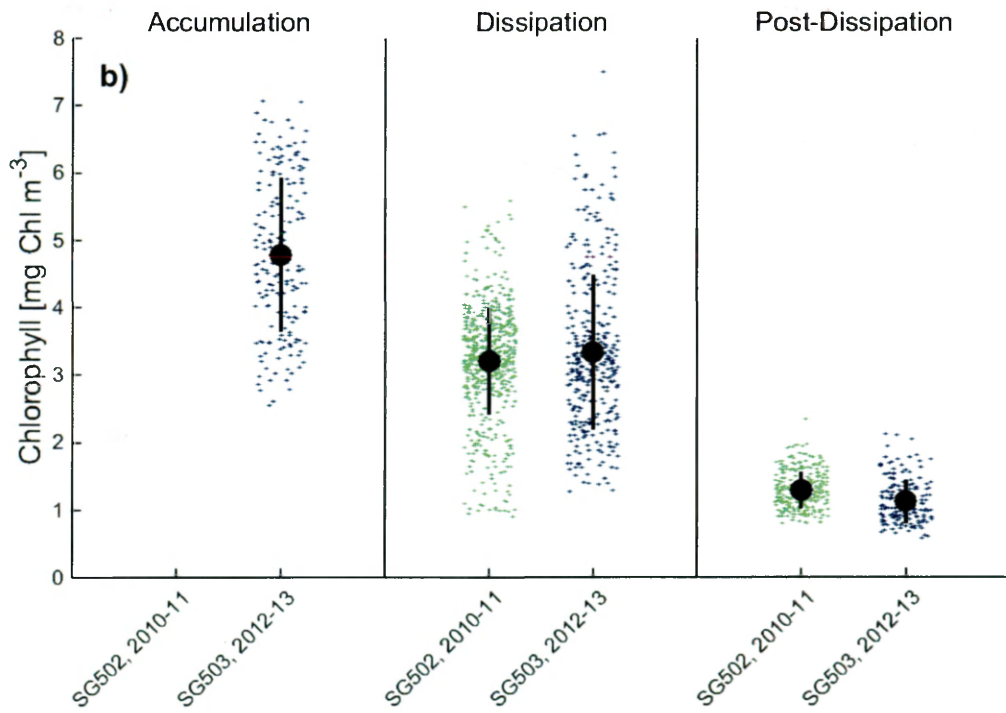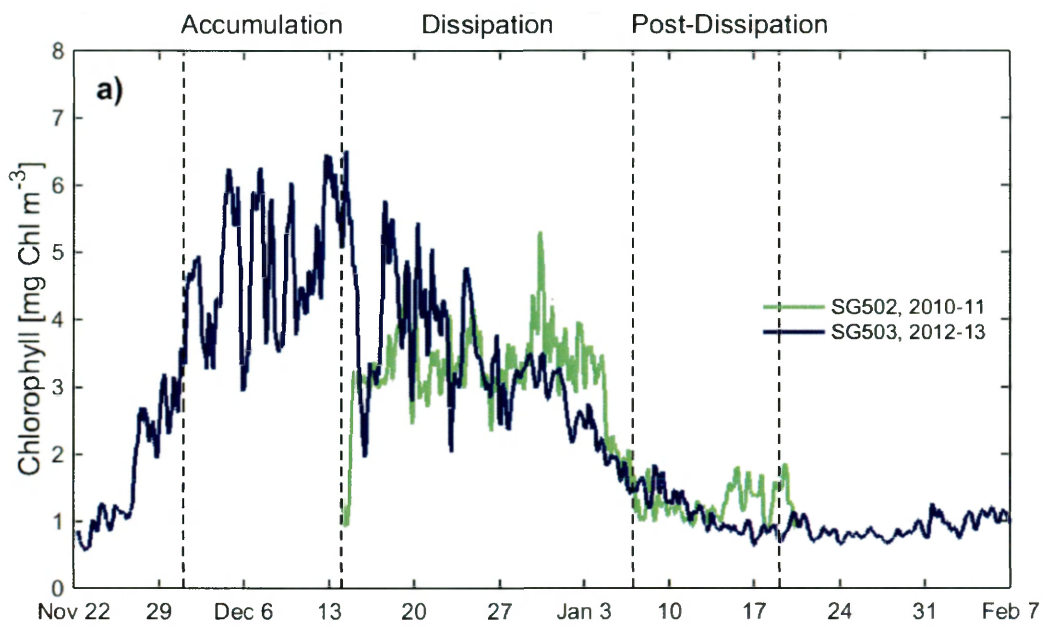
Appendix A.5: (**a**) Wind speeds from the Laurie II and Ferrell AMRC-AWSs for 2003-2004 (light orange line), 2004-2005 (orange line), 2005-2006 (dark red line), (**b**) 2010-2011 (green line), and 2012-2013 (dark blue line). Accumulation (December 1-14), dissipation (December 14 – January 7), and post-dissipation (January 7-19) periods are delineated by vertical, dashed lines. (**c**) Summary statistics for wind speed are displayed for the moorings and gliders during the three temporal periods. Averages are shown as black dots; one standard deviation both above and below the average are shown as black bars; individual data points are displayed as small points.
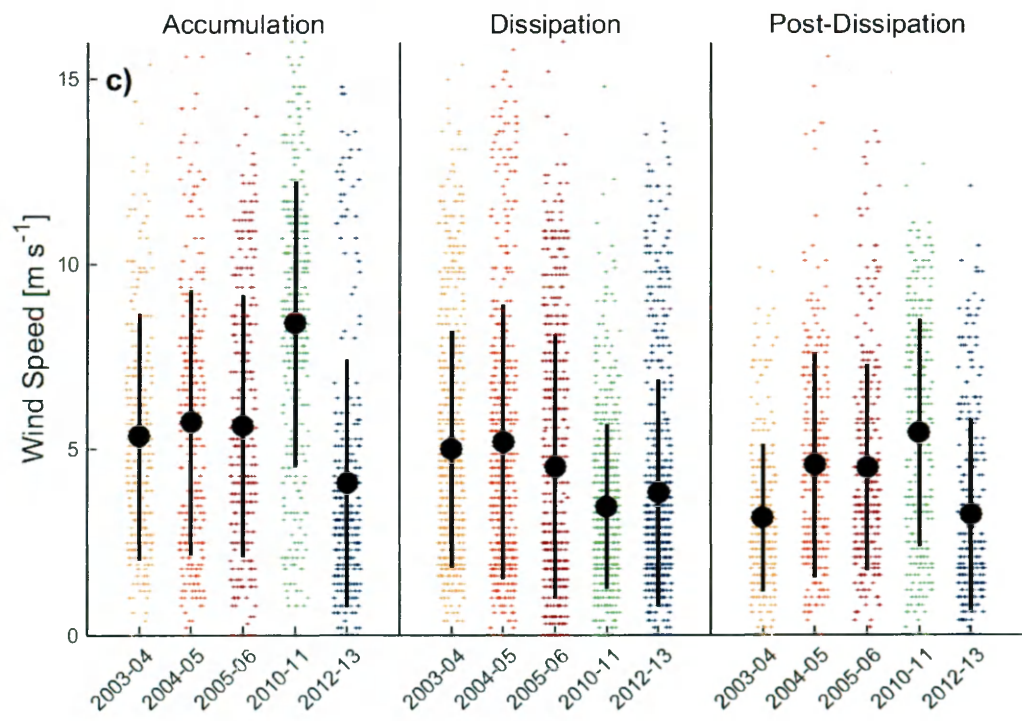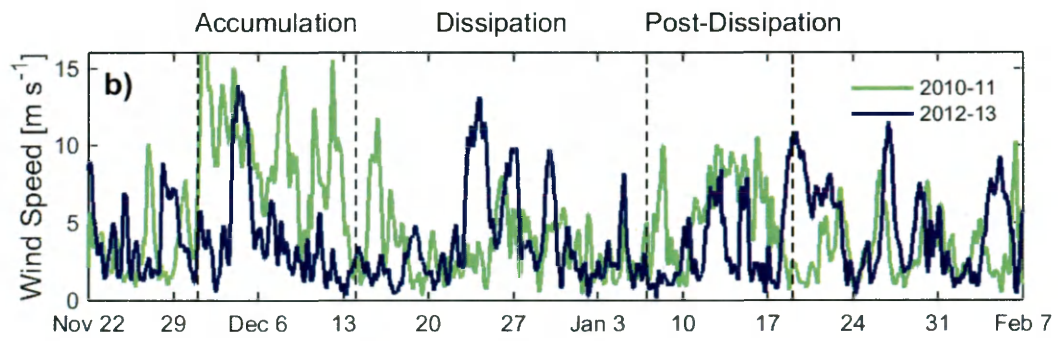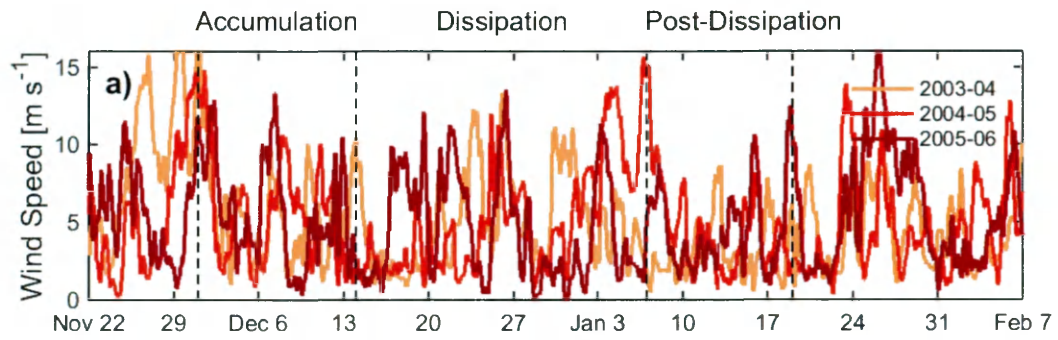
Appendix A.6: Temperature at 24 m from the (**a**) IVARS *Callinectes* mooring for 2004-2005 (orange line) and 2005-2006 (dark red line), (**b**) and from the gliders SG502, 2010-2011 (green line), SG503, 2010-2011 (light blue line), and SG503, 2012-2013 (dark blue line). Accumulation (December 1-14), dissipation (December 14 – January 7), and post-dissipation (January 7-19) periods are delineated by vertical, dashed lines. (**c**) Summary statistics for temperature at 24 m are displayed for the two mooring and three glider seasons during the three temporal periods. Averages are shown as black dots; one standard deviation both above and below the average are shown as black bars; individual data points are displayed as small points.

Appendix A.7: Density at 24 m from the (**a**) IVARS *Callinectes* mooring for 2004-2005 (orange line) and 2005-2006 (dark red line), (**b**) and from the gliders SG502, 2010-2011 (green line) and SG503, 2012-2013 (dark blue line). Accumulation (December 1-14), dissipation (December 14 – January 7), and post-dissipation (January 7-19) periods are delineated by vertical, dashed lines. (**c**) Summary statistics for density at 24 m are displayed for the two mooring and two glider seasons during the three temporal periods. Averages are shown as black dots; one standard deviation both above and below the average are shown as black bars; individual data points are displayed as small points.

143
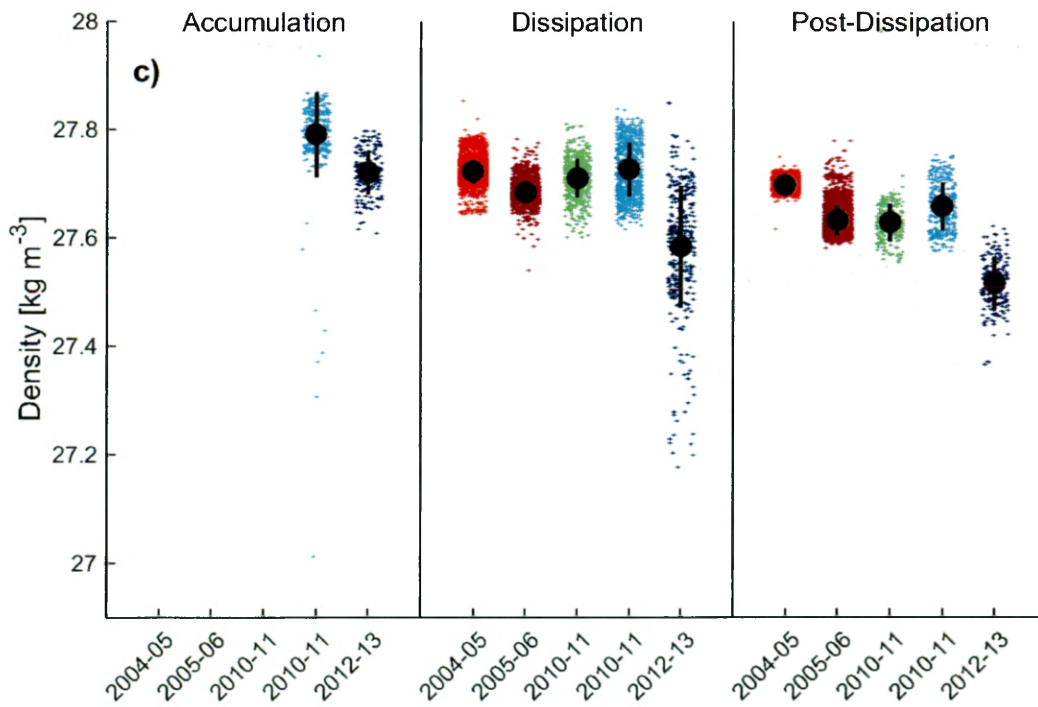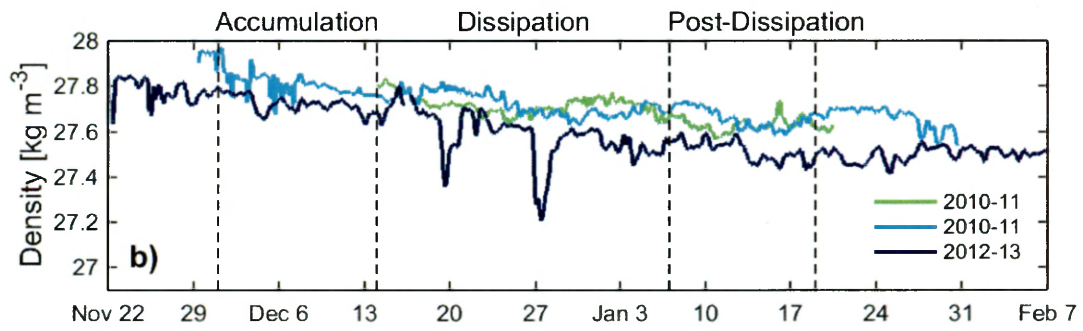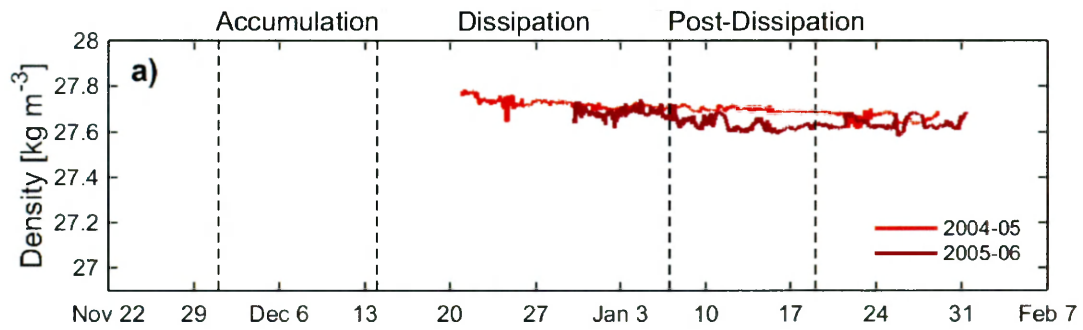
Appendix A.8: Fluorescence at 21 or 23 m from the (**a**) IVARS *Callinectes* mooring for 2003-2004 (21 m; light orange line), 2004-2005 (23 m; orange line), and 2005-2006 (21 m; dark red line), (**b**) and from the gliders SG502, 2010-2011 (21 m; green line) and SG503, 2012-2013 (21 m; dark blue line). Accumulation (December 1-14), dissipation (December 14 – January 7), and post-dissipation (January 7-19) periods are delineated by vertical, dashed lines. (**c**) Summary statistics for relative fluorescence at 24 m are displayed for the three mooring and two glider seasons during the three temporal periods. Averages are shown as black dots; one standard deviation both above and below the average are shown as black bars; individual data points are displayed as small points.
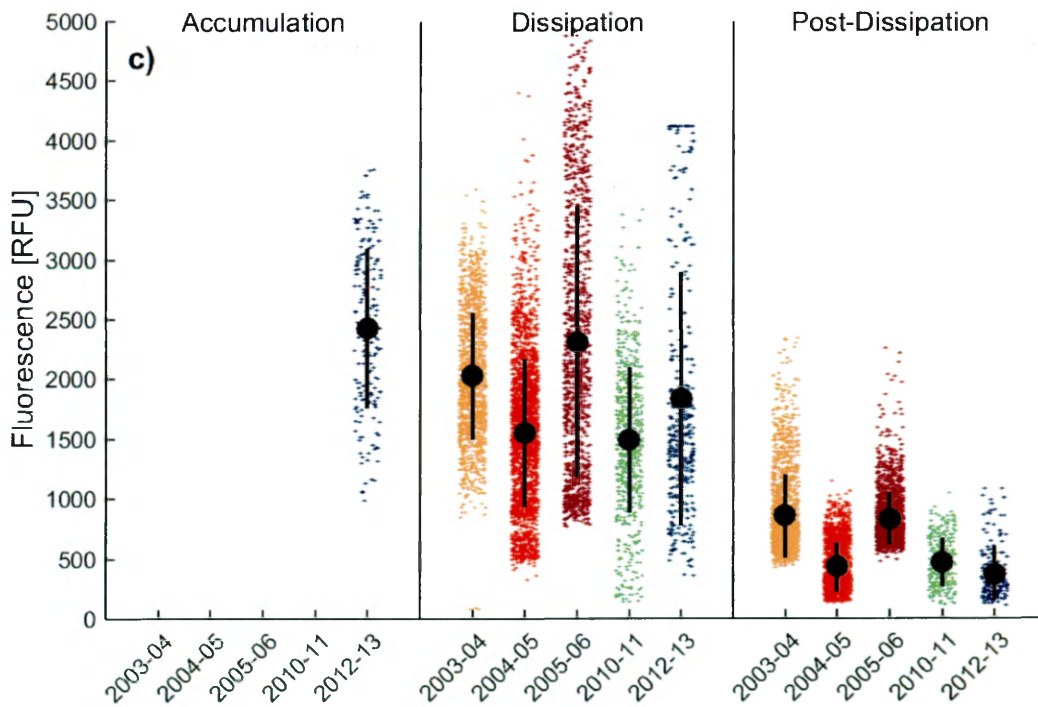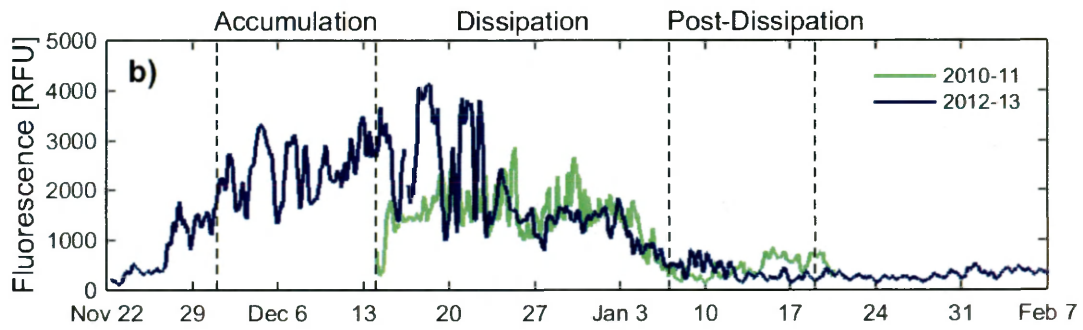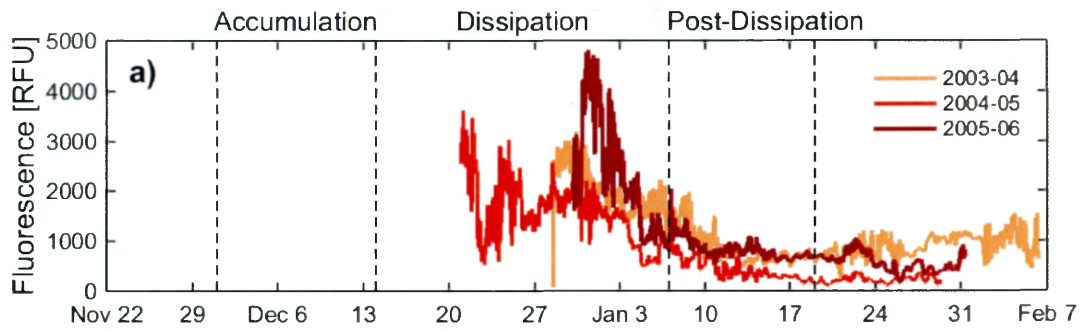
Appendix A.9: Moving correlations for SG503, 2012-2013 utilizing a moving window of 7 days between (**a**) 0-10 m, (**b**) 20-30 m, (**c**) 40-50 m, (**d**) 60-70 m, and (**e**) 80-90 m average 10 m chlorophyll with wind speed (blue lines), mixed layer depth (red lines), and the corresponding average 10 m temperature (yellow lines). Data are aligned on the x-axis at the window center.

147
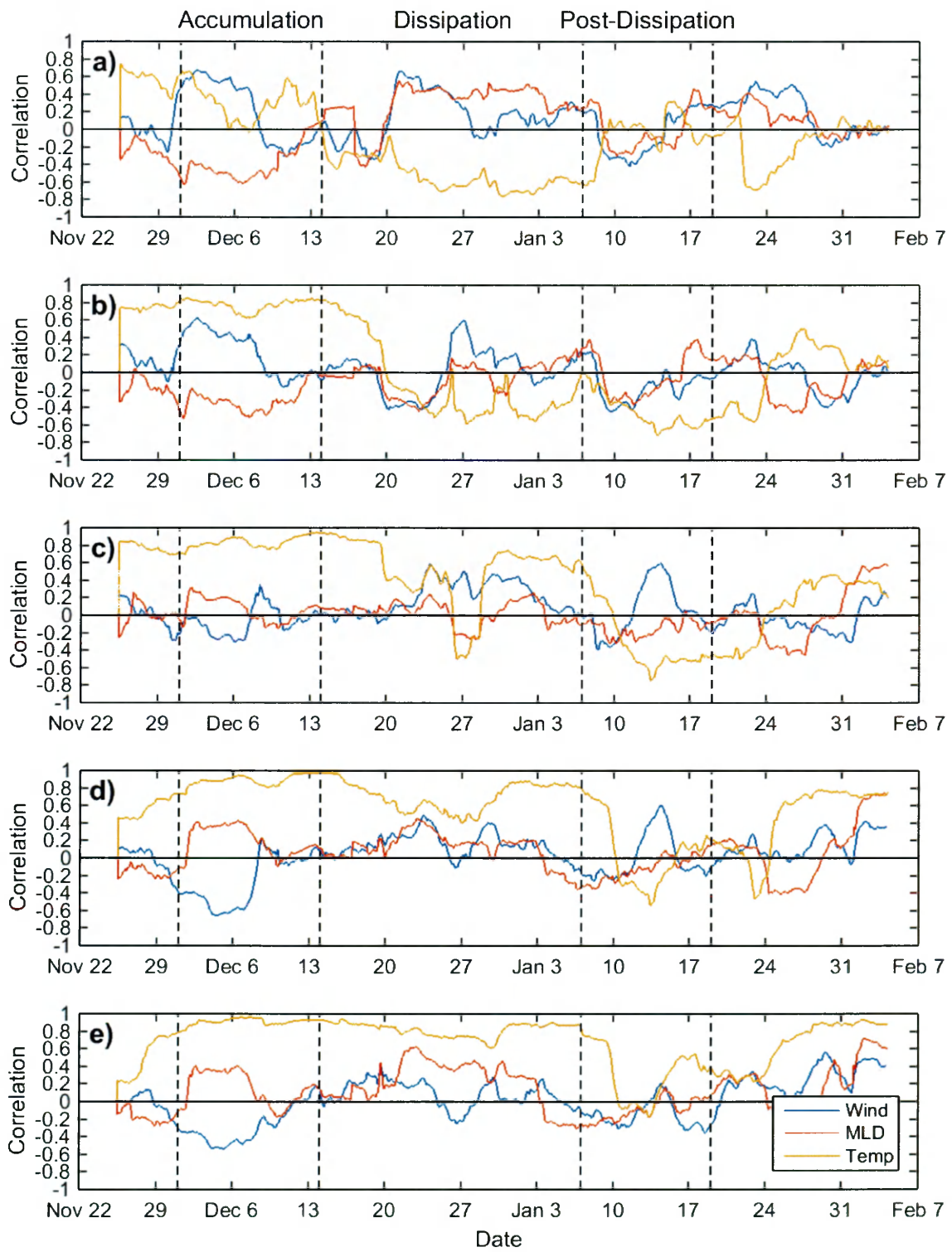
Appendix A.10: Moving correlations for SG502, 2010-2011 utilizing a moving window of 7 days between (**a**) 0-10 m, (**b**) 20-30 m, (**c**) 40-50 m, (**d**) 60-70 m, and (**e**) 80-90 m average 10 m chlorophyll with wind speed (blue lines), mixed layer depth (red lines), and the corresponding average 10 m temperature (yellow lines). Data are aligned on the x-axis at the window center.
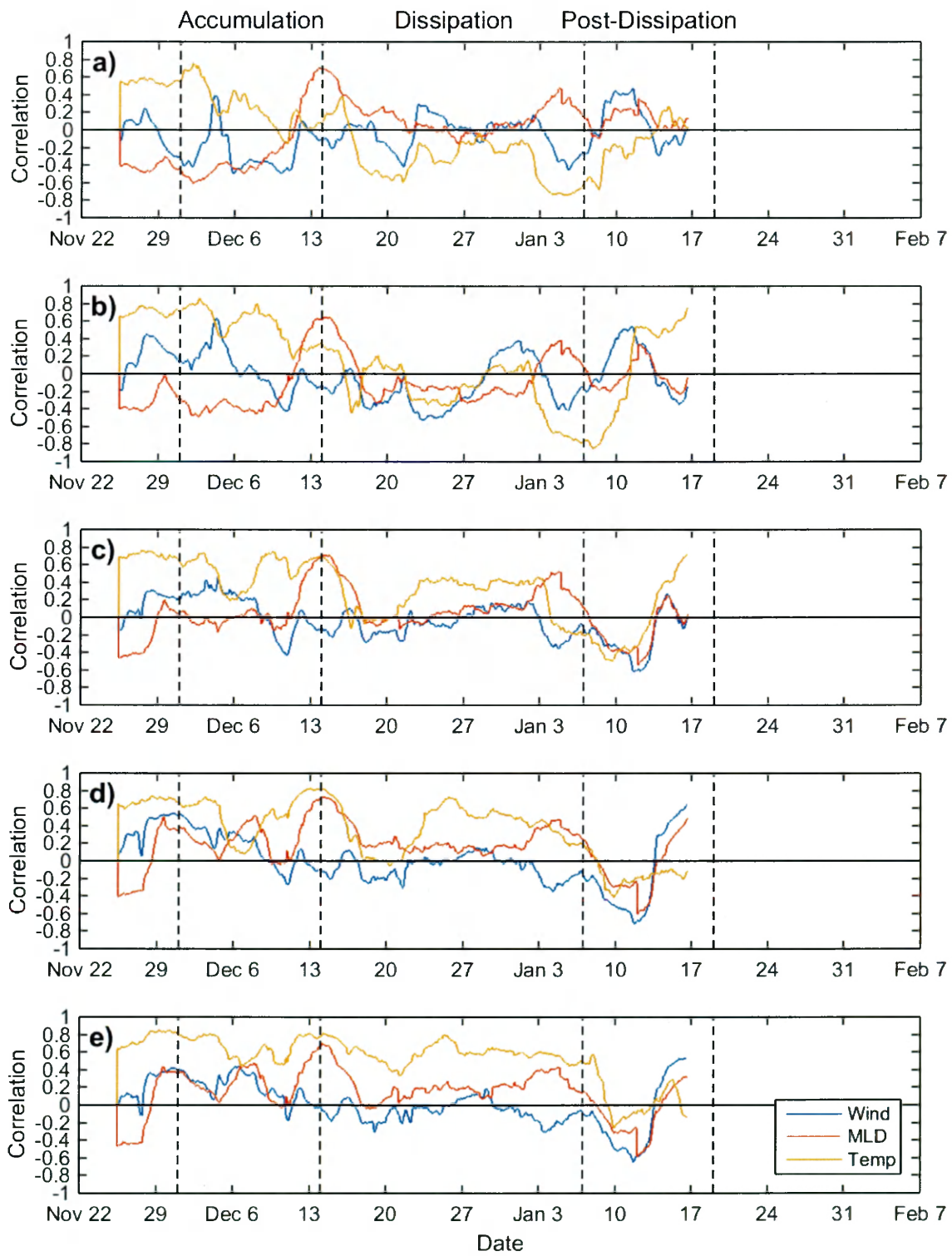
VITA

RANDOLPH MICHAEL JONES

Born in Boston, MA on February 17, 1984. Graduated from Xaverian Brothers High School in 2002. Earned a Bachelor's of Arts in Biology from Connecticut College in 2006. Employed as a research assistant at the Plum Island Ecosystems LTER in 2004 and 2005, and at the Darling Marine Center, University of Maine in 2006. Worked as a volunteer in the Peace Corps in Paraguay, South America in 2006-2007. Attended Friday Harbor Laboratories, University of Washington in Friday Harbor, WA as a research apprentice in 2007. Employed with Sea Education Association as an assistant scientist from 2009-2012. Entered the Master's of Science program at the Virginia Institute of Marine Science, College of William and Mary under graduate advisor Dr. Walker O. Smith, Jr. in 2012.